

THESIS

INTERACTION OF ADIPOSE-DERIVED STEM CELLS WITH
TITANIA NANOTUBE SURFACES

Submitted by

Kari Miller Cowden

Department of Mechanical Engineering

In partial fulfillment of the requirements

For the Degree of Master of Science

Colorado State University

Fort Collins, Colorado

Spring 2018

Master's Committee:

Advisor: Ketul C. Popat

Juyeon Park
Walajabad S. Sampath

Copyright by Kari Miller Cowden 2018

All Rights Reserved

ABSTRACT

INTERACTION OF ADIPOSE-DERIVED STEM CELLS WITH TITANIA NANOTUBE SURFACES

The need for joint replacement will continue to grow and increase significantly in the coming decades due to the aging population. Unfortunately, many joint implants experience failure after 10-15 years requiring revision surgery. With the growing need for more implants and the high cost of medical expenses for orthopedic surgery, it is imperative that implants are effective and have long term success. Since joint implant materials come into direct contact with bone it is vital that they mimic the structure of bone to improve osseointegration, or the direct structural and functional connection between living bone and the implant surface. Improving the osseointegration of the implant can increase the stability of the implant, thus, reducing micro motions that cause loosening and lead to implant failure. Current joint implants have microscale coatings and texturing, however, bone is composed of both micro and nano components. In order to mimic the nanostructure of bone, different nanotopographies are currently being studied. These nanostructures have been shown to improve cellular response in terms of adhesion, proliferation, and osteogenic differentiation. However, the optimal size of nanosurfaces to promote cell adhesion, proliferation, and differentiation is still disputed. Titania nanotubes (NT) have been shown to improve cellular response *in vitro* and improve integration in *in vivo* animal studies. This thesis investigates the surface characteristics of titania NT and

the effect of nanotube size on adhesion, proliferation, and differentiation of adipose-derived stem cells (ADSC) *in vitro*. The results presented in this thesis indicate that ADSC differentiated and performed better on NT surfaces than Ti surfaces. Additionally, the size of titania NT altered the proliferation and osteogenic differentiation of ADSC. Further studies should be directed toward *in vivo* animal studies to confirm that implants with NT surfaces enhance osseointegration and further define their potential to improve implant stability.

ACKNOWLEDGEMENTS

Foremost, I would like to express my sincere gratitude to my advisor Dr. Ketul C. Popat for his continuous support of my research, especially for his patience, motivation, enthusiasm, and immense knowledge. Also, a thank you to Dr. Juyeon Park and Dr. Walajabad S. Sampath for donating their time to serve on my committee.

I would also like to thank my fellow lab mates: Marcela Ferreira Dias-Netipanyj, Rachael Simon, Yanyi Zhang, Kevin Bartlett, Stephen Hughes, and Hieu Bui for training, research discussions, and additional help provided during the research process. Thanks to my undergraduate assistant, Andrea Thorpe, for her countless hours at the microscope imaging samples.

I would also like to thank and acknowledge Dr. Patrick McCurdy and Dr. Roy Geiss for their assistance with SEM and XPS, Brian Newell for his assistance with XRD, and Dr. Kimberly Cox-York for isolating and donating the adipose-derived stem cells.

Finally, I would like to express my profound gratitude to my husband, Joshua, for providing me with unfailing support and continuous encouragement throughout my years of study and through the process of researching and writing this thesis. This accomplishment would not have been possible without him.

TABLE OF CONTENTS

ABSTRACT	ii
ACKNOWLEDGEMENTS	iv
LIST OF FIGURES.....	vii
HYPOTHESIS AND SPECIFIC AIMS	1
Chapter 1 LITERATURE REVIEW	3
1.1 Introduction.....	3
1.2 Titanium as a Material for Orthopedic Implants	4
1.3 Implant Surface Modifications.....	6
1.4 Structure of Bone.....	9
1.5 Nano Structured Ti Surfaces	10
1.6 Adipose-derived Stem Cells	11
1.7 Focus of Research	15
REFERENCES.....	16
Chapter 2 FABRICATION AND CHARACTERIZATION OF TITANIA NANOTUBE SURFACES.....	24
2.1 Methods and Materials	25
2.1.1 Fabrication of Nanotube Surfaces.....	25
2.1.2 Characterization of Nanotube Surfaces.....	26
2.1.3 Statistical analysis	27
2.2 Results and Discussion	28
2.3 Conclusions.....	36
REFERENCES.....	37
Chapter 3 EVALUATION OF THE EFFECT OF TITANIA NANOTUBES ON ADHESION AND PROLIFERATION OF ADIPOSE-DERIVED STEM CELLS	40
3.1 Methods and Materials	41
3.1.1 Adipose-Derived Stem Cell (ADSC) Culture	41

3.1.2	ADSC Adhesion and Proliferation	41
3.1.3	Statistical analysis	43
3.2	Results and Discussion	44
3.3	Conclusions.....	53
	REFERENCES.....	54
	Chapter 4 EVALUATION OF THE EFFECT OF TITANIA NANOTUBES ON THE DIFFERENTIATION OF ADIPOSE-DERIVED STEM CELLS	56
4.1	Methods and Materials	57
4.1.1	ADSC Differentiation	57
4.1.2	Statistical analysis	59
4.2	Results and Discussion	59
4.3	Conclusions.....	67
	REFERENCES.....	69
	Chapter 5 CONCLUSIONS AND FUTURE WORK	72
5.1	Conclusions.....	72
5.2	Future Work.....	74
	Appendix I.....	76

LIST OF FIGURES

- Figure 1.1 Titanium is commonly used for the acetabular shell and/or the femoral stem in hip implants and the stemmed tibial plate in knee implants. Components of (a) hip (Reprinted from [21], Copyright (2018) Stryker Corp.) and (b) knee implants (Adapted from www.hss.edu/conditions_understanding-implants-in-knee-and-hip-replacement.asp [22]). 6
- Figure 1.2 Examples of hydroxyapatite coatings on current hip and knee implants. (a) Hydroxyapatite coating on acetabular shell for hip implant (Reprinted from [21], Copyright (2018) Stryker Corp.) (b) Tibial base plate with hydroxyapatite coated beads for knee implant (Adapted from rcmclinic.com/patient-information/knee-information/athletic-knee-implant-overview/athletic-knee-implant-technology-v2 [31])..... 7
- Figure 1.3 Examples of micro-scale topographies on titanium implant surfaces. (a) Micromachining on titanium screw (Reprinted from [39], Copyright (2018) Micropat) (b) Titanium surface structure after sandblasting with aluminum oxide grit (Reprinted from [40], Copyright (2018) 101Bios) (c) Titanium plasma spray coating on hip stem implant (Reprinted from [41], Copyright (2018) Medacta) (d) Surface structure after acid etching on titanium screw (Reprinted from [40], Copyright (2018) 101Bios) 8
- Figure 1.4 Example of the hierarchical structure of bone. (a) At the macrostructure level, bone consists of a dense shell of cortical bone with porous cancellous bone at both ends. (b) At the microstructure level, bone consists of repeating osteon units within the cortical bone. (c) At the nanostructure level, bone consists of collagen fibers (100–2,000 nm) that are composed of collagen fibrils (10’s nm). (Reprinted from [42], Copyright (2015) Bone Research)..... 9
- Figure 1.5 Examples of and nano-scale topographies on Ti surfaces. (a) Titanium nanofibers (Reprinted from [47], Copyright (2014) Int. J. Nanomedicine) (b) Titanium nanofibers with stem cells (Reprinted from [47], Copyright (2014) Int. J. Nanomedicine) (c) Titanium nanopores (Reprinted from [49], Copyright (2016) Int. J. Nanomedicine) (d) Titanium nanopores with stem cells (Reprinted from [49], Copyright (2016) Int. J. Nanomedicine) (e) Titania nanotubes (f) Titania nanotubes with stem cells 11
- Figure 1.6 Potential cell lineages for mesenchymal stem cells (Reprinted from [81] Copyright (2014), Stem Cells in Aesthetic Procedures: Art, Science, and Clinical Techniques)..... 12

Figure 1.7 Adipose-derived stem cells are present in fat tissue and are easily removed (Reprinted from [82], Copyright (2017) Journal of Limb Lengthening and Reconstruction).....	13
Figure 1.8 Adipose-derived stem cells can be induced to differentiate along the adipogenic, chondrogenic, and osteogenic cell lines. (AdaptedS from [79], Copyright (2008) Methods)	14
Figure 2.1 Schematic of anodization setup for fabrication of titania nanotube surfaces (Reprinted from [5], Copyright (2012) Smith, B.).....	26
Figure 2.2 SEM images of Titanium (Ti) and nanotubes made at 30 V (NT30), 45 V (NT45), and 60 V (NT60) at (A) 10,000 and (B) 50,000 magnification. (C) SEM images to look at the cross sectional length of NT30, NT45, and NT60 at 2,500 magnification.....	29
Figure 2.3 Average inner diameter and cross sectional length of nanotubes made at 30 V (NT30), 45 V (NT45), and 60 V (NT60). All NT inner diameter and tube length are significantly different. (*Tukey's HSD $p < 0.05$).....	30
Figure 2.4 Water contact angle on Ti and NT surfaces with representative images. Ti control surface is significantly different from NT30, NT45, and NT60 indicating that nanotubes are more hydrophilic than Titanium. (*Tukey's HSD $p < 0.05$)	31
Figure 2.5 Glancing angle X-ray diffraction (GAXRD) of Ti and NT surfaces after annealing indicating anatase and rutile crystalline phases.....	33
Figure 2.6 Chemical Compositions (Oxygen, Carbon, Titanium and Fluoride) of Ti and nanotube (NT) surfaces measured by XPS.....	34
Figure 2.7 X-ray photoelectron spectroscopy (XPS) survey scans of Ti, NT30, NT45, and NT60 indicating chemicals present on the surface.....	35
Figure 3.1 Adipose-derived stem cell viability after 1, 4 and 7 days determined by percent reduction of alamarBlue assay for (a) 2,500 cells/well, (b) 3,750 cells/well and (c) 5,000 cells/well densities.	46
Figure 3.2 Cell count of adipose-derived stem cells after 1, 4 and 7 days for Ti and NT surfaces cultured at (a) 2,500 cells/well, (b) 3,750 cells/well and (c) 5,000 cells/well densities.....	46
Figure 3.3 Percentage increase in (a) cell viability and (b) cell count calculated using alamarBlue results and DAPI staining from day 1 to day 7.	47
Figure 3.4 Fluorescent microscopy images of adipose-derived stem cells cultured at 2,500 cells/well density on Ti and NT surfaces after day 1, 4, and 7 of proliferation (scale bar 100 μ m).	48

Figure 3.5 Fluorescent microscopy images of adipose-derived stem cells cultured at 3,750 cells/well density on Ti and NT surfaces after day 1, 4, and 7 of proliferation (scale bar 100µm).	49
Figure 3.6 Fluorescent microscopy images of adipose-derived stem cells cultured at 3,750 cells/well density on Ti and NT surfaces after day 1, 4, and 7 of proliferation (scale bar 100µm).	50
Figure 3.7 Scanning electron microscopy images of adipose-derived stem cells after 1, 4, and 7 days of proliferation at 100x (scale bar 100µm) and 1,000x (scale bar 10µm) magnification for 2,500 cells/well.	52
Figure 4.1 Alkaline Phosphatase Activity (ALP) normalized by total protein content (Micro BCA assay). ALP and BCA assays were performed 7, 14 and 21 days after induced osteogenesis of ADSC. When statistically comparing between weeks of the same treatment, Ti and NT60: no significance between weeks; NT30: Day 7 is significantly different from Day 14 and Day 21; NT45: Day 7 is significantly different from Day 14. When statistically comparing between treatments on the same week, Day 7: Ti is significantly different from NT45 and NT60; Day 14: Ti is significantly different from NT30 and NT45, also NT60 is significantly different from NT30; Day 21: no significance between treatments. (Tukey's HSD $p < 0.05$).....	61
Figure 4.2 Immunofluorescent images of adipose-derived stem cells taken at 20x magnification after 7, 14 and 21 days of induced osteogenesis (Scale bar 50µm). Circles enclose osteocalcin proteins.	63
Figure 4.3 Percentage area coverage of osteocalcin normalized by total protein content (Micro BCA assay) after 7, 14 and 21 days induced osteogenesis. When statistically comparing between weeks of the same treatment, Ti and NT60: Day 7 is significantly different from Day 14 and Day 21; NT30 and NT45: all weeks are significantly different from each other. When comparing between treatments on the same week, Day 7: NT30 is significantly different from Ti, NT45 and NT60; Day 14: NT30 is significantly different from NT45 and NT60; Day 21: NT30 is significantly different from Ti and NT60, also NT60 is significantly different from NT45. (Tukey's HSD $p < 0.05$).....	64
Figure 4.4 Calcium concentration on samples 7, 14 and 21 days after induced osteogenesis determined using a calcium reagent test. When statistically comparing between weeks of the same treatment, for all treatments (Ti, NT30, NT45, and NT60) Day 7 is significantly different from Day 14 and Day 21. When comparing between treatments on the same week, Day 7: Ti is significantly different from NT45 and NT60; Day 14: Ti is significantly different from NT30, NT45, and NT60; Day 21: Ti is significantly different from NT30, NT45, and NT60, NT60 is significantly different from NT30. (Tukey's HSD $p < 0.05$).....	66

Figure 4.5 SEM images of differentiated adipose-derived stem cells and mineral deposition after 21 days of induced osteogenesis at 1000x magnification (scale bar is 50µm). Arrows indicate mineral deposits. 68

HYPOTHESIS AND SPECIFIC AIMS

Fundamental Hypothesis: Titania nanotube surfaces with different diameters will affect stem cell adhesion, proliferation, and differentiation.

Sub Hypothesis 1: Titania nanotube surfaces can be fabricated in different nanotube sizes by varying the voltage during anodization.

Specific Aim 1: Fabrication and characterization of titania nanotube surfaces. This specific aim will be discussed in chapter 2 and will cover the following:

- (a) Fabrication of nanotubes surfaces with three different diameter sizes using an electrochemical anodization process.
- (b) Characterization of nanotube and titanium surfaces by evaluating tube size, surface wettability, crystalline structure, and chemical composition.

Sub Hypothesis 2: Titania nanotube surfaces can affect the adhesion and proliferation of adipose-derived stem cells.

Specific Aim 2: Investigate adipose-derived stem cell (ADSC) adhesion and proliferation on nanotube and titanium surfaces. This specific aim will be discussed in chapters 3 and will cover the following:

- (a) Evaluation of ADSC viability via alamarBlue reduction.
- (b) Evaluation of ADSC adhesion and proliferation via fluorescent staining and DAPI cell count.
- (c) Evaluation of ADSC morphology via scanning electron microscopy.

Sub hypothesis 3: Titania nanotube surfaces can affect the differentiation response of adipose-derived stem cells.

Specific Aim 3: Investigate adipose-derived stem cell (ADSC) differentiation on nanotube surfaces. This specific aim will be discussed in chapter 4 and will cover the following:

- (a) Evaluation of ADSC alkaline phosphatase activity.
- (b) Evaluation of non-collagen protein osteocalcin produced by ADSC.
- (c) Evaluation of calcium deposition from ADSC.
- (d) Evaluation of ADSC morphology and mineral deposition via immunofluorescence staining and scanning electron microscopy.

CHAPTER 1

LITERATURE REVIEW

1.1 Introduction

The adult human body has 206 bones that provide mechanical support, protect various organs, and perform metabolic functions such as storing calcium, phosphorus, and other essential ions to be used by the body. Strong, healthy bones are essential, but bones will become weak and brittle when affected by injury, disease, or just simply age. The number of orthopedic implants needed in the United States will increase dramatically over the next few decades largely due to growth of the older population. In 2050, the population aged 65 and over is projected to be 83.7 million, and by 2030, more than 20 percent of U.S. residents are projected to be aged 65 and over, compared with 13 percent in 2010 and 9.8 percent in 1970 [1]. Additionally, the average body mass index in the united states is also increasing and studies are showing a potential correlation between high body mass index and joint replacement [2,3]. Already there are many people living with a joint implant. A study estimated in 2010 there were 4.5 million people living with an artificial hip and 6.7 million people living with an artificial knee in the United States [4]. Because hip and knee joints often experience failure after 10-15 years, revision surgeries for total hip and knee replacement from 2012 to 2015 ranged from 9.9% to 10.4% (hips) and 7.2% to 9.4% (knees) [5]. The cost of implant surgery and revision surgery is a major concern for the patients and hospitals. The national average price for just the implant in a total knee replacement was \$16,109 in 2016 [6]. Revision surgery implants for knees can cost \$7498 (for one component) up to \$13,640 (for all three components)

and implant costs are typically only 25-35% of the total hospital bill [6]. With the growing need for more implants and the high cost of medical expenses for orthopedic surgery, it is imperative that implants are effective and have long term success.

1.2 Titanium as a Material for Orthopedic Implants

Titanium (Ti) and its alloys are widely used in dental, orthopedic, and reconstructive surgery implants [7] due their biocompatible properties. Biocompatibility is a term that has been redefined and debated over the last few decades. As biomaterials are being used in increasingly diverse and complex situations, with applications now involving tissue engineering, invasive sensors, drug delivery, nanotechnologies, and implantable medical devices, the definition of biocompatible is becoming increasingly more complicated. Williams defined biocompatibility as the “ability of a biomaterial to perform its desired function with respect to a medical therapy, without eliciting any undesirable local or systemic effects in the recipient or beneficiary of that therapy, but generating the most appropriate beneficial cellular or tissue response in that specific situation, and optimizing the clinically relevant performance of that therapy” [8].

Titanium is considered biocompatible in bone applications because it does not react to the surrounding tissue (bio inert) due to its inherent corrosion resistance. Ti exhibits corrosion resistance because an inert oxide layer spontaneously forms on the surface of Ti when it is exposed to oxygen. This oxide film is very stable and does not break down under normal physiological conditions, thus, it provides a protective layer for the Ti. Titanium also displays other desirable properties that make it suitable for orthopedic applications: high specific strength, low elastic modulus, low density, and

fatigue strength [7,8]. The low elastic modulus of titanium and its alloys range from 55-110 GPa and this is generally viewed as a biomechanical advantage as it is much smaller than cobalt–chromium–molybdenum alloy (200-230 GPa) or stainless steel (~200 GPa) [7,9], which are other metals commonly used in orthopedic implants. For comparison, the elastic modulus of cortical bone ranges between 6-20 GPa [10], thus, titanium implants display smaller stress shielding than other metals due to their elastic modulus being closer to that of bone [7,9,11]. Commercially pure Ti (CP Ti, grade 2 and 4) and Ti-6Al-4V (grade 5) alloy are the most common titanium alloys used in orthopedic implants today [11,12]. Even though Ti possesses a lot of biocompatible properties that are desirable in orthopedic applications, its bone-binding activity is pretty low compared to other materials like calcium phosphates [10]. This limitation of Ti negatively affects its biological performance and leads to poor anchorage of bone which then leads to decelerated bone regeneration and healing after implantation.

Although Ti implants have improved over the years, they still experience a degree of failure when implanted due to mechanical issues [13,14], biological issues [15,16], or a combination of both. Titanium is commonly used in the fabrication of the acetabular shell and/or the femoral stem in hip implants and the stemmed tibial plate in knee implants (**Figure 1.1**). Although companies have been improving these particular joint implants, many of them will still experience failure between 10-30 years resulting in revision surgery [17]. The most common cause for failure of knee and hip implants is impaired implant fixation, called aseptic loosening [18,19]. It is not entirely sure what causes aseptic loosening, but it is likely due to inadequate initial fixation, mechanical loss of fixation over time, and/or biologic loss of fixation caused by particle-induced osteolysis around the

implant [20]. By improving the direct structural and functional connection between living bone and the implant surface, or osseointegration, the life of the implant may be significantly increased reducing the need for revision surgery.

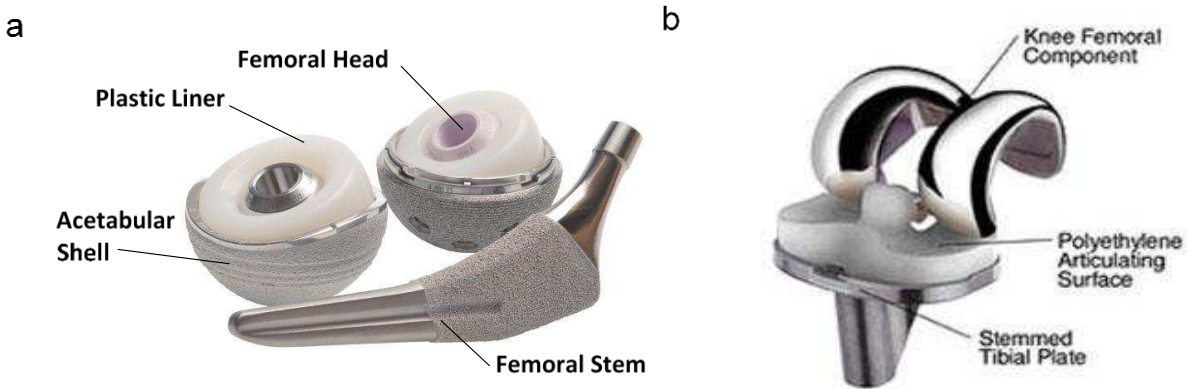


Figure 1.1 Titanium is commonly used for the acetabular shell and/or the femoral stem in hip implants and the stemmed tibial plate in knee implants. Components of (a) hip (Reprinted from [21], Copyright (2018) Stryker Corp.) and (b) knee implants (Adapted from www.hss.edu/conditions_understanding-implants-in-knee-and-hip-replacement.asp [22]).

1.3 Implant Surface Modifications

Studies have shown that cell adhesion, proliferation, and differentiation on an implant can be manipulated by altering the surface of the implant. Adding a surface coating to Ti is one approach to altering cell response on the surface. Studies have explored Ti surfaces with hydroxyapatite [23,24], calcium phosphate [25–28], and other cell enhancing biomolecules [29] to encourage cells to adhere and proliferate on the surface. Research studies have shown that these types of coatings enhance the cells response to the surface *in vitro* [23,24] and improve bone formation around the implant in *in vivo* animal studies [28]. Clinical studies looking at differences between coated and uncoated implants in human total hip replacement disagree on whether the coating actually improves the stability of the implant. Some studies have shown improved fixation

with the coating while others show no benefit [30]. There is also controversy on the effects of bioresorption, or degradation, of hydroxyapatite and other coatings when implanted in the body [30]. Today hydroxyapatite is a common coating that can be added to some components of hip and knee implants (**Figure 1.2**).

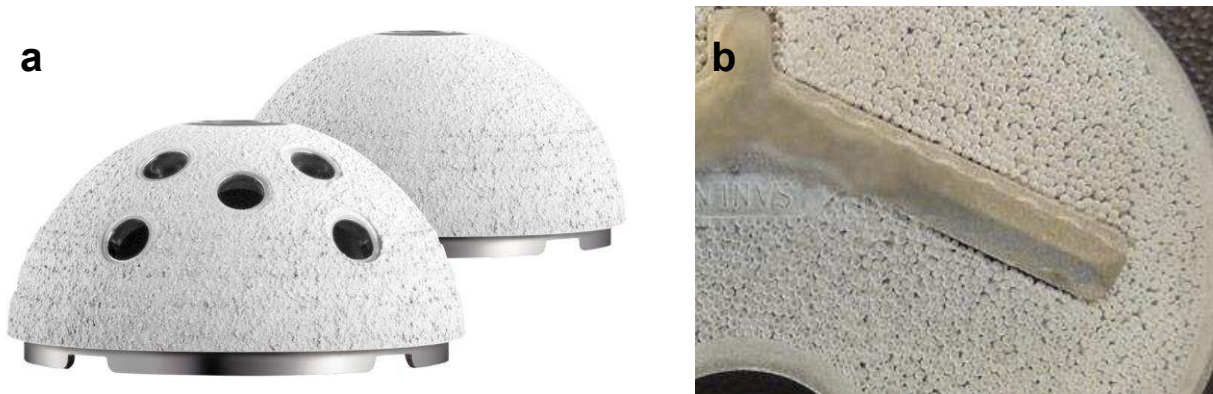


Figure 1.2 Examples of hydroxyapatite coatings on current hip and knee implants. (a) Hydroxyapatite coating on acetabular shell for hip implant (Reprinted from [21], Copyright (2018) Stryker Corp.) (b) Tibial base plate with hydroxyapatite coated beads for knee implant (Adapted from rcmclinic.com/patient-information/knee-information/athletic-knee-implant-overview/athletic-knee-implant-technology-v2 [31])

Altering the topography of the surface is another approach to enhancing cell response to encourage bone formation on the implant. Some examples of microscale topographical modifications are micromachining [32], sanding/grit blasting [33–35] plasma spraying [16,36], and acid etching [37] to name a few (**Figure 1.3**). Today plasma spraying is the technique most commonly used to micro-structure the surface of titanium components in both hip and knee implants. Some companies offer an additional coating such as hydroxyapatite to the plasma sprayed surface to further improve the fixation of

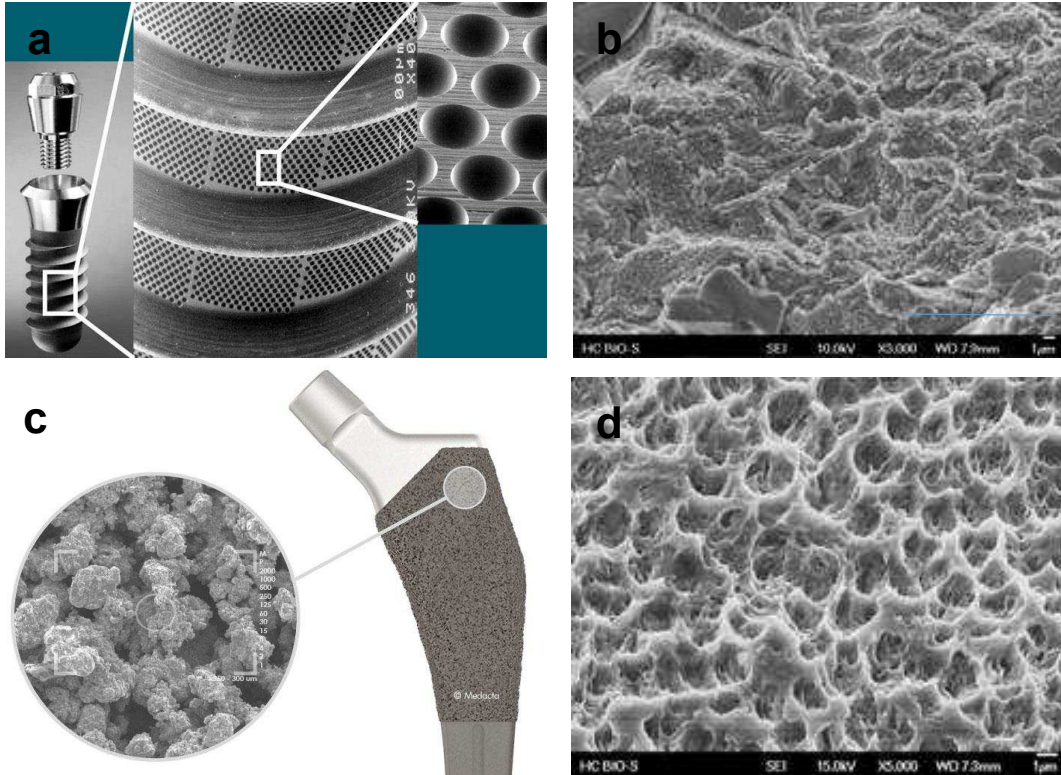


Figure 1.3 Examples of micro-scale topographies on titanium implant surfaces. (a) Micromachining on titanium screw (Reprinted from [39], Copyright (2018) Micropat) (b) Titanium surface structure after sandblasting with aluminum oxide grit (Reprinted from [40], Copyright (2018) 101Bios) (c) Titanium plasma spray coating on hip stem implant (Reprinted from [41], Copyright (2018) Medacta) (d) Surface structure after acid etching on titanium screw (Reprinted from [40], Copyright (2018) 101Bios)

the implant. Micro-coated and micro-structured joint implants have now been in continuous clinical use for thirty years to improve osseointegration of the implant. All though these implants are better they still experience a degree of failure [4,38] and the revision rate for knee and hip joints has not significantly decreased since these micro surfaces were introduced [5]. Because bone has a structure that has micro and nano components, implants surfaces that better mimic this structural hierarchy of bone may be the key for optimal fixation of the joint implant.

1.4 Structure of Bone

In the human body, bone is found either in a porous trabecular framework or a dense cortical structure. Bone has a hierarchical organization over length scales that span several orders of magnitude from the macro-scale to the nano-scale (**Figure 1.4**).

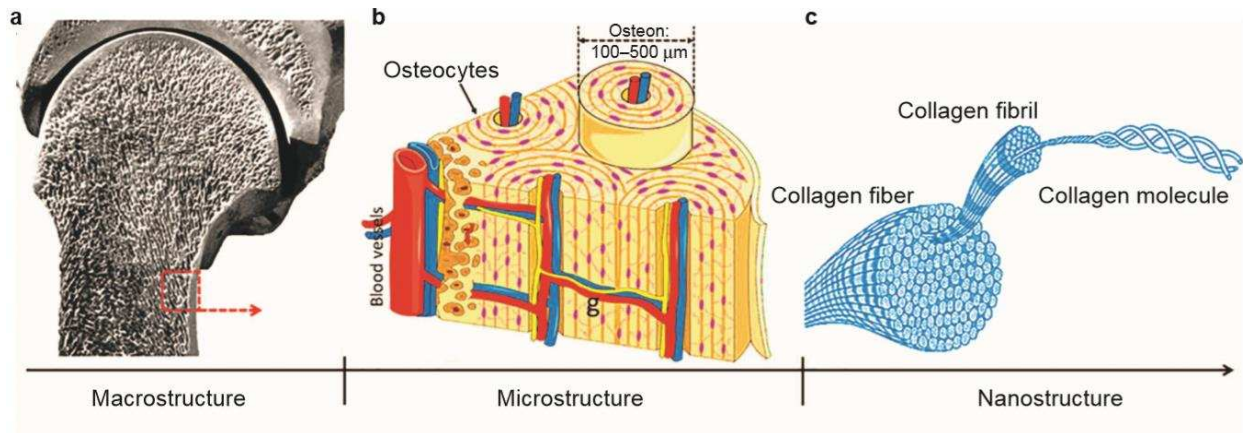


Figure 1.4 Example of the hierarchical structure of bone. (a) At the macrostructure level, bone consists of a dense shell of cortical bone with porous cancellous bone at both ends. (b) At the microstructure level, bone consists of repeating osteon units within the cortical bone. (c) At the nanostructure level, bone consists of collagen fibers (100–2,000 nm) that are composed of collagen fibrils (10's nm). (Reprinted from [42], Copyright (2015) Bone Research)

The macrostructure level of bone consists of a dense shell of cortical bone with porous cancellous bone at both ends. Within the cortical bone there are repeating osteon units (170–250 μm diameter) which are the units of bone produced during remodeling. Osteons are composed of 20–30 concentric layers of collagen fibers, called lamellae (2–9 μm thickness). These lamellae all surround a central vascular canal called the Haversian canal (60–90 μm diameter) where blood vessels and nerves reside. Collagen fibers (100–2,000 nm) that make up the lamellae are composed of collagen fibrils (80–100 nm diameter) [42]. Within the fibrils, type I collagen molecules (1.5 nm diameter, 300 nm length) and hydroxyapatite nanocrystals form a composite structure [43].

1.5 Nano Structured Ti Surfaces

Since bone tissue is composed of various components that are nanoscale [44], a surface that mimics this structural hierarchy and provides cues at the nanoscale may further improve the response of cells on the surface to enhance bone formation and improve long term stability of the implant [45,46]. Thus far, nanosurfaces have not been implemented for joint implants, however, many studies are currently directed towards understanding how nanoscale topographies on Ti surfaces can improve implant integration. Some nano-topographies that have been explored in research are nanofibers [47,48], nanopores [49–52], nanotubes (NT) [51,53–58], and other nanosurfaces [15,35] (**Figure 1.5**). Studies have shown that a Ti surface with a nanotopography not only promotes cell adhesion and proliferation of cells [47,59–61], it also supports differentiation of stem cells along the osteogenic line [49,62–64]. It can be hypothesized that a nanotopography on a Ti surface replicates the porous structure of native bone and creates an ideal environment for osteogenesis.

Previous studies have shown that titania NT, fabricated on the surface of titanium using an anodization technique, provide a template with a hierarchy similar to that of natural tissue [51,56,62,65–67] and have been shown to alter cellular functionality on the surface similar to that of natural tissue [51,68]. Additionally, titanium implants with a NT surface topography have been shown to improve fixation of solid implants to the surrounding bone tissues in *in vivo* animal studies [69,70]. However the optimal size of nanosurfaces to promote cell adhesion, proliferation, and differentiation is still disputed [53,54,60,64,71,72]. Because stem cells are important in the healing process, it is

essential to study the response of stem cells on these nanostructured surfaces *in vitro* and *in vivo*.

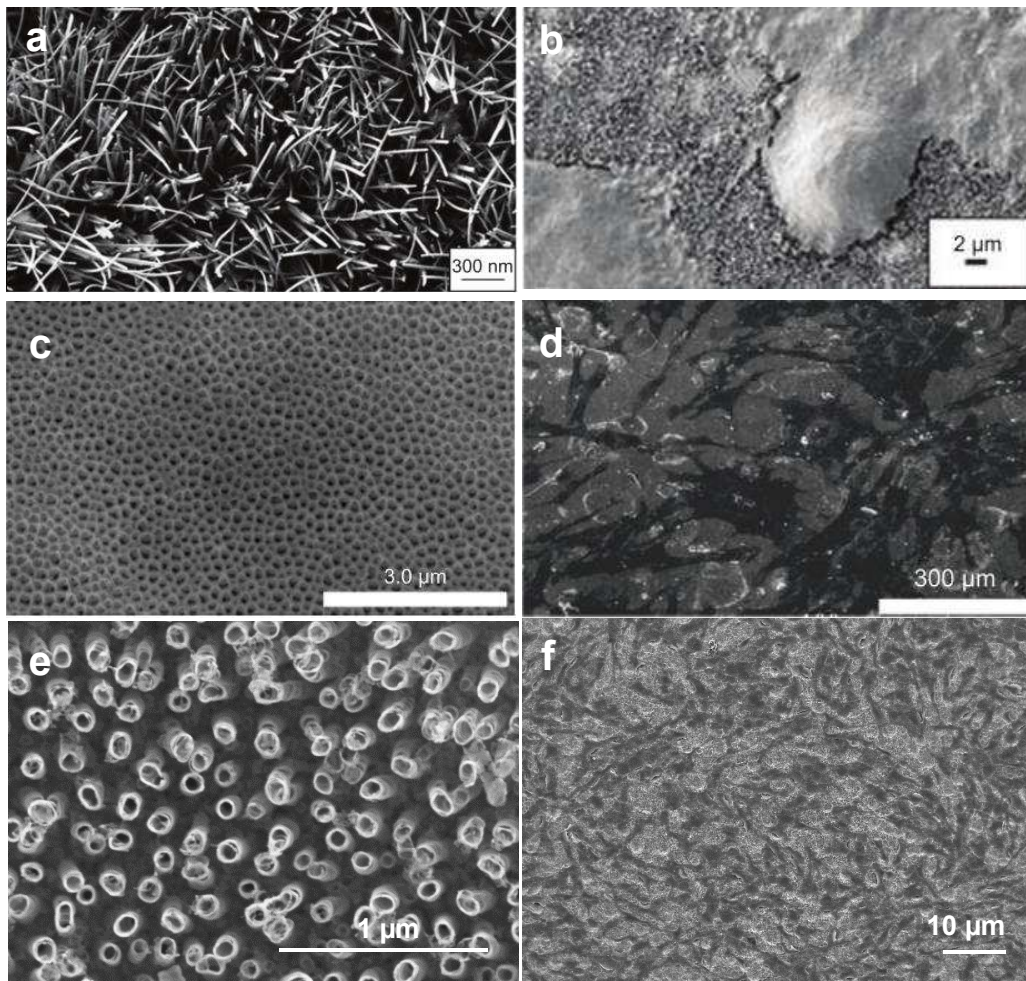


Figure 1.5 Examples of and nano-scale topographies on Ti surfaces. (a) Titanium nanofibers (Reprinted from [47], Copyright (2014) Int. J. Nanomedicine) (b) Titanium nanofibers with stem cells (Reprinted from [47], Copyright (2014) Int. J. Nanomedicine) (c) Titanium nanopores (Reprinted from [49], Copyright (2016) Int. J. Nanomedicine) (d) Titanium nanopores with stem cells (Reprinted from [49], Copyright (2016) Int. J. Nanomedicine) (e) Titania nanotubes (f) Titania nanotubes with stem cells

1.6 Adipose-derived Stem Cells

Stem cells are unspecialized cells capable of renewing themselves through self-renewal and can be induced to become specialized cells within specific tissue by providing specific cues. In all tissues of the body, stem cells become activated when an injury occurs and are recruited to the injury site to aid in the tissue repair process [73].

When a biomaterial is implanted, the body reacts similar to an injury and stem cells are recruited to the implant site. Since, stem cells play an important role in tissue repair in the body, their interaction with biomaterials is critical for long term success of medical devices. Bone marrow-derived mesenchymal stem cells (BMSC) are obtained from bone marrow and can be induced to differentiate into multiple cell lineages (**Figure 1.6**) [74].

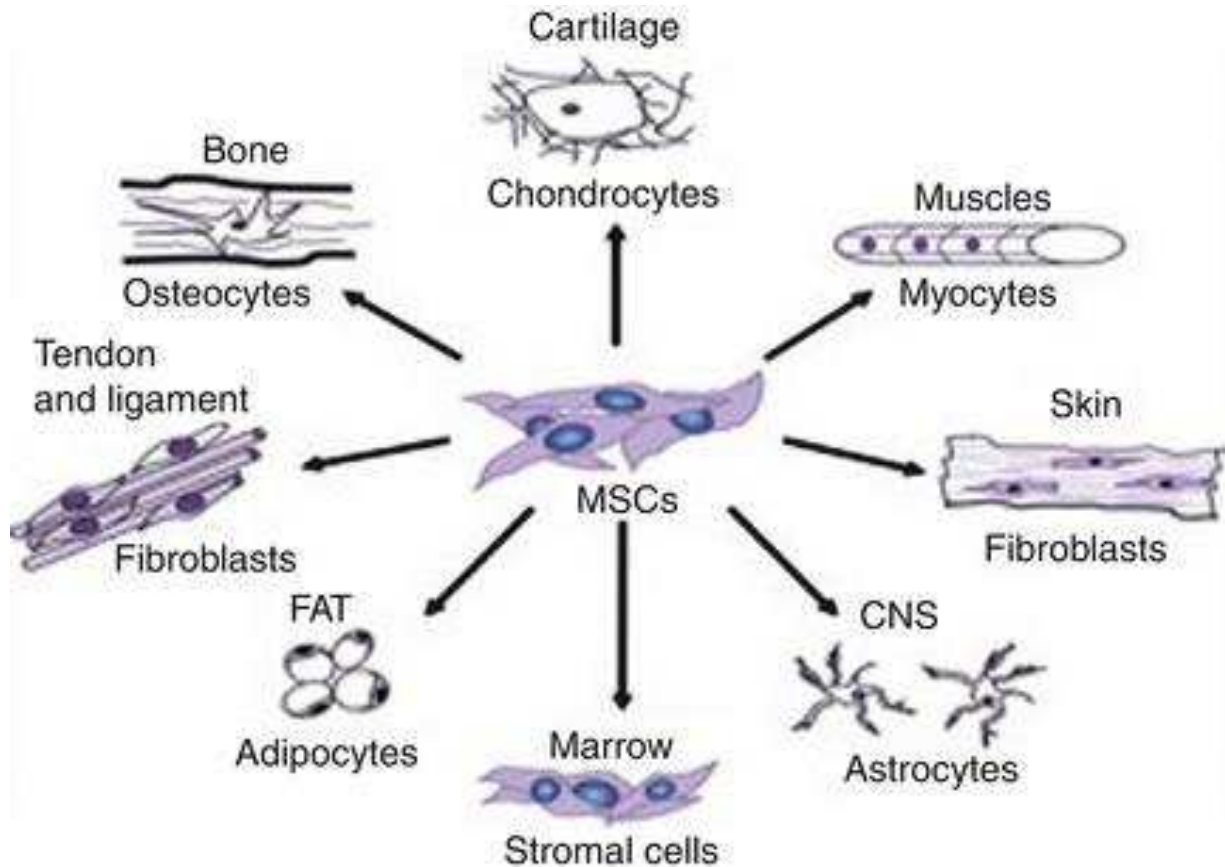


Figure 1.6 Potential cell lineages for mesenchymal stem cells (Reprinted from [81] Copyright (2014), Stem Cells in Aesthetic Procedures: Art, Science, and Clinical Techniques).

Because bone marrow-derived mesenchymal stem cells differentiate into osteoblasts, bone forming cells, they are commonly used in orthopedic biomaterial studies. However, obtaining these stem cells from bone marrow is an invasive procedure and the yield rate of cells is often low [75]. An alternative to BMSC are adipose-derived stem cells (ADSC) which are mesenchymal stem cells obtained from adipose tissue and

have been identified as a putative population of multipotent stem cells since 2001 (**Figure 1.7**) [76]. ADSC are easily accessible, available in large numbers, and attach and proliferate rapidly in culture, making them an attractive source for studies that aim to evaluate stem cell interaction with biomaterials [77,78]. Additionally, studies have demonstrated that ADSC possess an *in vitro* bone formation capacity similar to that of bone marrow-derived mesenchymal stem cells [79,80].

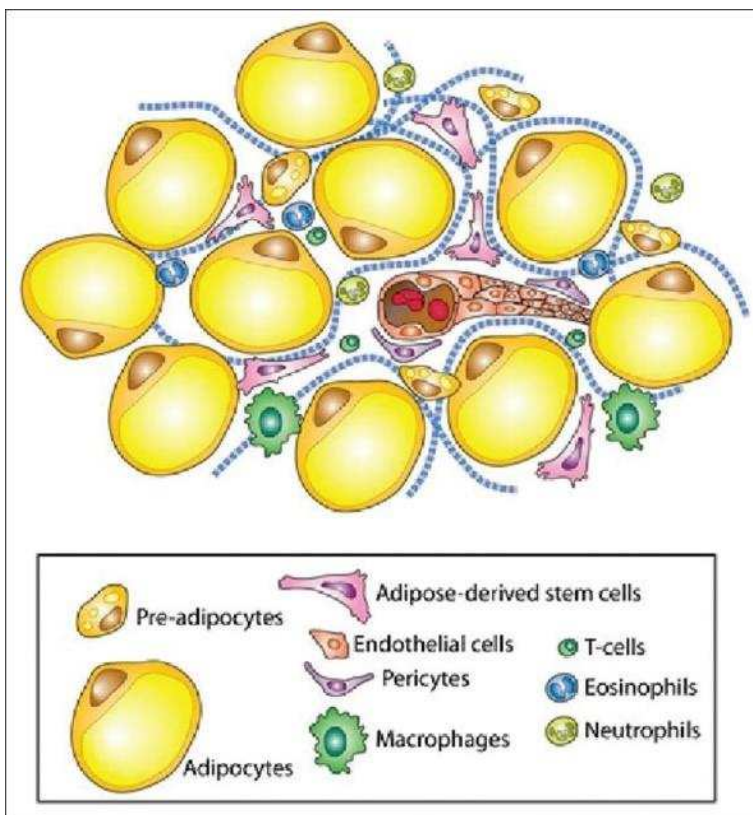


Figure 1.7 Adipose-derived stem cells are present in fat tissue and are easily removed (Reprinted from [82], Copyright (2017) Journal of Limb Lengthening and Reconstruction).

To date, very few studies have investigated the adhesion, proliferation, and differentiation of ADSC on titania NT surfaces. ADSC are easily proliferated in culture and on titanium surfaces using MEM Alpha Modification (Hyclone) media. Fluorescent staining of the stem cells allows visualization of ADSC distribution and the ability to quantify cell proliferation through nuclei counting. ADSC display multipotency in culture

studies, meaning they retain the ability to differentiate into cell types of multiple different lineages. By providing specific cues via chemicals in the media, ADSC can be induced to differentiate along the adipogenic, chondrogenic, and osteogenic cell lines (**Figure 1.8**) [75,78,79]. Osteogenic differentiation is achieved by using culture medium supplemented with dexamethasone, β -glycerol-phosphate and ascorbate-2-phosphate [79]. After differentiation, osteoblast-like cells began to produce calcium phosphate within the ECM which can be assessed using different assay tests. Alkaline phosphatase, type I collagen, osteopontin, osteocalcin, bone sialoprotein, Runx-1, BMP-2, BMP-4, parathyroid hormone receptor, BMP receptor 1 and 2 are all common genes that are up-regulated during osteogenesis process and can be investigated to confirm differentiation of the ADSC [78].

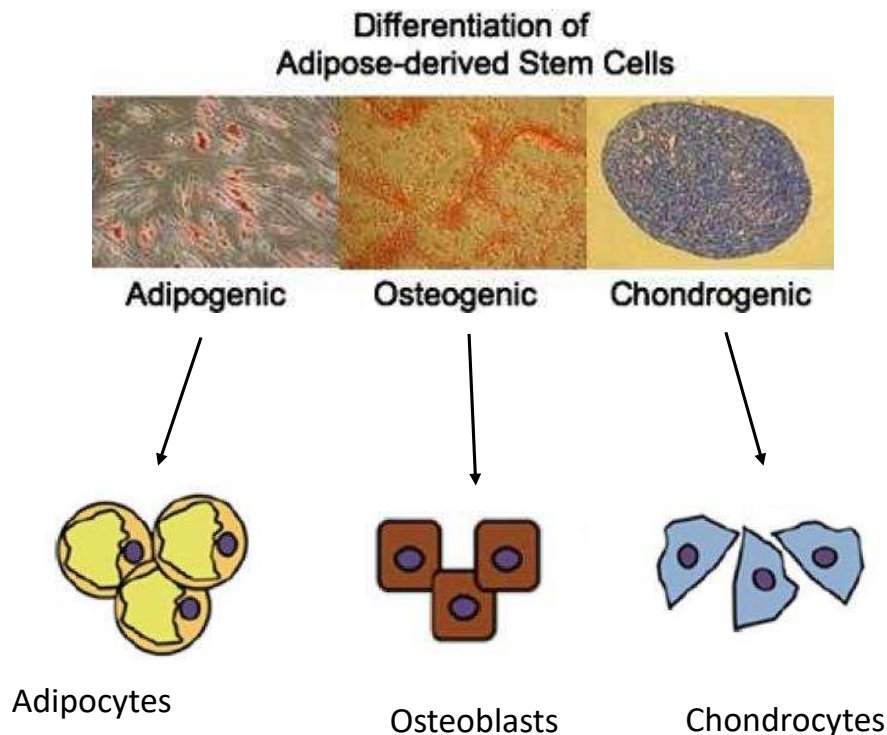


Figure 1.8 Adipose-derived stem cells can be induced to differentiate along the adipogenic, chondrogenic, and osteogenic cell lines. (Adapted from [79], Copyright (2008) Methods)

1.7 Focus of Research

Since many joint implants still experience loosening and eventual failure [13–16], implants with nanostructured surfaces could help improve their fixation to the surrounding bone tissues [44,62,68,83,84] and reduce the need for revision surgery. In order to develop these nanostructured surfaces it is important to understand how stem cells interact in an *in vitro* environment before moving into *in vivo* studies. The focus of this research is to better understand the effect of nanostructure size on adhesion, proliferation, and differentiation of ADSC *in vitro*. In chapter 2, the fabrication of titania nanotubes (NT) with three different diameters is discussed and they are characterized via scanning electron microscopy, wettability using contact angle, crystallinity using glancing angle X-ray diffraction, and surface chemistry using X-ray photoelectron spectroscopy. In chapter 3, the effect of nanotube size and cell density on the adhesion and proliferation of human adipose-derived stem cells (ADSC) is discussed and evaluated. In chapter 4, the effect of NT size on the differentiation of ADSC is discussed and evaluated. By fully understanding the effect of nanostructure size on the adhesion, proliferation, and osteogenic differentiation of stem cells, implants could be specifically designed to achieve the optimal stem cell response from the bone tissue in which they are implanted.

REFERENCES

- [1] J.M. Ortman, V. a. Velkoff, H. Hogan, An aging nation: The older population in the United States, *Econ. Stat. Adm. US Dep. Commer.* 1964 (2014) 1–28. doi:10.1016/j.jaging.2004.02.002.
- [2] D. Culliford, J. Maskell, A. Judge, C. Cooper, D. Prieto-alhambra, N.K. Arden, C. Study, Future projections of total hip and knee arthroplasty in the UK : results from the UK Clinical Practice Research Datalink, *Osteoarthr. Cartil.* 23 (2015) 594–600. doi:10.1016/j.joca.2014.12.022.
- [3] J.A. Singh, D.G. Lewallen, Time Trends in the Characteristics of Patients Undergoing Primary Total Knee Arthroplasty, *Arthritis Care Res. (Hoboken)*. 66 (2014) 897–906. doi:10.1002/acr.22233.
- [4] H. Maradit Kremers, D.R. Larson, C.S. Crowson, W.K. Kremers, R.E. Washington, C.A. Steiner, W.A. Jiranek, D.J. Berry, Prevalence of Total Hip and Knee Replacement in the United States., *J. Bone Joint Surg. Am.* 97 (2015) 1386–97. doi:10.2106/JBJS.N.01141.
- [5] K.J. Berry, Daniel J., Bozic, American Joint Replacement Registry ANNUAL REPORT 2016, 2016.
- [6] A.M. Elbuluk, A.B. Old, J.A. Bosco, R. Schwarzkopf, R. Iorio, Strategies for reducing implant costs in the revision total knee arthroplasty episode of care, *Arthroplast. Today*. 3 (2017) 286–288. doi:10.1016/j.artd.2017.03.004.
- [7] M. Long, H.J. Rack, Titanium alloys in total joint replacement--a materials science perspective., *Biomaterials*. 19 (1998) 1621–1639. doi:10.1016/S0142-9612(97)00146-4.
- [8] D.F. Williams, On the mechanisms of biocompatibility, *Biomaterials*. 29 (2008) 2941–2953. doi:10.1016/j.biomaterials.2008.04.023.
- [9] Y. Li, C. Yang, H. Zhao, S. Qu, X. Li, Y. Li, New developments of ti-based alloys for biomedical applications, *Materials (Basel)*. 7 (2014) 1709–1800. doi:10.3390/ma7031709.
- [10] F. Barrère, T.A. Mahmood, K. de Groot, C.A. van Blitterswijk, Advanced biomaterials for skeletal tissue regeneration: Instructive and smart functions, *Mater. Sci. Eng. R Reports*. 59 (2008) 38–71. doi:10.1016/j.mser.2007.12.001.
- [11] E. Sáenz de Viteri, Virginia and Fuentes, Titanium and Titanium Alloys as Biomaterials, in: *Tribol. - Fundam. Adv.*, 2013: pp. 155–181.

- [12] F. Mahyudin, L. Widhiyanto, H. Hermawan, Biomaterials in orthopaedics, *Adv. Struct. Mater.* 58 (2016) 161–181. doi:10.1007/978-3-319-14845-8_7.
- [13] J.M. Banovetz, R. Sharp, R. a Probe, J.O. Anglen, Titanium plate fixation: a review of implant failures., *J. Orthop. Trauma.* 10 (1996) 389–94. <http://www.ncbi.nlm.nih.gov/pubmed/8854316>.
- [14] J.P. Berthet, A. Gomez Caro, L. Solovei, M. Gilbert, S. Bommart, P. Gaudard, L. Canaud, P. Alric, C.H. Marty-Ane, Titanium Implant Failure After Chest Wall Osteosynthesis, *Ann Thorac Surg.* 99 (2015) 1945–1952. doi:10.1016/j.athoracsur.2015.02.040.
- [15] M. Geetha, A.K. Singh, R. Asokamani, A.K. Gogia, Ti based biomaterials, the ultimate choice for orthopaedic implants - A review, *Prog. Mater. Sci.* 54 (2009) 397–425. doi:10.1016/j.pmatsci.2008.06.004.
- [16] M. Yaszemski, D.J. Trantolo, *Corrosion and Biocompatibility of Orthopedic Implants*, 2004.
- [17] T. Camus, W.J. Long, Total knee arthroplasty in young patients: Factors predictive of aseptic failure in the 2nd–4th decade, *J. Orthop.* 15 (2018) 28–31. doi:10.1016/j.jor.2017.11.004.
- [18] D. Apostu, O. Lucaciu, C. Berce, D. Lucaciu, D. Cosma, Current methods of preventing aseptic loosening and improving osseointegration of titanium implants in cementless total hip arthroplasty: a review, *J. Int. Med. Res.* 0 (2017) 30006051773269. doi:10.1177/0300060517732697.
- [19] M. Fernandez-Sampedro, C. Salas-Venero, C. Fariñas-Álvarez, M. Sumillera, L. Pérez-Carro, M. Fakkas-Fernandez, J. Gómez-Román, L. Martínez-Martínez, M.C.M. Fariñas, 26 Postoperative diagnosis and outcome in patients with revision arthroplasty for aseptic loosening, *BMC Infect. Dis.* 15 (2015) 1–7. doi:10.1186/s12879-015-0976-y.
- [20] Y. Abu-Amer, I. Darwech, J.C. Clohisy, Aseptic loosening of total joint replacements: Mechanisms underlying osteolysis and potential therapies, *Arthritis Res. Ther.* 9 (2007) 1–7. doi:10.1186/ar2170.
- [21] Stryker, Hip Implant, (n.d.). www.stryker.com/us/en/portfolios/orthopaedics/joint-replacement/hip.html%0A (accessed July 2, 2018).
- [22] D.E. Padgett, R.E. Windsor, Knee Implant, (2013). www.hss.edu/conditions_understanding-implants-in-knee-and-hip-replacement.asp (accessed July 2, 2018).
- [23] C. Knabe, C.R. Howlett, F. Klar, H. Zreiqat, The effect of different titanium and hydroxyapatite-coated dental implant surfaces on phenotypic expression of human bone-derived cells, *J. Biomed. Mater. Res. - Part A.* 71 (2004) 98–107.

doi:10.1002/jbm.a.30130.

- [24] R. Bosco, M. Iafisco, A. Tampieri, J.A. Jansen, S.C.G. Leeuwenburgh, J.J.J.P. Van Den Beucken, Hydroxyapatite nanocrystals functionalized with alendronate as bioactive components for bone implant coatings to decrease osteoclastic activity, *Appl. Surf. Sci.* 328 (2015) 516–524. doi:10.1016/j.apsusc.2014.12.072.
- [25] H.S. Alghamdi, R. Bosco, J.J.J.P. van den Beucken, X.F. Walboomers, J.A. Jansen, Osteogenicity of titanium implants coated with calcium phosphate or collagen type-I in osteoporotic rats, *Biomaterials.* 34 (2013) 3747–3757. doi:10.1016/j.biomaterials.2013.02.033.
- [26] H.S. Alghamdi, R. Bosco, S.K. Both, M. Iafisco, S.C.G. Leeuwenburgh, J.A. Jansen, J.J.J.P. Van den Beucken, Synergistic effects of bisphosphonate and calcium phosphate nanoparticles on peri-implant bone responses in osteoporotic rats, *Biomaterials.* 35 (2014) 5482–5490. doi:10.1016/j.biomaterials.2014.03.069.
- [27] A.A. Campbell, Bioceramics for implant coatings, *Mater. Today.* 6 (2003) 26–30. doi:10.1016/S1369-7021(03)01128-3.
- [28] E. Schiegnitz, V. Palarie, V. Nacu, B. Al-Nawas, P.W. Kämmerer, Vertical osteoconductive characteristics of titanium implants with calcium-phosphate-coated surfaces - a pilot study in rabbits, *Clin. Implant Dent. Relat. Res.* 16 (2014) 194–201. doi:10.1111/j.1708-8208.2012.00469.x.
- [29] H. Kokkonen, H. Niiranen, H.A. Schols, M. Morra, F. Stenbäck, J. Tuukkanen, Pectin-coated titanium implants are well-tolerated in vivo, *J. Biomed. Mater. Res. - Part A.* 93 (2010) 1404–1409. doi:10.1002/jbm.a.32649.
- [30] Stuart B. Goodman, Zhenyu Yao, Michael Keeney, Fan Yang, The Future of Biologic Coatings for Orthopaedic Implants, *Biomaterials.* 34 (2013) 3174–3183. doi:10.1016/j.biomaterials.2013.01.074.
- [31] M. Roosenberg, Cooley, Stryker Triathlon tibial base plate with hydroxyapatite coated beads as porous coat, (n.d.). rcmclinic.com/patient-information/knee-information/athletic-knee-implant-overview/athletic-knee-implant-technology-v2/ (accessed August 2, 2018).
- [32] C. Prakash, M.S. Uddin, Surface modification of β -phase Ti implant by hydroxyapatite mixed electric discharge machining to enhance the corrosion resistance and in-vitro bioactivity, *Surf. Coatings Technol.* 326 (2017) 134–145. doi:10.1016/j.surfcoat.2017.07.040.
- [33] C. Aparicio, A. Padrós, F.J. Gil, In vivo evaluation of micro-rough and bioactive titanium dental implants using histometry and pull-out tests, *J. Mech. Behav. Biomed. Mater.* 4 (2011) 1672–1682. doi:10.1016/j.jmbbm.2011.05.005.
- [34] Z. Schwartz, P. Raz, G. Zhao, Y. Barak, M. Tauber, H. Yao, B.D. Boyan, Effect of

- Micrometer-Scale Roughness of the Surface of Ti6Al4V Pedicle Screws in Vitro and in Vivo, *J. Bone Jt. Surgery-American* Vol. 90 (2008) 2485–2498. doi:10.2106/JBJS.G.00499.
- [35] A. Jemat, M.J. Ghazali, M. Razali, Y. Otsuka, Surface modifications and their effects on titanium dental implants, *Biomed Res. Int.* 2015 (2015). doi:10.1155/2015/791725.
- [36] C.A. Simmons, N. Valiquette, R. Pilliar, Osseointegration of sintered porous-surfaced and plasma spray-coated implants: an animal model study of early postimplantation healing response and mechanical stability, *J. Biomed. Mater. Res.* 47 (1999) 127–138.
- [37] S. Ban, Y. Iwaya, H. Kono, H. Sato, Surface modification of titanium by etching in concentrated sulfuric acid, *Dent. Mater.* 22 (2006) 1115–1120. doi:10.1016/j.dental.2005.09.007.
- [38] W.T. Long, M. Dastane, M.J. Harris, Z. Wan, L.D. Dorr, Failure of the durom metasul® acetabular component, *Clin. Orthop. Relat. Res.* 468 (2010) 400–405. doi:10.1007/s11999-009-1071-8.
- [39] Micropat, Composite image showing the patterned implant, 2018. (n.d.). micropat.ch/application/prototypes-for-the-functional-micropatterning-of-a-titanium-dental-implant/ (accessed July 2, 2018).
- [40] 101 Bios, Titanium Surface Structure after Sandblasting with Aluminum Oxide Grit and Acid Etching, (n.d.). <http://101bios.com/blasting-etching.html> (accessed August 2, 2017).
- [41] Medacta, Titanium plasma spray coating on hip implant stem, (n.d.). www.medacta.com/EN/masterloc (accessed August 2, 2018).
- [42] T. Gong, J. Xie, J. Liao, T. Zhang, S. Lin, Y. Lin, Nanomaterials and bone regeneration, *Bone Res.* 3 (2015). doi:10.1038/boneres.2015.29.
- [43] E.A. Zimmermann, E. Schaible, B. Gludovatz, F.N. Schmidt, C. Riedel, M. Krause, E. Vettorazzi, C. Acevedo, M. Hahn, K. Puschel, S. Tang, M. Amling, R.O. Ritchie, B. Busse, Intrinsic mechanical behavior of femoral cortical bone in young, osteoporotic and bisphosphonate-treated individuals in low-and high energy fracture conditions, *Sci. Rep.* 6 (2016) 1–12. doi:10.1038/srep21072.
- [44] M.M. Stevens, Biomaterials for bone tissue engineering, *Mater. Today.* 11 (2008) 18–25. doi:10.1016/S1369-7021(08)70086-5.
- [45] G. Mendonça, D.B.S. Mendonça, F.J.L. Aragão, L.F. Cooper, Advancing dental implant surface technology - From micron- to nanotopography, *Biomaterials.* 29 (2008) 3822–3835. doi:10.1016/j.biomaterials.2008.05.012.

- [46] M. Kulkarni, A. Mazare, P. Schmuki, A. Iglič, Biomaterial surface modification of titanium and titanium alloys for medical applications, *Nanomedicine*. (2014) 111–136.
- [47] A.W. Tan, L. Tay, Proliferation and stemness preservation of human adipose-derived stem cells by surface-modified in situ TiO₂ nanofibrous surfaces, *Int. J. Nanomedicine*. 9 (2014) 5389–5401. doi:10.2147/IJN.S72659.
- [48] X. Wang, J. Zhu, L. Yin, S. Liu, X. Zhang, Y. Ao, H. Chen, Fabrication of electrospun silica-titania nanofibers with different silica content and evaluation of the morphology and osteoinductive properties, *J. Biomed. Mater. Res. - Part A*. 100 A (2012) 3511–3517. doi:10.1002/jbm.a.34293.
- [49] K. Malec, J. Goralska, M. Hubalewska-Mazgaj, P. Glowacz, M. Jarosz, P. Brzewski, G. Sulka, M. Jaskula, I. Wybranska, Effects of nanoporous anodic titanium oxide on human adipose derived stem cells, *Int. J. Nanomedicine*. Volume 11 (2016) 5349–5360. doi:10.2147/IJN.S116263.
- [50] D. Yu, Y. Song, X. Zhu, R. Yang, A. Han, Morphological evolution of TiO₂ nanotube arrays with lotus-root-shaped nanostructure, *Appl. Surf. Sci.* 276 (2013) 711–716. doi:10.1016/j.apsusc.2013.03.158.
- [51] Y. Wang, C. Wen, P. Hodgson, Y. Li, Biocompatibility of TiO₂ nanotubes with different topographies, *J. Biomed. Mater. Res. - Part A*. 102 (2014) 743–751. doi:10.1002/jbm.a.34738.
- [52] L. Salou, A. Hoornaert, G. Louarn, P. Layrolle, Enhanced osseointegration of titanium implants with nanostructured surfaces: An experimental study in rabbits, *Acta Biomater.* 11 (2015) 494–502. doi:10.1016/j.actbio.2014.10.017.
- [53] M. Kulkarni, A. Flašker, M. Lokar, K. Mrak-Poljšak, A. Mazare, A. Artenjak, S. Čučnik, S. Kralj, A. Velikonja, P. Schmuki, V. Kralj-Iglič, S. Sodin-Semrl, A. Iglič, Binding of plasma proteins to titanium dioxide nanotubes with different diameters, *Int. J. Nanomedicine*. 10 (2015) 1359–1373. doi:10.2147/IJN.S77492.
- [54] L. Lv, Y. Liu, P. Zhang, X. Zhang, J. Liu, T. Chen, P. Su, H. Li, Y. Zhou, The nanoscale geometry of TiO₂ nanotubes influences the osteogenic differentiation of human adipose-derived stem cells by modulating H3K4 trimethylation, *Biomaterials*. 39 (2015) 193–205. doi:10.1016/j.biomaterials.2014.11.002.
- [55] K.C. Popat, M. Eltgroth, T.J. LaTempa, C. a. Grimes, T. a. Desai, Decreased Staphylococcus epidermis adhesion and increased osteoblast functionality on antibiotic-loaded titania nanotubes, *Biomaterials*. 28 (2007) 4880–4888. doi:10.1016/j.biomaterials.2007.07.037.
- [56] S.J. Seunghan Oh, Chiara Daraio, Li-Han Chen, Thomas R. Pisanic, Rita R. Fin˜ones, Significantly accelerated osteoblast cell growth on aligned TiO₂ nanotubes, *J Biomed Mater Res A*. 78 (2006) 97–103. doi:10.1002/jbm.a.

- [57] S.-H. An, R. Narayanan, T. Matsumoto, H.-J. Lee, T.-Y. Kwon, K.-H. Kim, Crystallinity of anodic TiO₂ nanotubes and bioactivity., *J. Nanosci. Nanotechnol.* 11 (2011) 4910–4918. doi:10.1166/jnn.2011.4114.
- [58] R. Ge, W. Fu, H. Yang, Y. Zhang, W. Zhao, Z. Liu, C. Wang, H. Zhu, Q. Yu, G. Zou, Fabrication and characterization of highly-ordered titania nanotubes via electrochemical anodization, *Mater. Lett.* 62 (2008) 2688–2691. doi:10.1016/j.matlet.2008.01.015.
- [59] J. Park, S. Bauer, K.A. Schlegel, F.W. Neukam, K. Der Von Mark, P. Schmuki, TiO₂ nanotube surfaces: 15 nm - an optimal length scale of surface topography for cell adhesion and differentiation, *Small.* 5 (2009) 666–671. doi:10.1002/sml.200801476.
- [60] J. Park, S. Bauer, K. Von Der Mark, P. Schmuki, Nanosize and vitality: TiO₂ nanotube diameter directs cell fate, *Nano Lett.* 7 (2007) 1686–1691. doi:10.1021/nl070678d.
- [61] S. Bauer, J. Park, A. Pittrof, Y.-Y. Song, K. von der Mark, P. Schmuki, Covalent functionalization of TiO₂ nanotube arrays with EGF and BMP-2 for modified behavior towards mesenchymal stem cells., *Integr. Biol. (Camb).* 3 (2011) 927–936. doi:10.1039/c0ib00155d.
- [62] C.J. Frandsen, K.S. Brammer, S. Jin, Variations to the nanotube surface for bone regeneration, *Int. J. Biomater.* 2013 (2013). doi:10.1155/2013/513680.
- [63] K.S. Brammer, S. Oh, J.O. Gallagher, S. Jin, Enhanced cellular mobility guided by TiO₂ nanotube surfaces, *Nano Lett.* 8 (2008) 786–793. doi:10.1021/nl072572o.
- [64] S. Oh, K.S. Brammer, Y.S. Julie, D. Teng, A. Engler, S. Chien, S. Jin, Stem cell fate dictated solely by altered nanotube dimension, *Proceeding Natl. Acad. Sci.* 106 (2009) 2130–2135.
- [65] T.A. Popat, Ketul C.; Daniels, R. Hugh; Dubrow, Robert S.; Hardev, Veeral; Desai, Nanostructured Surfaces for Bone Biotemplating Applications, *Anticancer Res.* (2006) 619–627. doi:10.1002/jor.
- [66] a. W. Tan, B. Pinguan-Murphy, R. Ahmad, S. a. Akbar, Review of titania nanotubes: Fabrication and cellular response, *Ceram. Int.* 38 (2012) 4421–4435. doi:10.1016/j.ceramint.2012.03.002.
- [67] E. Anodization, J. Wang, Z. Lin, Freestanding TiO₂ Nanotube Arrays with Ultrahigh Aspect Ratio, (2008) 1257–1261.
- [68] M. Kulkarni, a Mazare, E. Gongadze, Š. Perutkova, V. Kralj-Iglič, I. Milošev, P. Schmuki, A Iglič, M. Mozetič, Titanium nanostructures for biomedical applications, *Nanotechnology.* 26 (2015) 62002. doi:10.1088/0957-4484/26/6/062002.

- [69] L.M. Bjursten, L. Rasmusson, S. Oh, G.C. Smith, K.S. Brammer, S. Jin, Titanium dioxide nanotubes enhance bone bonding in vivo, *J. Biomed. Mater. Res. - Part A*. 92 (2010) 1218–1224. doi:10.1002/jbm.a.32463.
- [70] N. Wang, H. Li, W. Lu, J. Li, J. Wang, Z. Zhang, Y. Liu, Effects of TiO₂ nanotubes with different diameters on gene expression and osseointegration of implants in minipigs, *Biomaterials*. 32 (2011) 6900–6911. doi:10.1016/j.biomaterials.2011.06.023.
- [71] M. Lai, K. Cai, L. Zhao, X. Chen, Y. Hou, Z. Yang, Surface Functionalization of TiO₂ Nanotubes with Bone Morphogenetic Protein 2 and Its Synergistic Effect on the Differentiation of Mesenchymal Stem Cells, (2011) 1097–1105.
- [72] R. Zhang, H. Wu, J. Ni, C. Zhao, Y. Chen, C. Zheng, X. Zhang, Guided proliferation and bone-forming functionality on highly ordered large diameter TiO₂ nanotube arrays, *Mater. Sci. Eng. C*. 53 (2015). doi:10.1016/j.msec.2015.04.046.
- [73] K.P. Krafts, The hidden drama Tissue repair, *Organogenesis*. 6 (2010) 225–233. doi:10.4161/org6.4.12555.
- [74] D.C. Colter, R. Class, C.M. DiGirolamo, D.J. Prockop, Rapid expansion of recycling stem cells in cultures of plastic-adherent cells from human bone marrow, *Proc. Natl. Acad. Sci.* 97 (2000) 3213–3218. doi:10.1073/pnas.97.7.3213.
- [75] B. Lindroos, R. Suuronen, S. Miettinen, The Potential of Adipose Stem Cells in Regenerative Medicine, *Stem Cell Rev. Reports*. 7 (2011) 269–291. doi:10.1007/s12015-010-9193-7.
- [76] P. Zuk, Adipose-Derived Stem Cells in Tissue Regeneration: A Review, *Int. Sch. Res. Not.* 2013 (2013) e713959. doi:10.1155/2013/713959.
- [77] A.S. Zanetti, C. Sabliov, J.M. Gimble, D.J. Hayes, Human adipose-derived stem cells and three-dimensional scaffold constructs: A review of the biomaterials and models currently used for bone regeneration, *J. Biomed. Mater. Res. - Part B Appl. Biomater.* 101 B (2013) 187–199. doi:10.1002/jbm.b.32817.
- [78] W. Tsuji, Adipose-derived stem cells: Implications in tissue regeneration, *World J. Stem Cells*. 6 (2014) 312. doi:10.4252/wjsc.v6.i3.312.
- [79] B.A. Bunnell, M. Flaat, C. Gagliardi, B. Patel, C. Ripoll, Adipose-derived stem cells: Isolation, expansion and differentiation, *Methods*. 45 (2008) 115–120. doi:10.1016/j.ymeth.2008.03.006.
- [80] Y.C. Halvorsen, D. Franklin, A.L. Bond, D.C. Hitt, C. Auchter, A.L. Boskey, D. Ph, E.P. Paschalis, Extracellular Matrix Mineralization and Osteoblast, *Tissue Eng.* 7 (2001) 729–41.
- [81] E. Bolletta, E. Petrucci, C. Tartaglione, D. Bordoni, Adipose-Derived Stem Cells

(ADSCs): Current Findings and Future Perspectives in Structural Facial Fat Grafting, in: M.A. Shiffman, A. Di Giuseppe, F. Bassetto (Eds.), *Stem Cells Aesthetic Proced. Art, Sci. Clin. Tech.*, Springer Berlin Heidelberg, Berlin, Heidelberg, 2014: pp. 383–414. doi:10.1007/978-3-642-45207-9_26.

- [82] R.H. Yasir Alabdulkarim, Bayan Ghalimah, Mohammad Al-Otaibi¹, Hadil F Al-Jallad, Mina Mekhael, Bettina Willie⁵, Recent advances in bone regeneration: The role of adipose tissue-derived stromal vascular fraction and mesenchymal stem cells, *J. Limb Lengthening Reconstr.* 3 (2017) 4–18.
- [83] D.L.C. Barbara D Boyan, ChristophH Lohmann, David D Dean, VictorLSylvia, and Z. Schwartz, Mechanisms Involved in Osteoblast Response to Implant Surface Morphology, *Annu. Rev. Mater. Res.* 31 (2001) 357–371.
- [84] H.-I. Chang, Y. Wang, *Cell Responses to Surface and Architecture of Tissue Engineering Scaffolds*, 2011. doi:10.5772/21983.

CHAPTER 2

FABRICATION AND CHARACTERIZATION OF TITANIA NANOTUBE SURFACES

Titania nanostructured surfaces were first discovered in the late 1990s. There are the three main methods to synthesize various nanostructured forms of titania; template-assisted, electrochemical, and hydrothermal [1]. Electrochemical anodization is a cost-effective and simple method to prepare titania nanotubes (NT). The anodization is performed in a two electrode system with a titanium anode and a platinum cathode immersed in a fluoride-ion containing electrolyte solution. The NT are formed by selective etching, followed by a chemical dissolution that results in the nucleation of nanopores on the surface [1]. Continuing the anodization process leads to a steady-state growth on the metal surface resulting in tubular geometries [1]. Over the last two decades, this synthesis process has improved through the discovery that altering the pH value of the electrolyte can improve the tube layer thickness and that a neutral pH value produces longer tubes [2]. Additionally, it was demonstrated that non-aqueous electrolytes produce smooth tubes with uniform ordering of the nanotubes [2]. Today there are many different electrolyte compositions being used to fabricate titania nanotubes and each result in a unique nanotube structure and ordering. Changing other parameters such as time, temperature, and voltage during anodization also alter nanotube size and structure.

This chapter addresses specific aim 1. In this chapter titania nanotubes (NT) were prepared on titanium surfaces by anodization using an organic electrolyte solution. The NT surfaces were made at three different diameters by altering the voltage and duration of the anodization process. Since these NT surfaces are being explored as a biomaterial

it is important to define their surface characteristics and therefore analyze their potential to support cellular activity. Cells interaction with a surface is driven by the proteins adhered on the surface [3,4]. There are several material factors that can affect how proteins adhere and interact with a biomaterial surface including, but not limited to, surface chemistry, surface wettability, surface roughness, crystallinity and size of the topography. Thus it is important to evaluate these material characteristics of the NT surface in order to determine the potential of NT as an implant surface before proceeding to *in vitro* cell studies. In this chapter, tube size, surface wettability, crystalline structure, and surface chemistry are evaluated and discussed for all three NT surfaces.

2.1 Methods and Materials

2.1.1 Fabrication of Nanotube Surfaces

Titania nanotubes (NT) surfaces were fabricated using electrochemical anodization. Titanium foil surfaces, 0.635 mm thick (CP Grade 1 Titanium), were cleaned with acetone, soap, and isopropanol before anodization. An electrochemical cell was developed with the titanium surfaces acting as the anode, and platinum foil acting as the cathode. The electrolyte solution was prepared by mixing diethylene glycol (DEG, 99% v/v) with 2% hydrofluoric acid (HF, 48% v/v) and 3% de-ionized water (**Figure 2.1**). NT with 65 nm diameter were obtained by anodizing at 30 V for 46 hours, 100 nm diameters at 45 V for 24 hours, and 160 nm diameters at 60 V for 24 hours. When anodization time was finished, the NT surfaces were rinsed with isopropanol, followed by DI water and

then dried with nitrogen gas. The surfaces were then annealed at 530°C for 3 hours. NT surfaces are denoted NT30, NT45, and NT60 and the titanium control surface is denoted Ti.

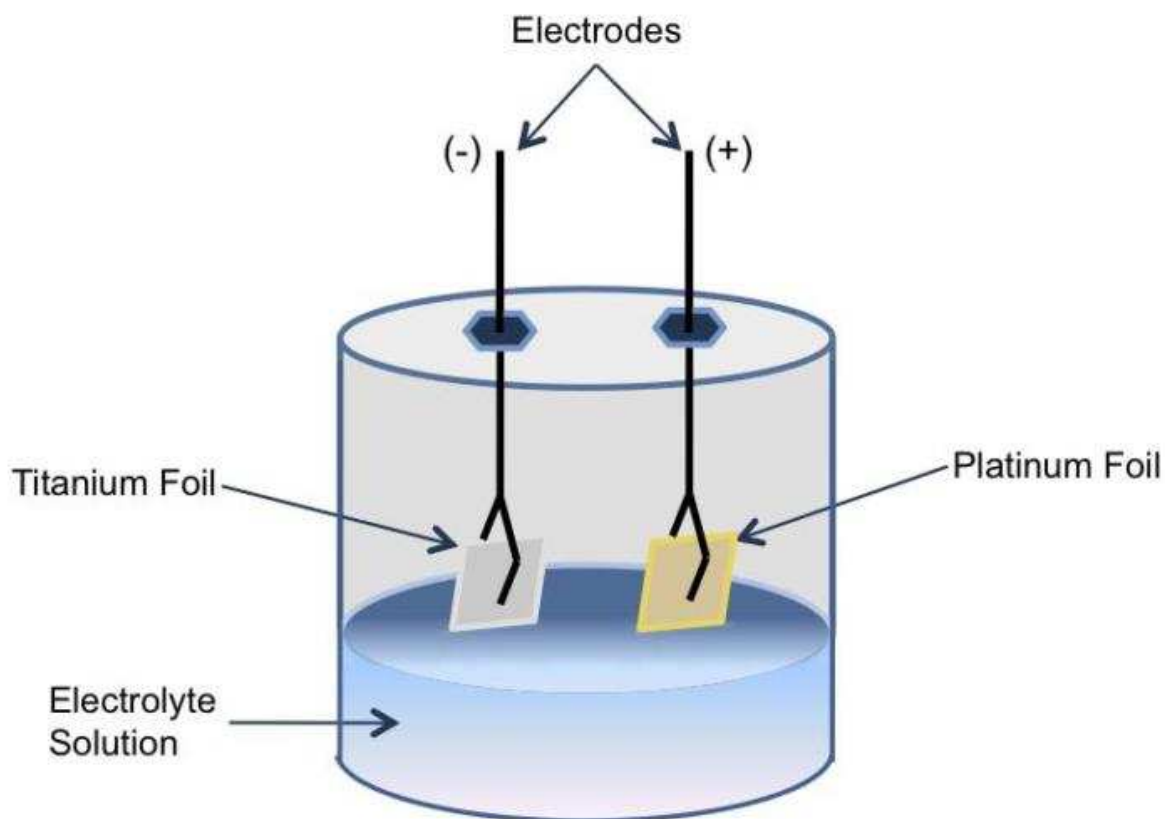


Figure 2.1 Schematic of anodization setup for fabrication of titania nanotube surfaces (Reprinted from [5], Copyright (2012) Smith, B.).

2.1.2 Characterization of Nanotube Surfaces

In order to characterize nanotube morphology, scanning electron microscopy (SEM, JEOL JSM-6500F) was employed at an accelerating voltage of 15kV. Images were taken at 2,500, 10,000, and 50,000 magnification on two different locations on each sample.

Material surface wettability was evaluated by using a water-drop method on a contact angle goniometer (ramé-hart 250). A predetermined volume of water was dropped onto the NT surfaces and images of the water droplet were immediately captured. The images were analyzed to determine the contact angles using DROPimage software.

Chemical composition on the NT and Ti surfaces was characterized by X-ray photoelectron spectroscopy (XPS, ESCA Systems X-ray Photoelectron Spectrometer 5800). XPS is a surface sensitive technique that detects trace levels of elements present on the surface. Ten minute survey spectra were collected from 0 to 1100eV with a pass energy of 187.85 eV using the binding energy of carbon (C1s: 284.8 eV) as the reference. Data for percent elemental composition, elemental ratios and peak fit analysis were calculated using Multipack software.

In order to determine the crystalline phases present on the NT surfaces, glancing angle X-ray diffraction (GAXRD) was performed with a Bruker D-8 Discover X-ray diffraction system with a Cu X-ray source and line focus optics on NT and Ti surfaces. A scintillation detector and soller slits ($\sim 0.4^\circ$ separation) were used on the diffracted beam side to record the XRD spectra. GAXRD measurements were performed with a fixed angle of incidence of 1.50° to maximize the signal from the films and a detector scan was carried out to record the diffracted X-ray intensity as a function of 2θ .

2.1.3 Statistical analysis

All studies were performed with $n_{\min} = 3$ for qualitative analyses and $n_{\min} = 5$ for quantitative analyses. The statistical differences were compared using one-way ANOVA analysis ($p < 0.05$) with a post-hoc Tukey's HSD (honest significant difference) test.

Minitab software was used to conduct the statistical analysis. All data is shown as the average \pm standard errors.

2.2 Results and Discussion

Different nanotube surfaces were fabricated using anodization at 30 V (NT30), 45 V (NT45), and 60 V (NT60). Scanning electron microscopy (SEM, JEOL JSM-6500F) was used at an accelerating voltage of 15kV to characterize NT morphology, inner diameter, and NT length (**Figure 2.2**). The titanium control (Ti) surface exhibited a smooth surface with visible grain boundaries and no unique features. The NT surfaces were uniform with NT attached at the base and formed perpendicular to the surface with occasional broken NT observed on the surfaces.

SEM images also confirmed that as the anodization voltage increased, the diameter of the NT increased resulting in average diameters of 65 ± 15 nm for 30 V, 95 ± 25 nm for 45 V, and 160 ± 30 nm for 60V (**Figure 2.3**). SEM images of NT cross-sectional lengths were obtained by fracturing the NT surfaces before imaging. The cross sectional tube lengths were 0.7 ± 0.1 μm for 30 V, 2.1 ± 0.2 μm for 45 V, and 3.3 ± 0.8 μm for 60 V. The inner diameter and tube length were assessed using ImageJ software with SEM images. Voltage, time, composition of electrolyte solution, and temperature of the electrolyte solution during anodization all influence NT formation [6,7]. Studies have shown that NT diameter and length have an almost linear relationship to the applied voltage, thus diameter and length increase as the voltage increases [2,8].

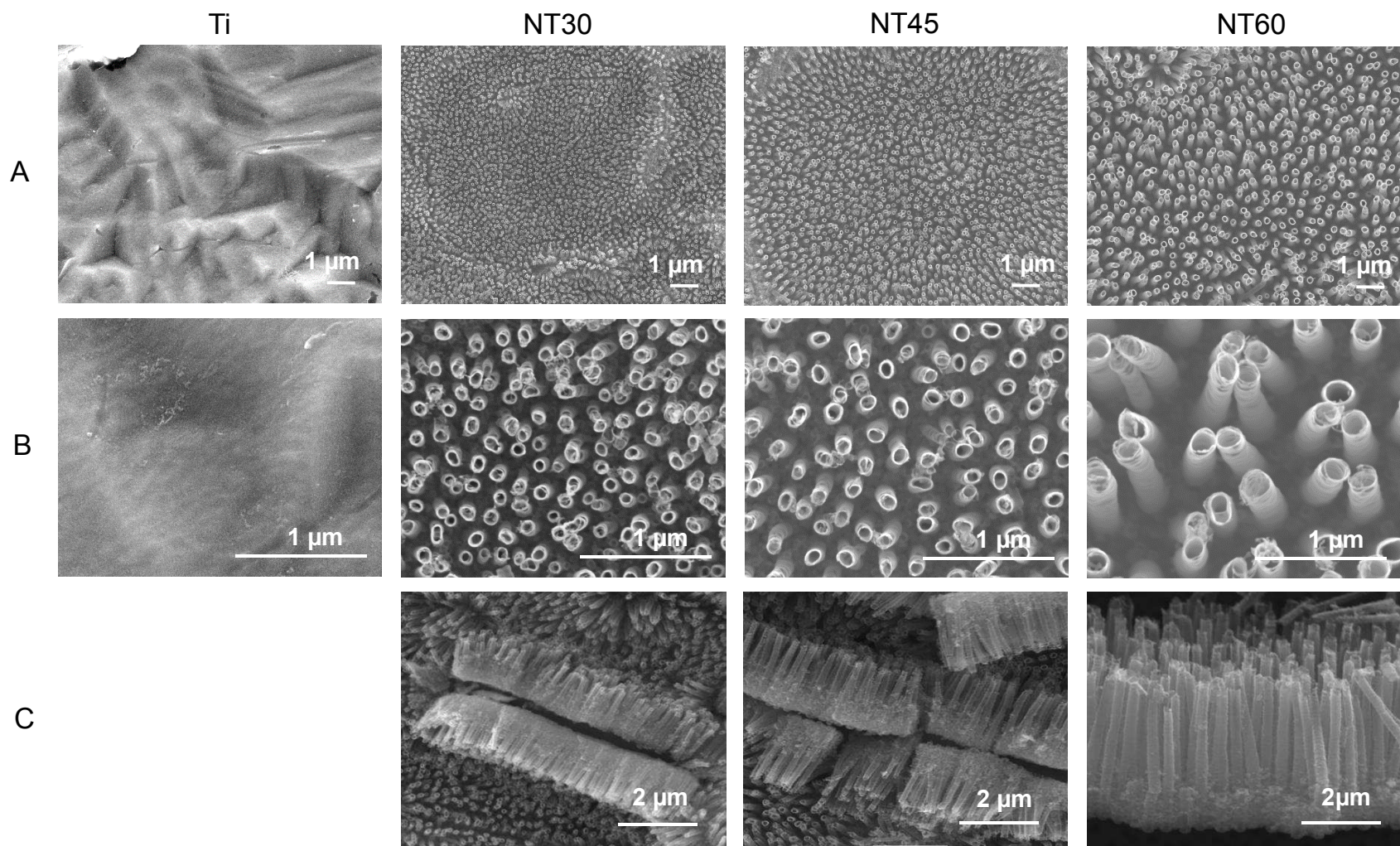


Figure 2.2 SEM images of Titanium (Ti) and nanotubes made at 30 V (NT30), 45 V (NT45), and 60 V (NT60) at (A) 10,000 and (B) 50,000 magnification. (C) SEM images to look at the cross sectional length of NT30, NT45, and NT60 at 2,500 magnification.

In this study, the tube length displayed a nearly linear relationship with the anodization voltage, while, inner diameter was not linear, but still increased as voltage increased (Figure 2.3).

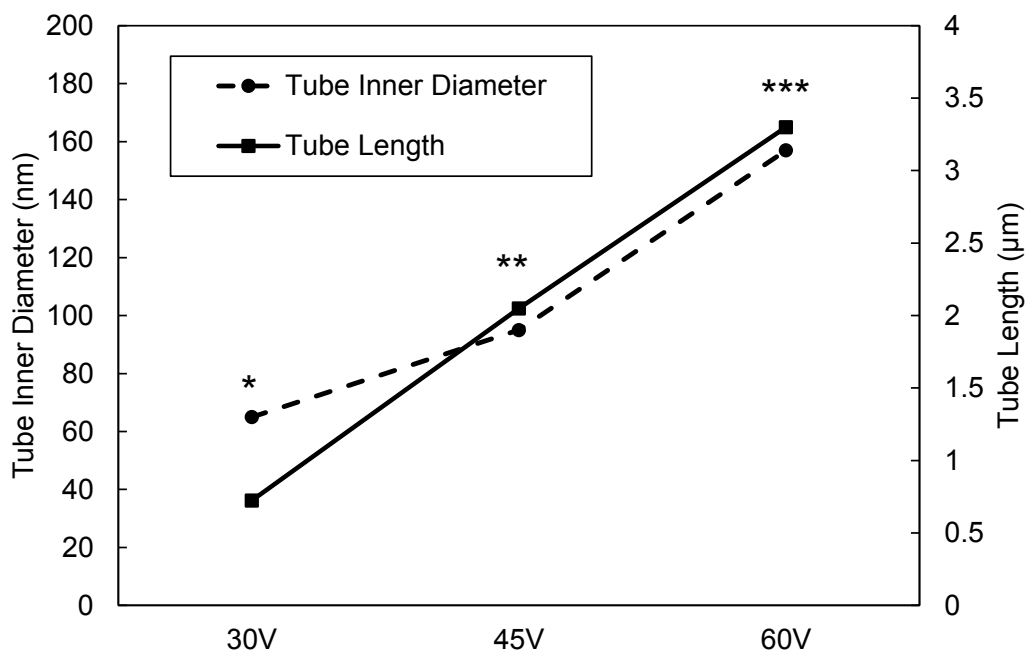


Figure 2.3 Average inner diameter and cross sectional length of nanotubes made at 30 V (NT30), 45 V (NT45), and 60 V (NT60). All NT inner diameter and tube length are significantly different. (*Tukey's HSD $p < 0.05$) Full statistical analysis found in Appendix I.

Wettability plays an important role in cell-surface interaction as the wetting characteristic affects the protein adsorption and the proteins direct cell adhesion and proliferation [9,10]. A wettable surface is termed hydrophilic and a non-wettable surface hydrophobic. A surface with a contact angle lower than 90° is considered hydrophilic and a contact angle higher than 90° is considered hydrophobic. Earlier studies have shown that hydrophilic surfaces not only enhance cell adhesion and proliferation [3] but improve the initial blood contact, accelerating implant osseointegration [11]. In this study wettability was evaluated by determining the water contact angle for the Ti and NT surfaces. The

results indicate that the Ti surface was hydrophilic at 57°, however, the NT surfaces displayed improved hydrophilic properties with contact angles <10° (**Figure 2.4**).

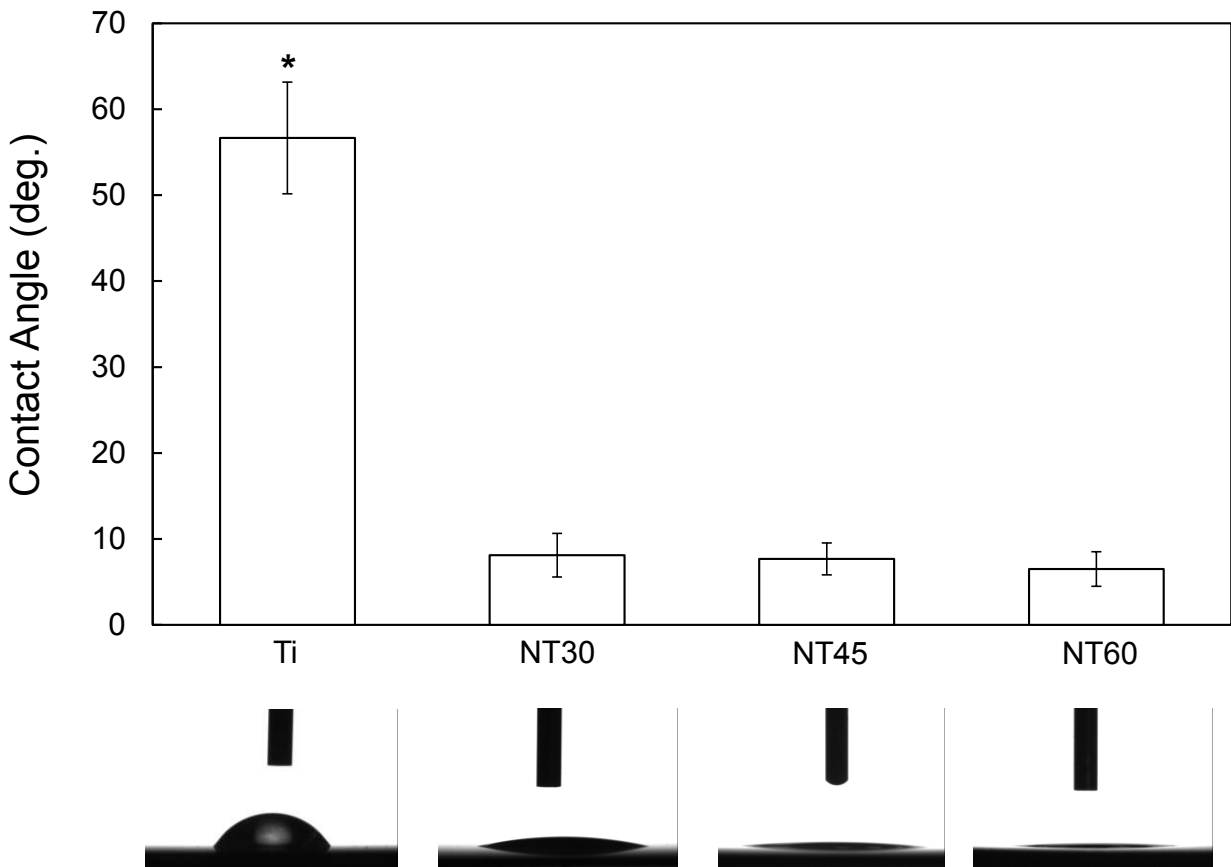


Figure 2.4 Water contact angle on Ti and NT surfaces with representative images. Ti control surface is significantly different from NT30, NT45, and NT60 indicating that nanotubes are more hydrophilic than Titanium. (*Tukey's HSD $p < 0.05$) Full statistical analysis found in Appendix I.

The crystallinity of a surface is also important as cells respond differently to different crystal structures. Nanotubes are primarily titanium dioxide (TiO_2) also known as titania. Titania can exist as an amorphous layer or in crystalline phases: anatase (tetragonal), rutile (tetragonal) and brookite (orthorhombic). Only rutile phase is thermodynamically stable at high temperatures. Titania nanotubes are amorphous right after the anodization process however annealing the samples at a high temperature causes the titania to crystallize. The temperatures at which anatase and rutile crystalline

structure appear vary based on the anodization parameters and chemicals present on the NT surface [2]. Typically, titania nanotubes annealed above 250°C will exhibit an anatase crystalline structure. At temperatures near or above 430°C-500 °C a rutile crystalline structure is present along with the anatase [12]. Above 680°C degrees the crystalline structure becomes completely rutile [13,14]. The crystallinity of the Ti and NT surfaces was determined using glancing angle X-ray diffraction (GAXRD). All the NT surfaces exhibited anatase (◆) and rutile (●) phases (**Figure 2.5**). NT60 exhibited a higher anatase phase and smaller rutile phase than the NT30 and NT45 (at 25° and 27°) indicating that the content of anatase phase decreases and the content of rutile increases with decreasing anodization voltage. Decreases in the anatase peak as voltage decreased can also be seen at 38° and 48° for all NT surfaces. Other studies have reported similar findings [15,16]. Studies have shown that cells performed better on annealed NT (crystalline) over non-annealed (amorphous) NT surfaces [17,18] and that osteoblasts preferred anatase coated titanium surfaces over rutile and amorphous surfaces [19]. Since all NT surfaces in this study exhibit high anatase content, the surfaces should be ideal for cell growth.

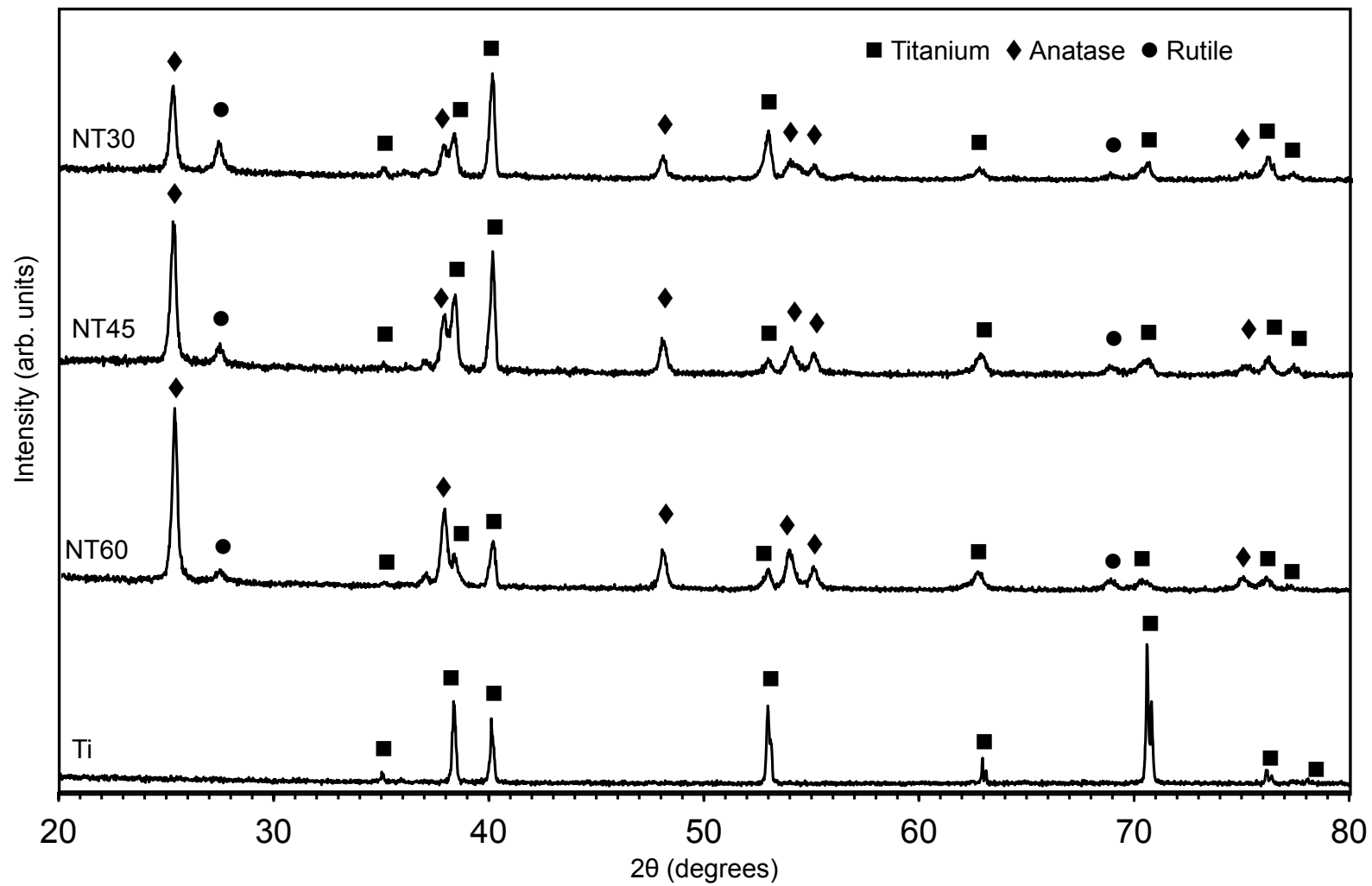


Figure 2.5 Glancing angle X-ray diffraction (GAXRD) of Ti and NT surfaces after annealing indicating anatase and rutile crystalline phases.

Many studies have shown that cells respond to chemicals found on an implant surface, thus X-ray photoelectron spectroscopy (XPS) was performed to determine the chemical composition on Ti and NT surfaces before cell culture was performed. From the survey scans it is clear that all surfaces contained carbon, titanium, and oxygen (**Figure 2.6**). Since nanotubes are compositionally TiO_2 , the titanium and oxygen content is expected (**Figure 2.7**). The high content of carbon was not expected and is probably a combination of environmental contamination and a carbon rich layer that forms on the outer part of the NT when using an organic electrolyte during anodization [20]. Carbon content on NT surfaces has been reported in several other NT studies as well [14,21,22]. All the NT surfaces exhibit fluoride on the surfaces due to the hydrofluoric (HF) acid used in the anodization process. At high concentrations, fluoride can be toxic to cells, but at low concentrations, fluoride has been shown to influence proliferation and migration of some cell types [23–27].

	O %	C %	Ti %	F %
Ti	52.7	35.2	12.1	0.0
NT30	53.9	32.3	11.2	2.6
NT45	56.3	21.4	20.3	2.0
NT60	46.0	37.4	15.7	0.9

Figure 2.6 Chemical Compositions (Oxygen, Carbon, Titanium and Fluoride) of Ti and nanotube (NT) surfaces measured by XPS.

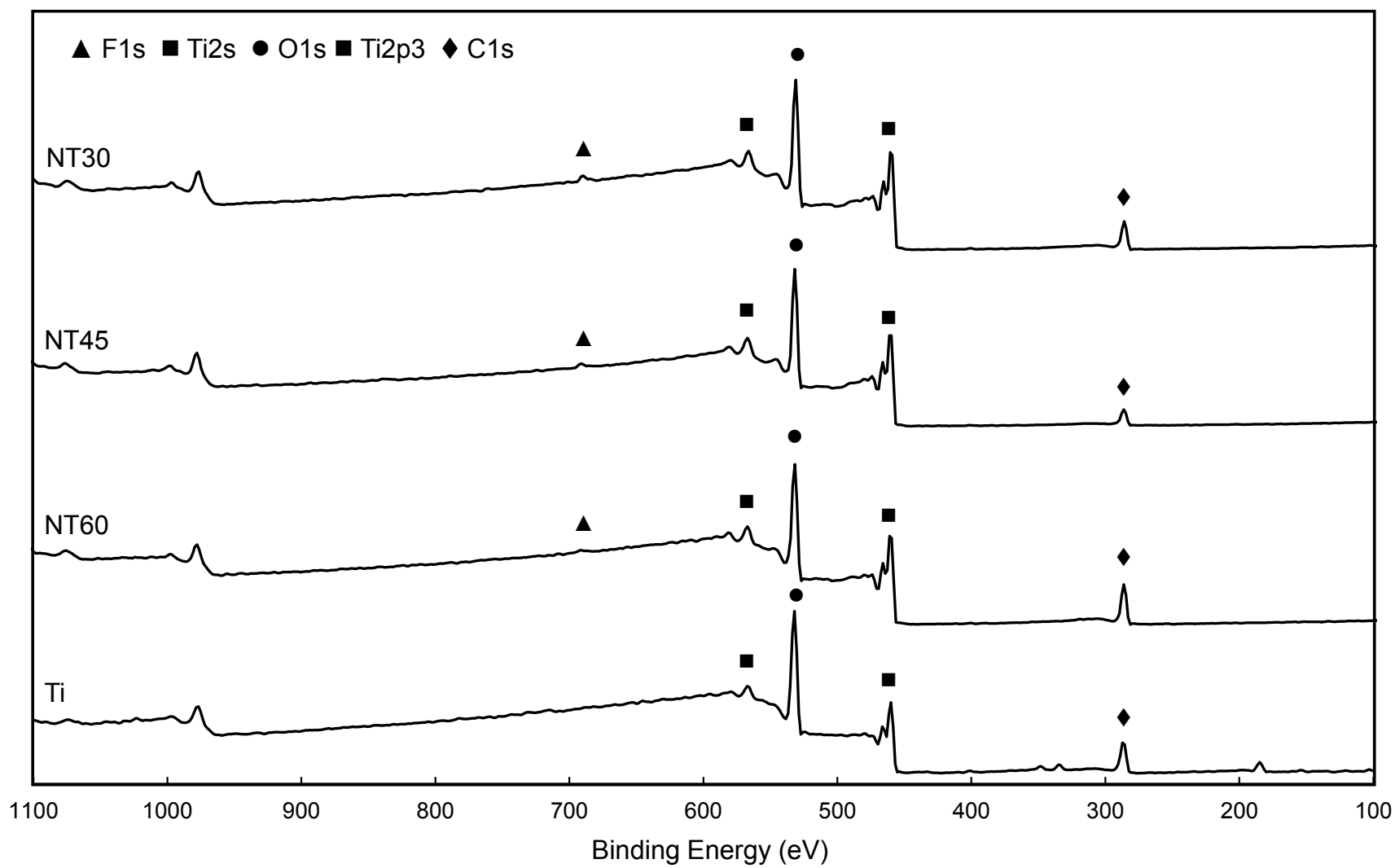


Figure 2.7 X-ray photoelectron spectroscopy (XPS) survey scans of Ti, NT30, NT45, and NT60 indicating chemicals present on the surface.

2.3 Conclusions

Titania nanotubes (NT) with three different diameters were fabricated and inner diameter and length of NT were characterized via scanning electron microscopy (SEM). Wettability of all NT surfaces is strong and exhibited higher hydrophilicity than Ti control. Glancing angle X-ray diffraction (GAXRD) revealed all NT surfaces in this study exhibit high anatase content after annealing with some rutile content. X-ray photoelectron spectroscopy (XPS) indicated small percentages of fluoride present on all three NT surfaces. In conclusion, all of these surface characterization tests suggest that all three NT surfaces should be ideal for *in vitro* cell studies and have the potential to promote cell adhesion, proliferation, and differentiation.

REFERENCES

- [1] V.B. Damodaran, D. Bhatnagar, V. Leszczak, K.C. Popat, Titania nanostructures: a biomedical perspective, *RSC Adv.* 5 (2015) 37149–37171. doi:10.1039/C5RA04271B.
- [2] P. Roy, S. Berger, P. Schmuki, TiO₂ nanotubes: Synthesis and applications, *Angew. Chemie - Int. Ed.* 50 (2011) 2904–2939. doi:10.1002/anie.201001374.
- [3] H.-I. Chang, Y. Wang, Cell Responses to Surface and Architecture of Tissue Engineering Scaffolds, 2011. doi:10.5772/21983.
- [4] K.S. Brammer, C.J. Frandsen, S. Jin, TiO₂ nanotubes for bone regeneration, *Trends Biotechnol.* 30 (2012) 315–322. doi:10.1016/j.tibtech.2012.02.005.
- [5] B.S. Smith, M. Gonzalez-juarrero, S. Dow, Dissertation: Titania Nanotube Arrays: Interfaces for Implantable Devices, (2012).
- [6] J.M. Macak, H. Tsuchiya, a. Ghicov, K. Yasuda, R. Hahn, S. Bauer, P. Schmuki, TiO₂ nanotubes: Self-organized electrochemical formation, properties and applications, *Curr. Opin. Solid State Mater. Sci.* 11 (2007) 3–18. doi:10.1016/j.cossms.2007.08.004.
- [7] Y. Wang, D. -I. Yu, B. Chong, D. -d. Li, Y. Song, S. -y. Zhang, W. -h. Ma, X. -f. Zhu, Simulation and Separation of Anodizing Current-Time Curves, Morphology Evolution of TiO₂ Nanotubes Anodized at Various Temperatures, *J. Electrochem. Soc.* 161 (2014) H891–H895. doi:10.1149/2.0411414jes.
- [8] A. Hamlekhan, A. Butt, S. Patel, D. Royhman, C. Takoudis, C. Sukotjo, J. Yuan, G. Jursich, M.T. Mathew, W. Hendrickson, A. Viridi, T. Shokuhfar, Fabrication of anti-aging TiO₂ nanotubes on biomedical Ti alloys, *PLoS One.* 9 (2014). doi:10.1371/journal.pone.0096213.
- [9] Roberto Cingolani, ed., *Bioinspired Approaches for Human-Centric Technologies*, illustrate, Springer, 2014.
- [10] Y. Yang, R. Cavin, J.L. Ong, Protein adsorption on titanium surfaces and their effect on osteoblast attachment, *J. Biomed. Mater. Res.* 67A (2003) 344–349. doi:10.1002/jbm.a.10578.
- [11] F. Rupp, L. Liang, J. Geis-Gerstorfer, L. Scheideler, F. Hüttig, Surface characteristics of dental implants: A review, *Dent. Mater.* (2017) 1–18. doi:10.1016/j.dental.2017.09.007.

- [12] Y. Wang, C. Wen, P. Hodgson, Y. Li, Biocompatibility of TiO₂ nanotubes with different topographies, *J. Biomed. Mater. Res. - Part A.* 102 (2014) 743–751. doi:10.1002/jbm.a.34738.
- [13] R. Ge, W. Fu, H. Yang, Y. Zhang, W. Zhao, Z. Liu, C. Wang, H. Zhu, Q. Yu, G. Zou, Fabrication and characterization of highly-ordered titania nanotubes via electrochemical anodization, *Mater. Lett.* 62 (2008) 2688–2691. doi:10.1016/j.matlet.2008.01.015.
- [14] G.K. Mor, O.K. Varghese, M. Paulose, K. Shankar, C. a. Grimes, A review on highly ordered, vertically oriented TiO₂ nanotube arrays: Fabrication, material properties, and solar energy applications, *Sol. Energy Mater. Sol. Cells.* 90 (2006) 2011–2075. doi:10.1016/j.solmat.2006.04.007.
- [15] P. Kar, Effect of anodization voltage on the formation of phase pure anatase nanotubes with doped carbon, *Inorg. Mater.* 46 (2010) 377–382. doi:10.1134/S0020168510040102.
- [16] Z. Su, L. Zhang, F. Jiang, M. Hong, Formation of crystalline TiO₂ by anodic oxidation of titanium, *Prog. Nat. Sci. Mater. Int.* 23 (2013) 294–301. doi:10.1016/j.pnsc.2013.04.004.
- [17] A. Mazare, M. Dilea, D. Ionita, I. Titorencu, V. Trusca, E. Vasile, Changing bioperformance of TiO₂ amorphous nanotubes as an effect of inducing crystallinity, *Bioelectrochemistry.* 87 (2012) 124–131. doi:10.1016/j.bioelechem.2012.01.002.
- [18] K.S. Brammer, S. Oh, C.J. Cobb, L.M. Bjursten, H. Van Der Heyde, S. Jin, Improved bone-forming functionality on diameter-controlled TiO₂ nanotube surface, *Acta Biomater.* 5 (2009) 3215–3223. doi:10.1016/j.actbio.2009.05.008.
- [19] J. He, W. Zhou, X. Zhou, X. Zhong, X. Zhang, P. Wan, B. Zhu, W. Chen, The anatase phase of nanotopography titania plays an important role on osteoblast cell morphology and proliferation, *J. Mater. Sci. Mater. Med.* 19 (2008) 3465–3472. doi:10.1007/s10856-008-3505-3.
- [20] S.P. Albu, P. Schmuki, TiO₂ nanotubes grown in different organic electrolytes: Two-size self-organization, single vs. double-walled tubes, and giant diameters, *Phys. Status Solidi - Rapid Res. Lett.* 4 (2010) 215–217. doi:10.1002/pssr.201004244.
- [21] M. Lai, K. Cai, L. Zhao, X. Chen, Y. Hou, Z. Yang, Surface Functionalization of TiO₂ Nanotubes with Bone Morphogenetic Protein 2 and Its Synergistic Effect on the Differentiation of Mesenchymal Stem Cells, (2011) 1097–1105.
- [22] S.P. Albu, D. Kim, P. Schmuki, Growth of aligned TiO₂ bamboo-type nanotubes and highly ordered nanolace, *Angew. Chemie - Int. Ed.* 47 (2008) 1916–1919. doi:10.1002/anie.200704144.
- [23] O. Barbier, L. Arreola-Mendoza, L.M. Del Razo, Molecular mechanisms of fluoride

- toxicity, *Chem. Biol. Interact.* 188 (2010) 319–333. doi:10.1016/j.cbi.2010.07.011.
- [24] M.A. Khokher, P. Dandona, Fluoride stimulates [3H]thymidine incorporation and alkaline phosphatase production by human osteoblasts, *Metabolism.* 39 (1990) 1118–1121. doi:10.1016/0026-0495(90)90081-M.
- [25] W.J. Qu, D.B. Zhong, P.F. Wu, J.F. Wang, B. Han, Sodium fluoride modulates caprine osteoblast proliferation and differentiation, *J. Bone Miner. Metab.* 26 (2008) 328–334. doi:10.1007/s00774-007-0832-2.
- [26] H.Y. Liu, X.J. Wang, L.P. Wang, F.Y. Lei, X.F. Wang, H.J. Ai, Effect of fluoride-ion implantation on the biocompatibility of titanium for dental applications, *Appl. Surf. Sci.* 254 (2008) 6305–6312. doi:10.1016/j.apsusc.2008.03.075.
- [27] J.E. Ellingsen, Pre-treatment of titanium implants with fluoride improves their retention in bone, *J. Mater. Sci. Mater. Med.* 6 (1995) 749–753. doi:10.1007/BF00134312.

CHAPTER 3

EVALUATION OF THE EFFECT OF TITANIA NANOTUBES ON ADHESION AND PROLIFERATION OF ADIPOSE-DERIVED STEM CELLS

The success of any clinical implant is dependent on the interaction of cells with the implant surface. A successful orthopedic implant will promote cell adhesion and proliferation in order to stimulate osseointegration of the implant with the surrounding bone tissue. When a surface is initially exposed to *in vitro* culture conditions, proteins in the cell culture media adsorb to the material's surface and mediate cell adhesion through signals to the cells through the cell's adhesion receptors (integrins) and protein functional groups (ligands) [1,2]. Cells then adhere on the surfaces and release active compounds for signaling, perform extra-cellular matrix deposition, proliferate and differentiate [1]. So one of the first steps in determining the potential of a new implant is to study the adhesion and proliferation of cells on the surface *in vitro*, specifically stem cells. When a biomaterial is implanted, the body reacts similar to an injury and stem cells are recruited to the implant site. Since, stem cells play an important role in tissue repair in the body, it is essential to understand their interaction with the implant surface. Adipose-derived stem cells (ADSC) are mesenchymal stem cells obtained from adipose tissue that are easily accessible, available in large numbers, and attach and proliferate rapidly in culture, making them an attractive source for studies that aim to evaluate stem cell interaction with implant surfaces [3,4]. Additionally, studies have demonstrated that ADSC possess an *in vitro* bone formation capacity similar to that of bone marrow-derived mesenchymal stem cells [5,6].

This chapter addresses specific aim 2. In this chapter the culturing of adipose-derived stem cells (ADSC) for one week on titanium (Ti) and nanotube (NT) surfaces is evaluated and discussed. Not only does surface topography affect cell proliferation, but cell density does as well, thus, ADSC were cultured at three different cell densities to determine the optimal cell density for further studies. Adhesion and proliferation are investigated using a viability assay, fluorescent staining, and scanning electron microscope to visualize cell morphology.

3.1 Methods and Materials

3.1.1 Adipose-Derived Stem Cell (ADSC) Culture

ADSC were isolated from abdominal and femoral subcutaneous adipose tissue biopsy surfaces as described previously [7]. When ready for culturing the ADSC were thawed and expanded using standard cell culture techniques. All ADSC used in this study were below passage five. Following expansion, ADSC were detached using 0.25% Trypsin and suspended in growth media (MEM Alpha Modification, HyClone™) with 10% fetal bovine serum and 1% penicillin/streptomycin added. NT and Ti surfaces were sterilized by incubation in 70% ethanol at room temperature for 10 minutes and then rinsed twice with warm phosphate buffered saline (PBS). Following sterilization, the surfaces were exposed to UV light for 30 mins.

3.1.2 ADSC Adhesion and Proliferation

ADSC were cultured on NT and Ti surfaces in 48-well plates at 500 μ l per well with three different cell densities: 2,500, 3,750, and 5,000 cells/well. The surfaces were

incubated at 37 °C and 5% CO₂ for the entire duration of the study. Media changes were done on day 2 and 5 with prepared growth media. Fluorescent staining and proliferation assays were done after 1, 4, and 7 days.

A measurement of cell viability is important in evaluating the capacity for a scaffold to support initial cell proliferation. Viability of ADSC was assessed using alamarBlue® (ThermoFisher Scientific) cell viability assay after 1, 4, and 7 days of proliferation. Surfaces were moved to a new well plate on day one to mitigate the effect from ADSC adhered in the well plate. 300 µl fresh media was added to surfaces along with 30 µl of alamarBlue®. Well plates were covered with foil and incubated for 4 hours. After incubation, 100 µl was removed from each well and placed in a 96 well plate. Absorbance was read at 570 nm and 600 nm. A control well with media plus alamarBlue® was used to determine the percent reduction of alamarBlue® for each surface.

Fluorescent staining was used to characterize cell adhesion. Media was removed and the NT and Ti surfaces were washed twice with warm PBS and then moved to a new well plate. ADSC were stained with 5-chloromethylfluorescein diacetate (CellTracker green CMFDA, Invitrogen) live stain. The surfaces were incubated with 10 µM CMFDA in PBS for 30 min at 37 °C and 5% CO₂. CMFDA was removed and ADSC were rinsed three times in PBS and incubated for another 30 min at 37 °C and 5% CO₂. The surfaces were fixed in 3.7 wt % formaldehyde in PBS for 15 min at room temperature, followed by three washes (5 min per wash) with PBS. Adhered ADSC were permeabilized by incubation in 1% Triton-X in PBS for 3 min and rinsed with PBS. After transferring surfaces to a new well plate, ADSC were incubated in 70nM of Rhodamine Phalloidin (Cytoskeleton) in PBS at room temperature for 25 minutes. DAPI (ThermoFisher Scientific) nuclear stain (300

nM) was added for 5 min at room temperature and surfaces were rinsed twice with PBS and imaged with a fluorescence microscope (Zeiss). ADSC cell count was determined by counting the number of DAPI stained nuclei from the fluorescence images at 10x magnification.

In order to examine cell morphology and cell–substrate interaction, the ADSC were fixed and dehydrated after 1, 4 and 7 days proliferation in growth media. Surfaces were removed from media and placed in the primary fixative of 3% glutaraldehyde (Ted Pella, Inc.), 0.1 M of sodium cacodylate (ACROS Organics), and 0.1 M sucrose (Fisher) for 45 minutes. Surfaces were then moved to the buffer solution containing 0.1M sodium cacodylate and 0.1 M sucrose. The ADSC were then dehydrated by replacing the buffer with increasing concentrations of ethanol (35%, 50%, 70%, and 100%) for 10 minutes each. The ADSC were then dried by hexamethyldisilazane (HMDS, Aldrich) for 10 min. After HMDS was removed, the surfaces were air dried for 30 minutes and then placed in a desiccator. The surfaces were sputter coated with 10nm of gold before imaging using a Scanning Electron Microscope (JEOL JSM-6500F) at an accelerating voltage of 10 kV.

3.1.3 Statistical analysis

All studies were performed with $n_{\min} = 3$ for qualitative analyses and $n_{\min} = 5$ for quantitative analyses. The statistical differences were compared using one-way ANOVA analysis ($p < 0.05$) with a post-hoc Tukey's HSD (honest significant difference) test. Minitab software was used to conduct the statistical analysis. All data is shown as the average \pm standard errors.

3.2 Results and Discussion

Since titanium implants still experience loosening and eventual failure [8–11], implants with nanostructured surfaces could help improve their fixation to the surrounding bone tissues [1,12–15]. By more fully understanding the effect of nanostructure size on adhesion and proliferation of stem cells, implants could be specifically designed to achieve the optimal stem cell response from the tissue in which they are implanted. In this chapter, the effect of nanotube (NT) size and cell density on the adhesion and proliferation of human adipose-derived stem cells (ADSC) was evaluated.

The size of the surface topography can influence cell behavior, thus, titania nanotube surfaces were fabricated at three different sizing using anodization at 30 V (NT30) 45 V (NT45) and 60 V (NT60) as described in Chapter 2. Not only does surface topography affect cell proliferation, but cell density does as well, thus, ADSC were cultured on Ti and NT surfaces for 7 days at three different cell densities: 2,500, 3,750, and 5,000 cells/well. It is important to evaluate the ability of a surface to support initial cell proliferation by measuring the cell viability. AlamarBlue®, a commercially available assay, was used to investigate cell viability. AlamarBlue® is a proven cell viability indicator that uses the natural reducing power of living cells to convert a cell permeable compound (resazurin) to a fluorescent molecule (resorufin). The amount of absorbance is proportional to the number of living cells and corresponds to the cells metabolic activity. In this study, the percent reduction of alamarBlue® from a control well was calculated from the absorbance readings after 1, 4, and 7 days (**Figure 3.1**). The percent increase from day 1 to day 7 was calculated in order to determine the cell density that had the highest increase in viability during the week (**Figure 3.3**). The 2,500 and 3,750 cells/well

densities showed similar increases across all surfaces, whereas, the 5000 cells/well density exhibited a much lower percent increase from day 1 to day 7 for all surfaces. Since these results were not conclusive as to which cell density was the best, cells were stained and fluorescent microscopy was used to count the cells and to visualize ADSC distribution.

Fluorescent staining was performed after 1 and 7 days (**Figures 3.4-3.6**). From the fluorescent images it is clear that the ADSC proliferated on all the surfaces for all cell densities from day 1 to day 7. However, the cells on the Ti surfaces tended to clump together, whereas the cells on the NT surfaces were dispersed with space between the cells. Cell count was determined using ImageJ software to count the DAPI nuclei stain on fluorescent (10x) images from each surface (**Figure 3.2**). The ADSC were spread and elongated on the NT surfaces and their nuclei were easy to count, however, cells on Ti surfaces were close together making the nuclei difficult to count and produced large standard deviations for Ti after day 7. It is interesting to note that viability for Ti is high but cell count for Ti is low after 7 days. This could be due to the ADSC on the Ti weakly adhering to the surface compared to the ADSC strongly adhering to NT surfaces.

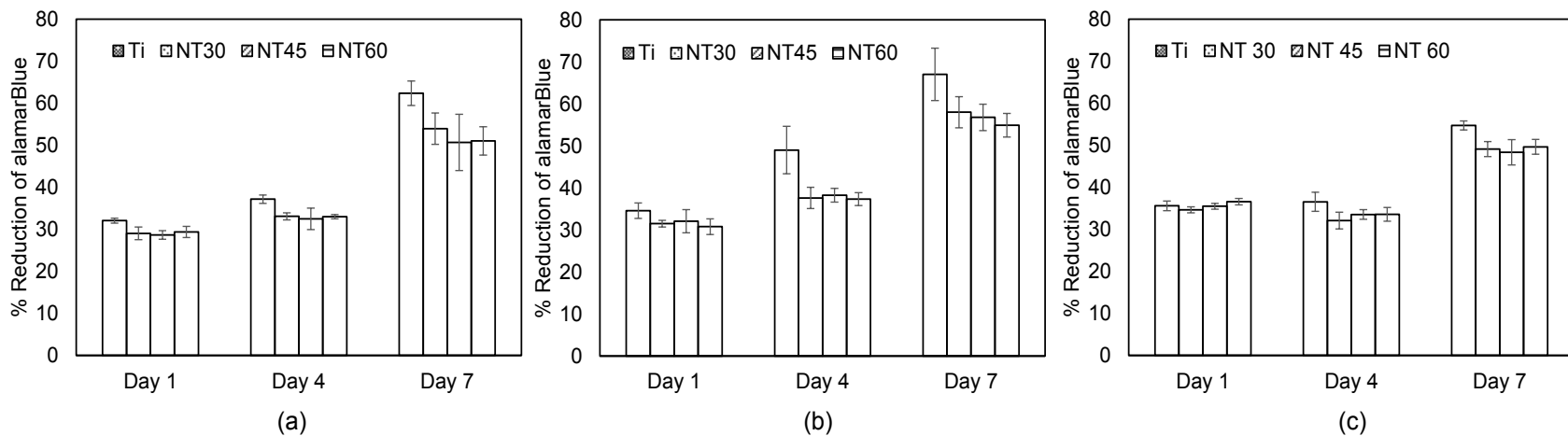


Figure 3.1 Adipose-derived stem cell viability after 1, 4 and 7 days determined by percent reduction of alamarBlue assay for (a) 2,500 cells/well, (b) 3,750 cells/well and (c) 5,000 cells/well densities.

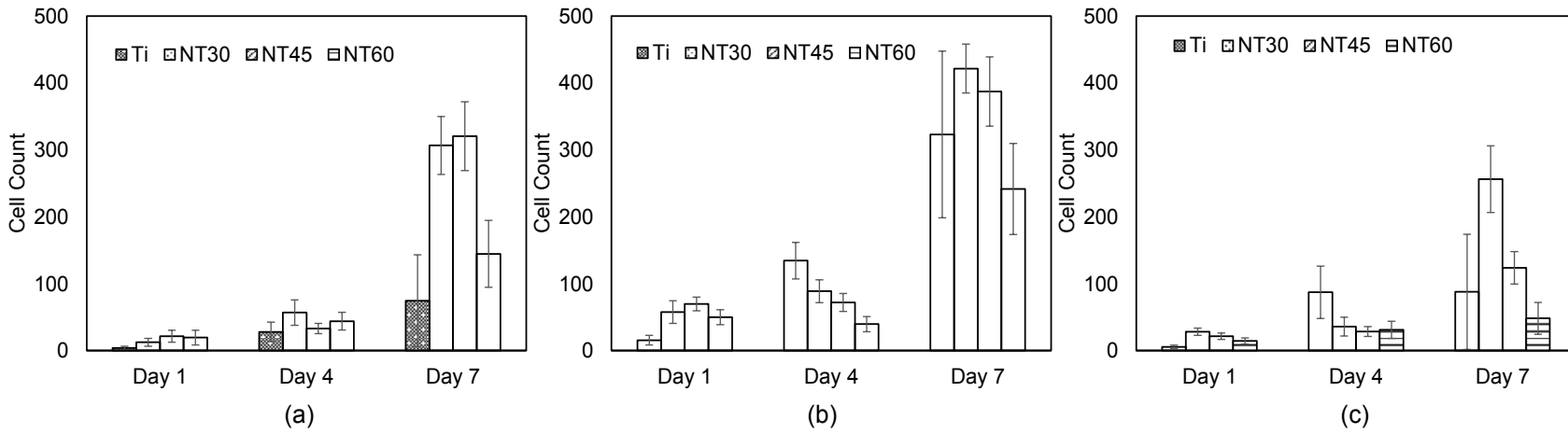
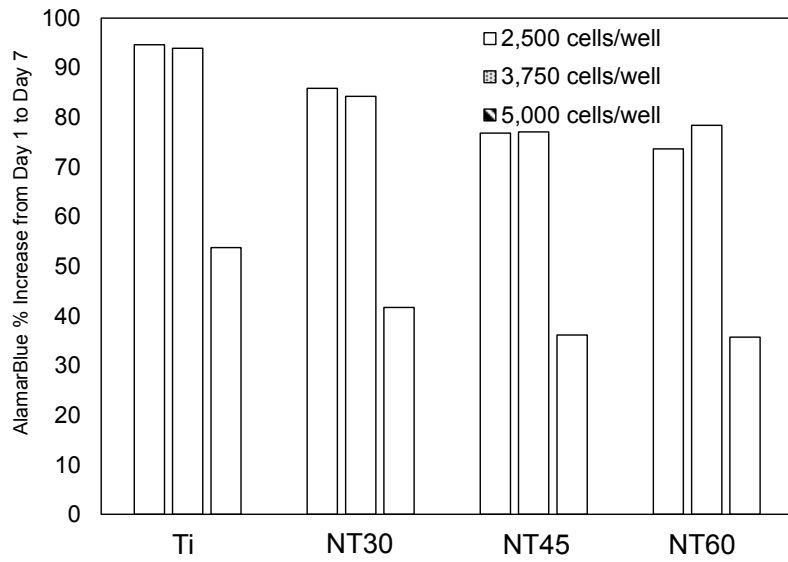
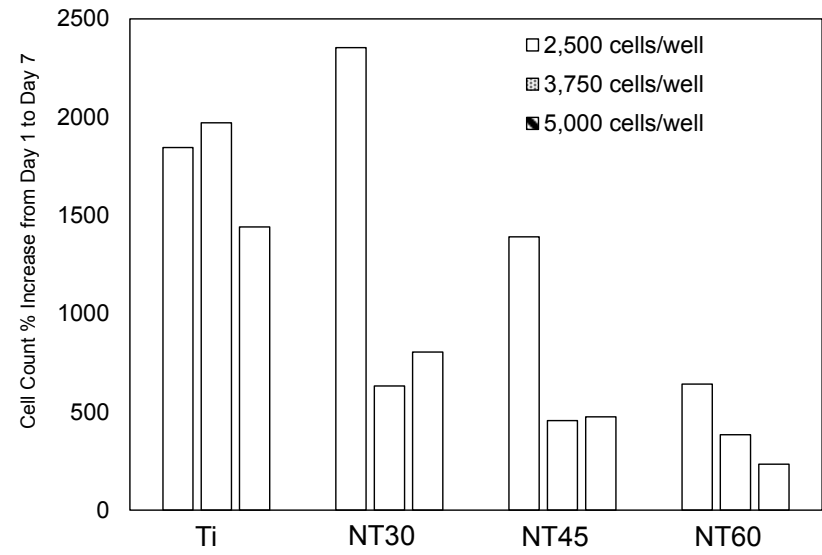


Figure 3.2 Cell count of adipose-derived stem cells after 1, 4 and 7 days for Ti and NT surfaces cultured at (a) 2,500 cells/well, (b) 3,750 cells/well and (c) 5,000 cells/well densities.



(a)



(b)

Figure 3.3 Percentage increase in (a) cell viability and (b) cell count calculated using alamarBlue results and DAPI staining from day 1 to day 7.

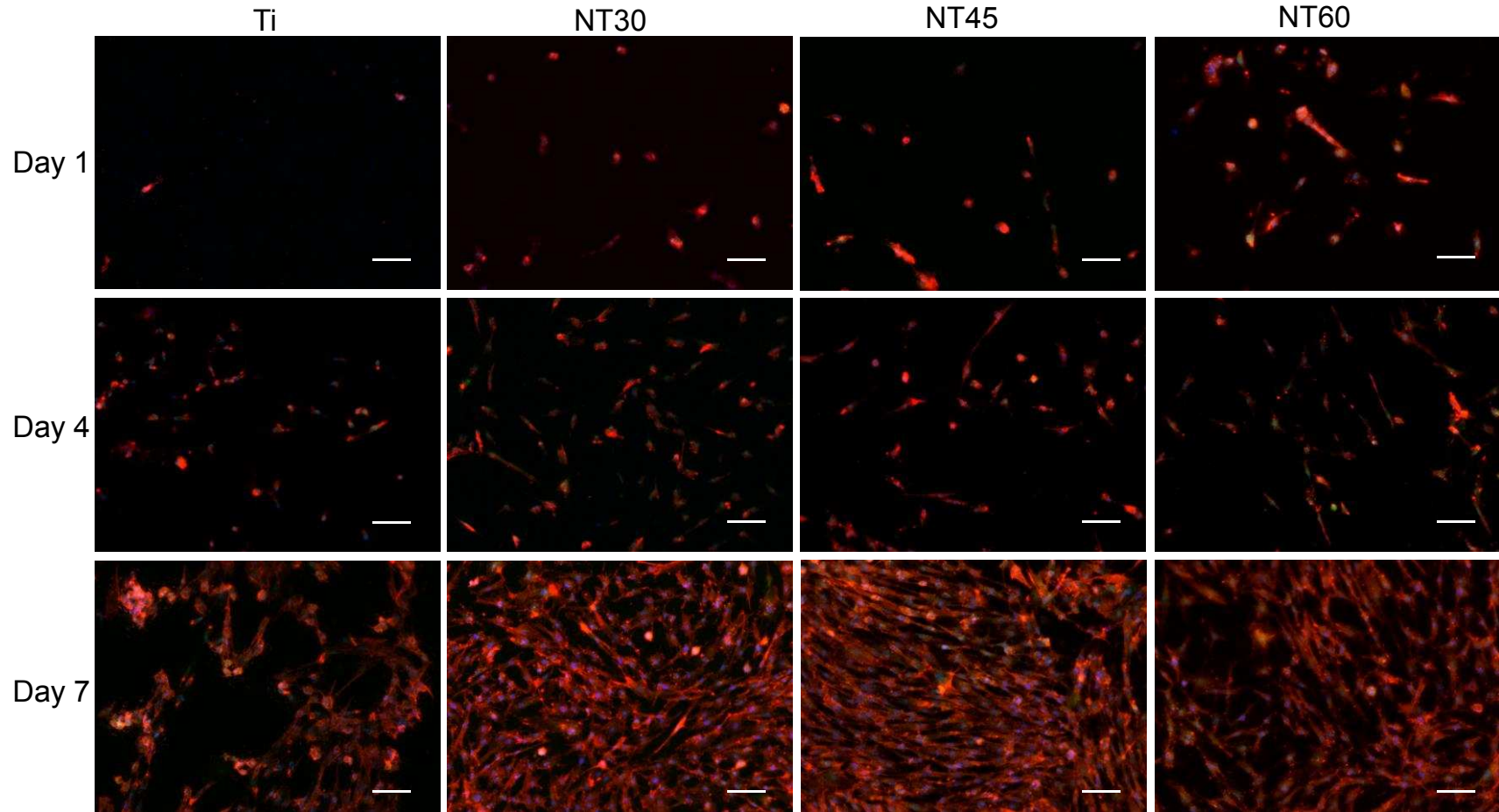


Figure 3.4 Fluorescent microscopy images of adipose-derived stem cells cultured at 2,500 cells/well density on Ti and NT surfaces after day 1, 4, and 7 of proliferation (scale bar 100 μ m).

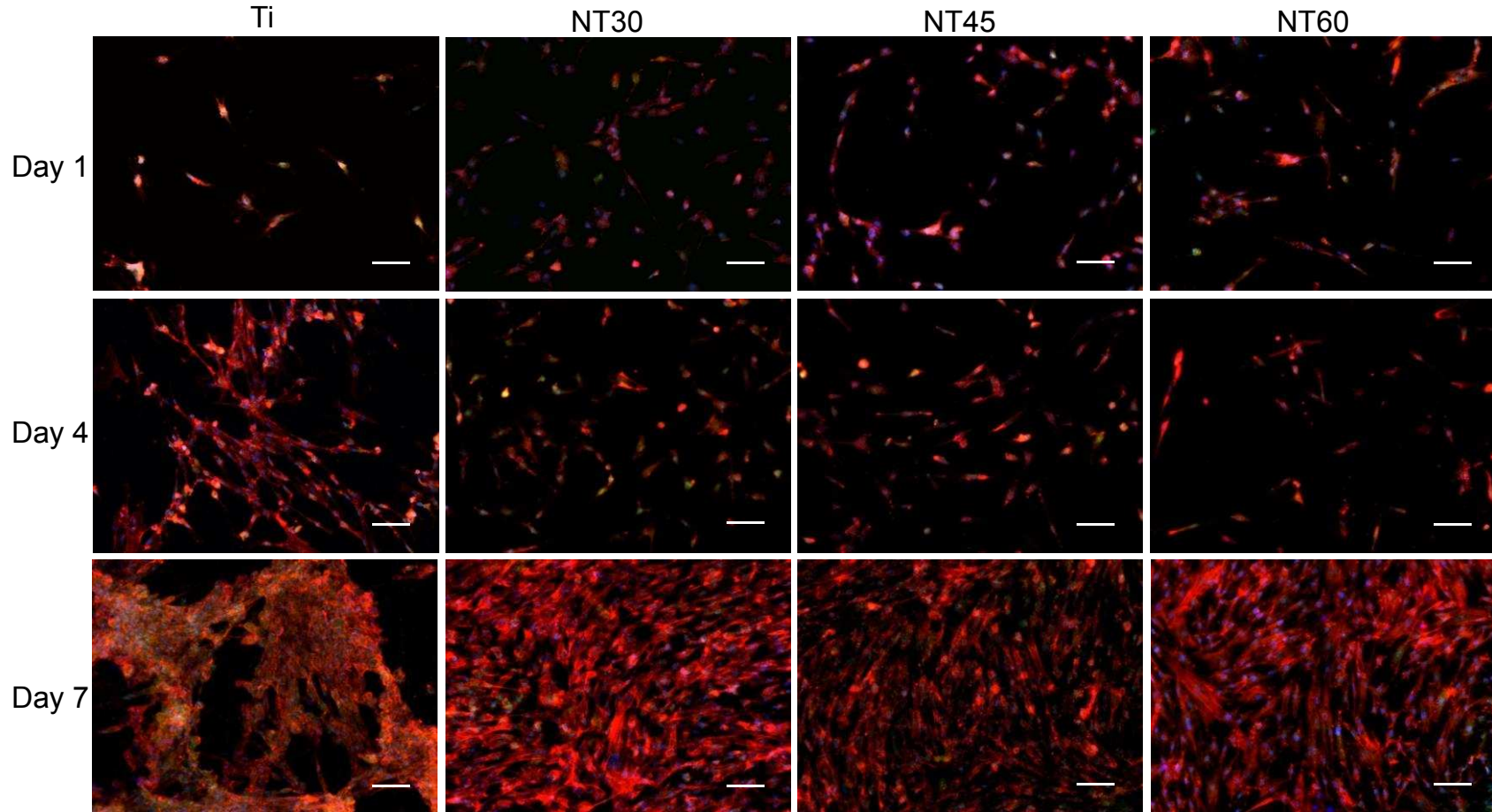


Figure 3.5 Fluorescent microscopy images of adipose-derived stem cells cultured at 3,750 cells/well density on Ti and NT surfaces after day 1, 4, and 7 of proliferation (scale bar 100 μ m).

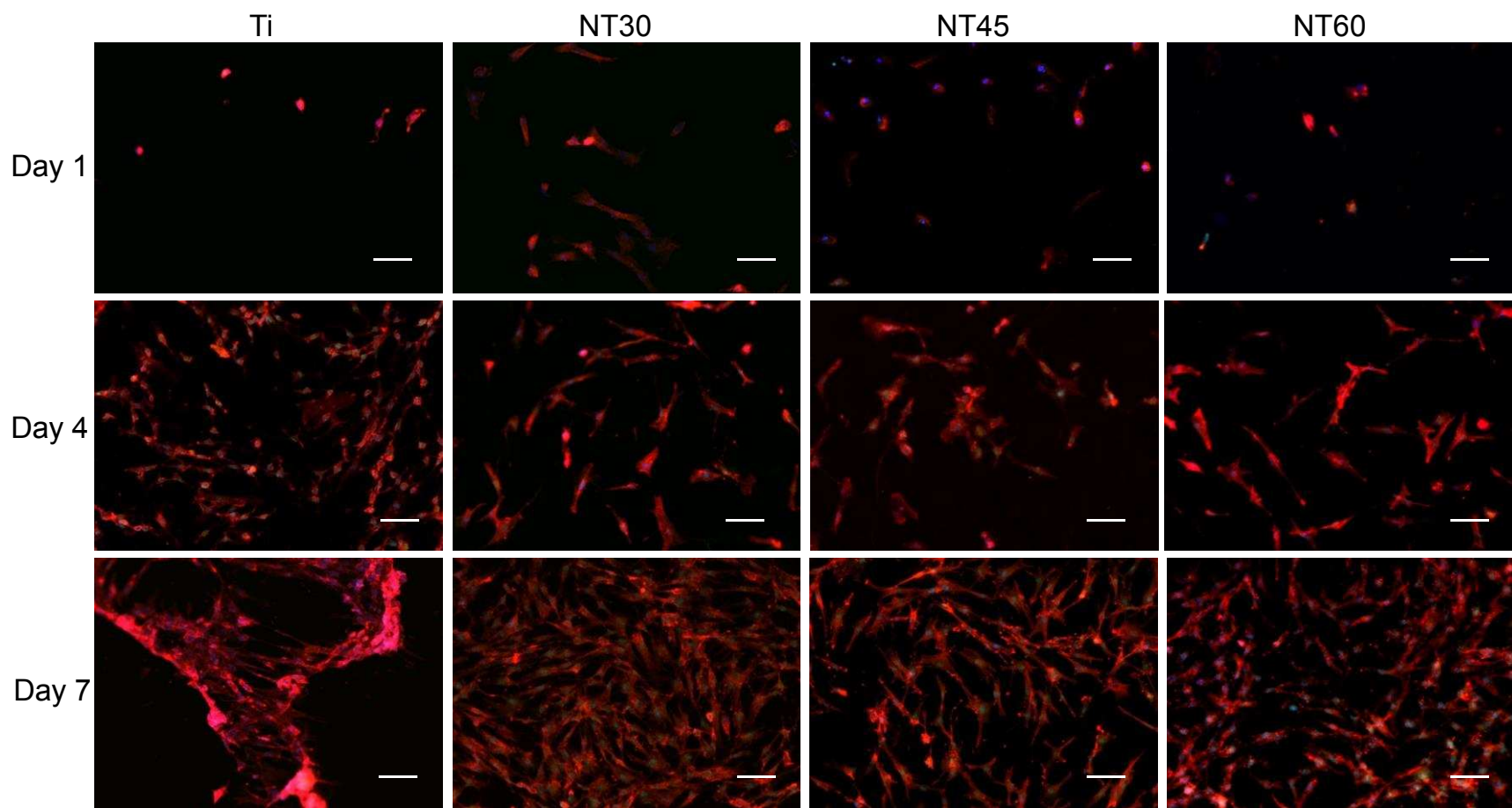


Figure 3.6 Fluorescent microscopy images of adipose-derived stem cells cultured at 3,750 cells/well density on Ti and NT surfaces after day 1, 4, and 7 of proliferation (scale bar 100 μ m).

Studies have reported that cells cultured on smooth Ti were easily removed, whereas cells cultured on rougher Ti surfaces require multiple treatments of trypsin and still some cells remain adhered to the surface [13]. Additionally on rough surfaces, cells divide slower, but adhere and differentiate faster [13].

In this study the results show that proliferation decreased as the size of NT increased. This decrease in proliferation may be due to the cells expending their energy to elongate and adhere firmly to the surface rather than proliferating. Overall, the ADSC count was higher on NT surfaces than Ti surfaces after 7 days for 2,500 and 3,750 cells/well densities, however, ADSC proliferation for the higher cell density (5,000 cells/well) experienced lower cell count on larger NT surface. The percent increase in cell count from day 1 to day 7 revealed the 2,500 cell density displayed a larger percent increase than 3,750 and 5,000 cell densities (**Figure 3.3**). The lower cell density may perform better due to more space for the cells to stretch, expand, and elongate which is an important part of cell division and differentiation.

Morphological analysis of cells is important in order to study the cellular organization, the physiological state of the cells, and the cell–surface interaction. The morphology of ADSC was investigated using SEM images of the surfaces after 1, 4, and 7 days of proliferation in growth media. Images of ADSC on the surfaces were only acquired for the 2,500 cells/well density as it was determined to be the optimal cell density (**Figure 3.7**). From the images it is clear that the ADSC were well spread across the surfaces after 7 days of culture. ADSC on the Ti are not as elongated as they are on the NT surfaces, with the most elongated ADSC being on NT60.

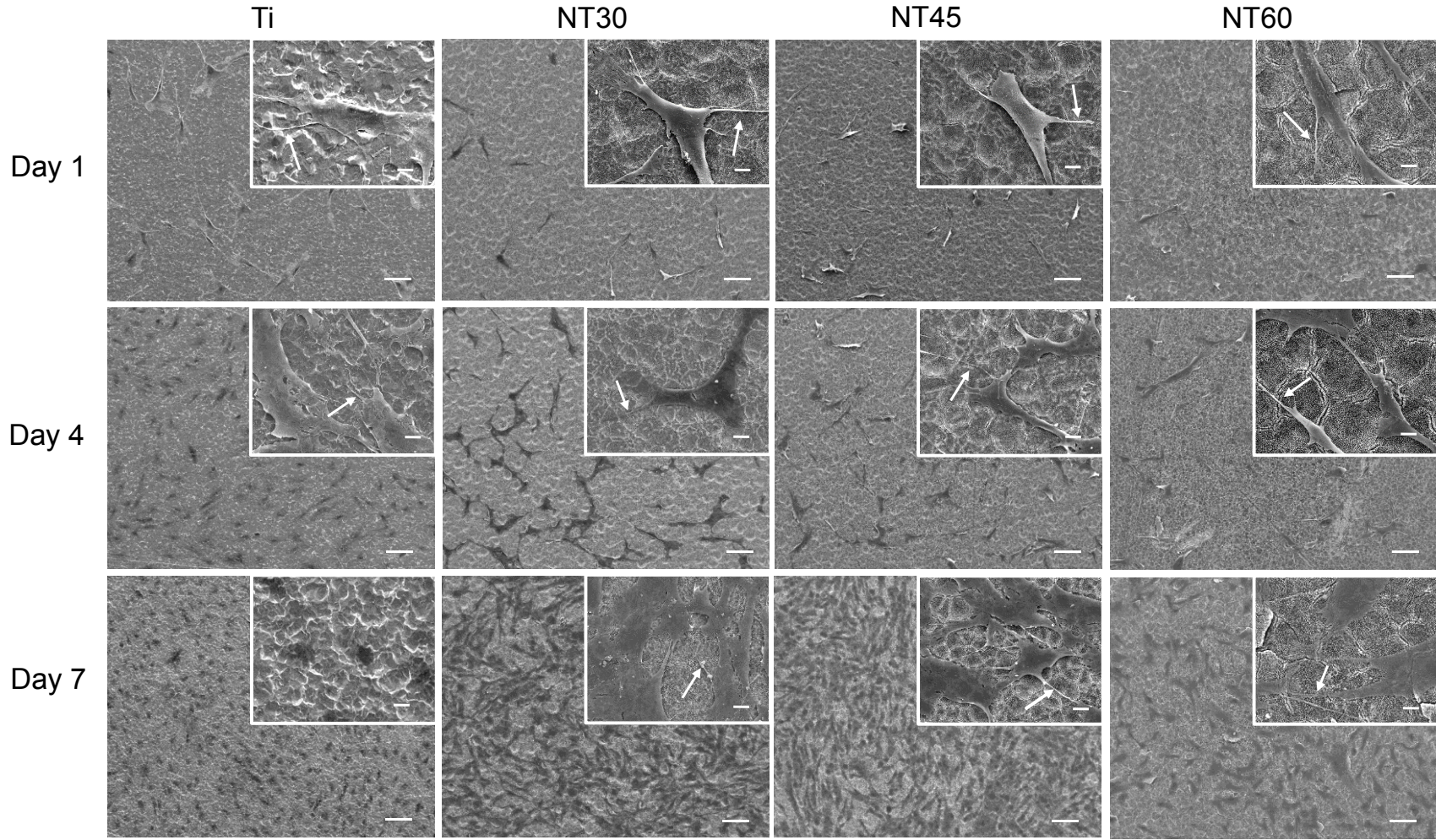


Figure 3.7 Scanning electron microscopy images of adipose-derived stem cells after 1, 4, and 7 days of proliferation at 100x (scale bar 100μm) and 1,000x (scale bar 10μm) magnification for 2,500 cells/well.

The images also revealed long filopodia protruding from the ADSC on all the surfaces (Arrows in high magnification SEM images **Figure 3.7**). Filopodia are actin-rich protrusions that play a significant role in topography sensing, migration, and cell-cell interaction [16,17]. Elongation is determined by the initial protein adsorption and protein adsorption is dependent on the surface characteristics. Studies have shown that cells cultured on smaller NT easily adhered to the surface because of the large number and thorough distribution of protein nanoparticles already covering the whole surface of the NT, however, proteins on larger NT only adhered sparsely to the surface due to the presence of large empty spaces around the NT. Thus, cells on the larger NT must expand further to find a protein-deposited surface, causing them to extend their filopodia across larger areas and eventually forming an elongated shape [18,19].

3.3 Conclusions

The purpose of this study was to determine the effect of nanotube (NT) size and cell density on the adhesion and proliferation of human adipose-derived stem cells (ADSC). Week long proliferation of ADSC on NT and Ti surfaces presented elongated cells on NT surfaces and ADSC cell count was greater than Ti on all nanotube surfaces after 7 days proliferation. The optimal cell density was 2,500 cells/well because it allowed the cells to proliferate more fully and elicited a higher increase in viability and cell count on nearly all surfaces. The smaller diameter nanotubes, NT30 and NT45, were better for ADSC proliferation as they elicited higher cell counts after day 7. This study confirms that NT surfaces promote ADSC adhesion and proliferation.

REFERENCES

- [1] H.-I. Chang, Y. Wang, Cell Responses to Surface and Architecture of Tissue Engineering Scaffolds, 2011. doi:10.5772/21983.
- [2] K.S. Brammer, C.J. Frandsen, S. Jin, TiO₂ nanotubes for bone regeneration, Trends Biotechnol. 30 (2012) 315–322. doi:10.1016/j.tibtech.2012.02.005.
- [3] A.S. Zanetti, C. Sabliov, J.M. Gimble, D.J. Hayes, Human adipose-derived stem cells and three-dimensional scaffold constructs: A review of the biomaterials and models currently used for bone regeneration, J. Biomed. Mater. Res. - Part B Appl. Biomater. 101 B (2013) 187–199. doi:10.1002/jbm.b.32817.
- [4] W. Tsuji, Adipose-derived stem cells: Implications in tissue regeneration, World J. Stem Cells. 6 (2014) 312. doi:10.4252/wjsc.v6.i3.312.
- [5] B.A. Bunnell, M. Flaat, C. Gagliardi, B. Patel, C. Ripoll, Adipose-derived stem cells: Isolation, expansion and differentiation, Methods. 45 (2008) 115–120. doi:10.1016/j.ymeth.2008.03.006.
- [6] Y.C. Halvorsen, D. Franklin, A.L. Bond, D.C. Hitt, C. Auchter, A.L. Boskey, D. Ph, E.P. Paschalis, Extracellular Matrix Mineralization and Osteoblast, Tissue Eng. 7 (2001) 729–41.
- [7] K.A. Cox-York, C.B. Erickson, R.I. Pereira, D.H. Bessesen, R.E. Van Pelt, Region-specific effects of oestradiol on adipose-derived stem cell differentiation in post-menopausal women, J. Cell. Mol. Med. 21 (2017) 677–684. doi:10.1111/jcmm.13011.
- [8] J.M. Banovetz, R. Sharp, R. a Probe, J.O. Anglen, Titanium plate fixation: a review of implant failures., J. Orthop. Trauma. 10 (1996) 389–94. <http://www.ncbi.nlm.nih.gov/pubmed/8854316>.
- [9] J.P. Berthet, A. Gomez Caro, L. Solovei, M. Gilbert, S. Bommart, P. Gaudard, L. Canaud, P. Alric, C.H. Marty-Ane, Titanium Implant Failure After Chest Wall Osteosynthesis, Ann Thorac Surg. 99 (2015) 1945–1952. doi:10.1016/j.athoracsur.2015.02.040.
- [10] M. Geetha, A.K. Singh, R. Asokamani, A.K. Gogia, Ti based biomaterials, the ultimate choice for orthopaedic implants - A review, Prog. Mater. Sci. 54 (2009) 397–425. doi:10.1016/j.pmatsci.2008.06.004.
- [11] M. Yaszemski, D.J. Trantolo, Corrosion and Biocompatibility of Orthopedic Implants, 2004.

- [12] C.J. Frandsen, K.S. Brammer, S. Jin, Variations to the nanotube surface for bone regeneration, *Int. J. Biomater.* 2013 (2013). doi:10.1155/2013/513680.
- [13] D.L.C. Barbara D Boyan, ChristophH Lohmann, David D Dean, VictorL Sylvia, and Z. Schwartz, Mechanisms Involved in Osteoblast Response to Implant Surface Morphology, *Annu. Rev. Mater. Res.* 31 (2001) 357–371.
- [14] M. Kulkarni, a Mazare, E. Gongadze, Š. Perutkova, V. Kralj-Iglič, I. Milošev, P. Schmuki, A Iglič, M. Mozetič, Titanium nanostructures for biomedical applications, *Nanotechnology.* 26 (2015) 62002. doi:10.1088/0957-4484/26/6/062002.
- [15] M.M. Stevens, Biomaterials for bone tissue engineering, *Mater. Today.* 11 (2008) 18–25. doi:10.1016/S1369-7021(08)70086-5.
- [16] J. Albuschies, V. Vogel, The role of filopodia in the recognition of nanotopographies, *Sci. Rep.* 3 (2013) 1658. doi:10.1038/srep01658.
- [17] Y. Zhukova, C. Hiepen, P. Knaus, M. Osterland, S. Prohaska, J.W.C. Dunlop, P. Fratzl, E. V. Skorb, The Role of Titanium Surface Nanostructuring on Preosteoblast Morphology, Adhesion, and Migration, *Adv. Healthc. Mater.* 1601244 (2017) 1601244. doi:10.1002/adhm.201601244.
- [18] K.S. Brammer, S. Oh, C.J. Cobb, L.M. Bjursten, H. Van Der Heyde, S. Jin, Improved bone-forming functionality on diameter-controlled TiO₂ nanotube surface, *Acta Biomater.* 5 (2009) 3215–3223. doi:10.1016/j.actbio.2009.05.008.
- [19] S. Oh, K.S. Brammer, Y.S. Julie, D. Teng, A. Engler, S. Chien, S. Jin, Stem cell fate dictated solely by altered nanotube dimension, *Proceeding Natl. Acad. Sci.* 106 (2009) 2130–2135.

CHAPTER 4

EVALUATION OF THE EFFECT OF TITANIA NANOTUBES ON THE DIFFERENTIATION OF ADIPOSE-DERIVED STEM CELLS

Stem cells are unspecialized cells capable of renewing themselves through self-renewal and can be induced to become specialized cells within specific tissue. In all tissues of the body, stem cells become activated when an injury occurs and are recruited to the injury site to aid in the tissue repair process [1]. When a biomaterial is implanted, the body reacts similar to an injury and stem cells are recruited to the implant site. Since, stem cells play an important role in tissue repair in the body, their interaction with biomaterials is critical for long term success of medical devices. Adipose-derived stem cells (ADSC) are mesenchymal stem cells obtained from adipose tissue and have the ability to differentiate into osteoblasts, bone forming cells [2]. It is important for osteoblasts to be present and active on an implant surface to help create a structural connection between the living bone and the implant, or osseointegration. Thus, studying the differentiation of stem cells into osteoblasts and their subsequent activity level on an implant surface *in vitro* gives a first glimpse of the potential of that biomaterial surface as an orthopedic implant.

This chapter addresses specific aim 3. In this chapter the osteogenic differentiation of adipose-derived stem cells (ADSC) for three weeks on titanium (Ti) and nanotube (NT) surfaces is evaluated and discussed. Differentiation markers of alkaline phosphatase (ALP) activity, non-collagen protein osteocalcin (OCN), and calcium deposition to confirm

and analyze the differentiation of ADSC on the NT and Ti surfaces are discussed. Immunofluorescence staining is performed to examine production of osteocalcin by the differentiated ADSC. Scanning electron microscopy is also utilized to visualize differentiated cells and mineral deposition.

4.1 Methods and Materials

4.1.1 ADSC Differentiation

After 7 days of proliferation on the surfaces, osteogenic differentiation was induced using osteogenic media; growth media supplemented with 10 nM dexamethasone, 5.4 mM β -glycerolphosphate, and 300 μ M ascorbic acid. Differentiation media changes were done every 2-3 days.

To confirm osteogenic differentiation and to determine the level of activity of the differentiated ADSC, three assays were performed: alkaline phosphatase (ALP) activity, total protein content (micro BCA assay), and calcium concentration. After 7, 14 and 21 days of induced osteogenesis, the surfaces were washed with PBS and transferred to a new well plate. The ADSC were lysed with 500 μ l of 0.2% w/v Triton X-100 in sterile DI water for 20 minutes (while shaken at 150 rpm) to remove all proteins from the surfaces.

To determine total protein content, 150 μ L of Triton-protein mixture was placed in a 96 well plate with 150 μ L of working reagent made from micro BCA protein assay kit (Thermo Scientific). The well plate was covered with foil and incubated at 37 °C for two hours. Absorbance was read at 562 nm. The total proteins expressed by ADSC were determined from a standard absorbance curve versus known concentration of albumin run in a parallel experiment.

To assess ALP activity, 50 μ L of Triton-protein mixture was placed in a 96 well plate and 150 μ L of working reagent made from QuantiChrom™ Alkaline Phosphatase Assay Kit (BioAssay Systems) was added using a multichannel pipette. Absorbance was read at 405 nm and then repeated 4 minutes later.

To quantify calcium deposition on each surface a commercially available calcium reagent test (Teco Diagnostics) was used. After cell lysis, the surfaces were soaked in 500 μ L of 6 N HCl for two hours to dissolve deposited calcium. After two hours, 20 μ L of the calcium-acid solution was removed to a new well plate and 1 ml of working reagent was added. The absorbance of the calcium–acid solution was measured at 570 nm and was converted to concentration using the absorbance of a reference calcium solution.

The osteogenic differentiation of ADSCs was confirmed through immunofluorescent staining of the cells and the protein osteocalcin. After 7, 14, and 21 days of induced osteogenesis, differentiation media was removed and surfaces were washed twice with warm PBS and then moved to a new well plate. The surfaces were fixed in 3.7 wt% formaldehyde in PBS for 15 min at room temperature, followed by three washes (5 min per wash) with PBS. Adhered ADSC were permeabilized by incubation in 1% Triton-X in PBS for 3 minutes and rinsed with PBS. After transferring surfaces to a new well plate, non-specific sites were blocked by incubating the ADSC in 10% bovine serum albumin (BSA) (Sigma) for 30 minutes. Blocking serum was removed and osteocalcin primary antibody (Santa Cruz Biotechnology) was added at the dilution of 1:100 in 1% BSA for 60 minutes at room temperature, followed by three washes (5 min per wash) with PBS. Secondary antibody FITC (Santa Cruz Biotechnology) was applied at the dilution of 1:200 in 1% BSA for 45 minutes, followed by one wash with PBS. The

ADSC were then incubated in Rhodamine and DAPI nuclear stain with the same procedure discussed in ADSC adhesion and proliferation section. Surfaces were rinsed twice with PBS and imaged with a fluorescence microscope (Zeiss). The osteocalcin present was determined by calculating percentage area (ImageJ software) coverage of stained osteocalcin from the fluorescence images at 10x magnification.

The morphology and mineral deposition of ADSC on Ti surfaces was investigated using SEM images of the surfaces after 21 days of induced osteogenesis in differentiation media. SEM fixing was performed with the same procedure discussed in Chapter 3. A gold coating of 10 nm was utilized and images were taken at 10 kV. Dispersive X-Ray Spectrometry (EDS) was utilized to confirm calcium and phosphorous mineral deposition after 21 days. Gold coating was not done before performing EDS on the surfaces as the gold peak interferes with the phosphorous peak during spectrum analysis.

4.1.2 Statistical analysis

All studies were performed with $n_{\min} = 3$ for qualitative analyses and $n_{\min} = 5$ for quantitative analyses. Minitab software was used to conduct the statistical analysis. The statistical differences were compared using one-way ANOVA analysis ($p < 0.05$) with a post-hoc Tukey's HSD (honest significant difference) test. All data is shown as the average \pm standard errors.

4.2 Results and Discussion

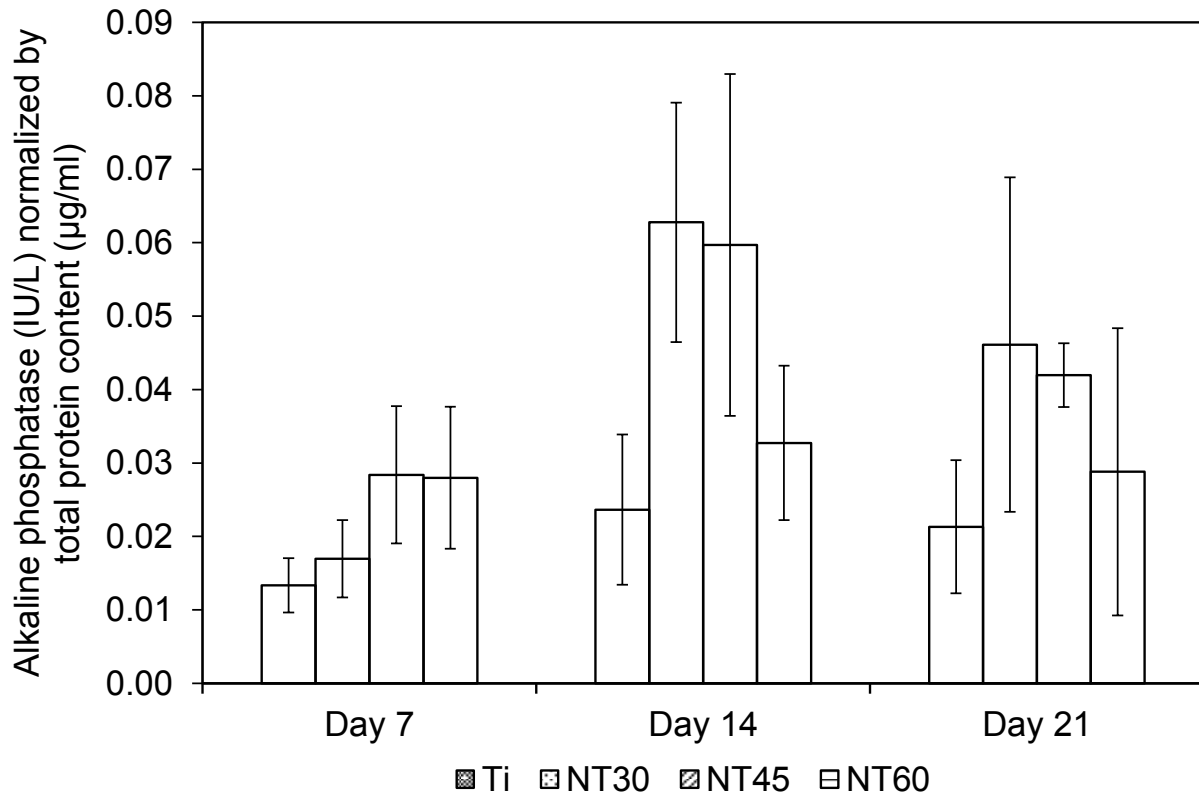
Since titanium implants still experience loosening and eventual failure [3–6], implants with nanostructured surfaces could help improve their fixation to the surrounding

bone tissues [7–11]. By fully understanding the effect of nanostructure size on the osteogenic differentiation of stem cells, implants could be specifically designed to achieve the optimal stem cell response from the tissue in which they are implanted. In this chapter, the effect of nanotube (NT) size on the differentiation of human adipose-derived stem cells (ADSC) was investigated.

Different NT surfaces were fabricated using anodization at 30 V, 45 V and 60 V as described in Chapter 2. After 7 days of proliferation on NT and Ti surfaces, osteogenesis of adhered ADSC was induced using growth media supplemented with 10 nM dexamethasone, 5.4 mM β -glycerolphosphate, and 300 μ M ascorbic acid. ADSC were allowed to proliferate on the surfaces for 7 days because that is when they reach 80–90% confluence, which is the optimal concentration to induce differentiation [12]. The concentrations of dexamethasone, β -glycerolphosphate, and ascorbic acid were chosen based on their proven ability to induce osteogenic differentiation in ADSC [12,13].

Alkaline phosphatase (ALP) is an enzyme found throughout the body and plays an integral role in the health of the liver and bone. In bone, ALP activity is associated with calcification because activity peaks just before mineralization begins. It is believed that high ALP leads to increased levels of inorganic phosphate, one of the components of apatite, the mineral phase of bone [8,14]. Thus, ALP activity is used as an early marker of osteoblast differentiation and hence was measured after 7, 14, and 21 days of induced osteogenesis. The ALP activity was normalized with total protein content of the cells to take into account the differences in number of cells on Ti and NT surfaces. Total protein content secreted by differentiated ADSC was also measured after 7, 14, and 21 days of induced osteogenesis using a micro BCA assay kit. ALP activity on NT30 and NT45 is

significantly higher (Tukey's HSD $p < 0.05$) than Ti after 14 days, but after 21 days ALP activity is back down for all surfaces and there is no significance between Ti and NT surfaces after 21 days (**Figure 4.1**).



Statistical significance presented in figure caption

Figure 4.1 Alkaline Phosphatase Activity (ALP) normalized by total protein content (Micro BCA assay). ALP and BCA assays were performed 7, 14 and 21 days after induced osteogenesis of ADSC. When statistically comparing between weeks of the same treatment, Ti and NT60: no significance between weeks; NT30: Day 7 is significantly different from Day 14 and Day 21; NT45: Day 7 is significantly different from Day 14. When statistically comparing between treatments on the same week, Day 7: Ti is significantly different from NT45 and NT60; Day 14: Ti is significantly different from NT30 and NT45, also NT60 is significantly different from NT30; Day 21: no significance between treatments. (Tukey's HSD $p < 0.05$) Full statistical analysis found in Appendix I.

These results are consistent with osteoblast activity in bone and calcifying cartilage. In early development, ALP is expressed but later in the cell development ALP expression declines, while other genes (e.g. osteocalcin production) are upregulated [14].

After 21 days, the results indicate that as the size of NT increases, ALP activity decreases suggesting slower osteoblast enzyme function. Several studies have found that ALP is higher on nanostructured surfaces [7,15–18], compared to Ti surfaces, however studies that compare ALP activity on different sizes of NT have varied results with some finding larger NT with higher ALP [7], and others finding that the smaller NT had higher ALP [17,19]. Clearly the size of NT is not the only factor that affects the ALP activity. The type of cell lineage used, concentrations of inducing chemicals in differentiation media, and the concentration of the cells cultured may also affect ALP and hence it is difficult to correlate ALP activity directly to NT size.

In order to deposit organic matrix necessary for mineralization, osteoblasts will also secrete collagen proteins, non-collagen proteins (e.g. osteocalcin, osteonectin, and osteopontin), and proteoglycan [20]. Osteocalcin (OCN) is a small molecular weight protein produced by osteoblasts that aids in mineralization and is considered a late marker of differentiation. In this study, immunofluorescent staining was used to visualize how OCN is distributed on the NT and Ti surfaces and was performed after 7, 14, and 21 days of induced osteogenesis (**Figure 4.2**). The immunofluorescent images show that OCN is well distributed across the surfaces and increasing each week. OCN proteins are small circular dots and some are circled in each image in **Figure 4.2**. OCN area coverage was calculated from immunofluorescent images of each surface using ImageJ software and was normalized using total protein content (**Figure 4.3**).

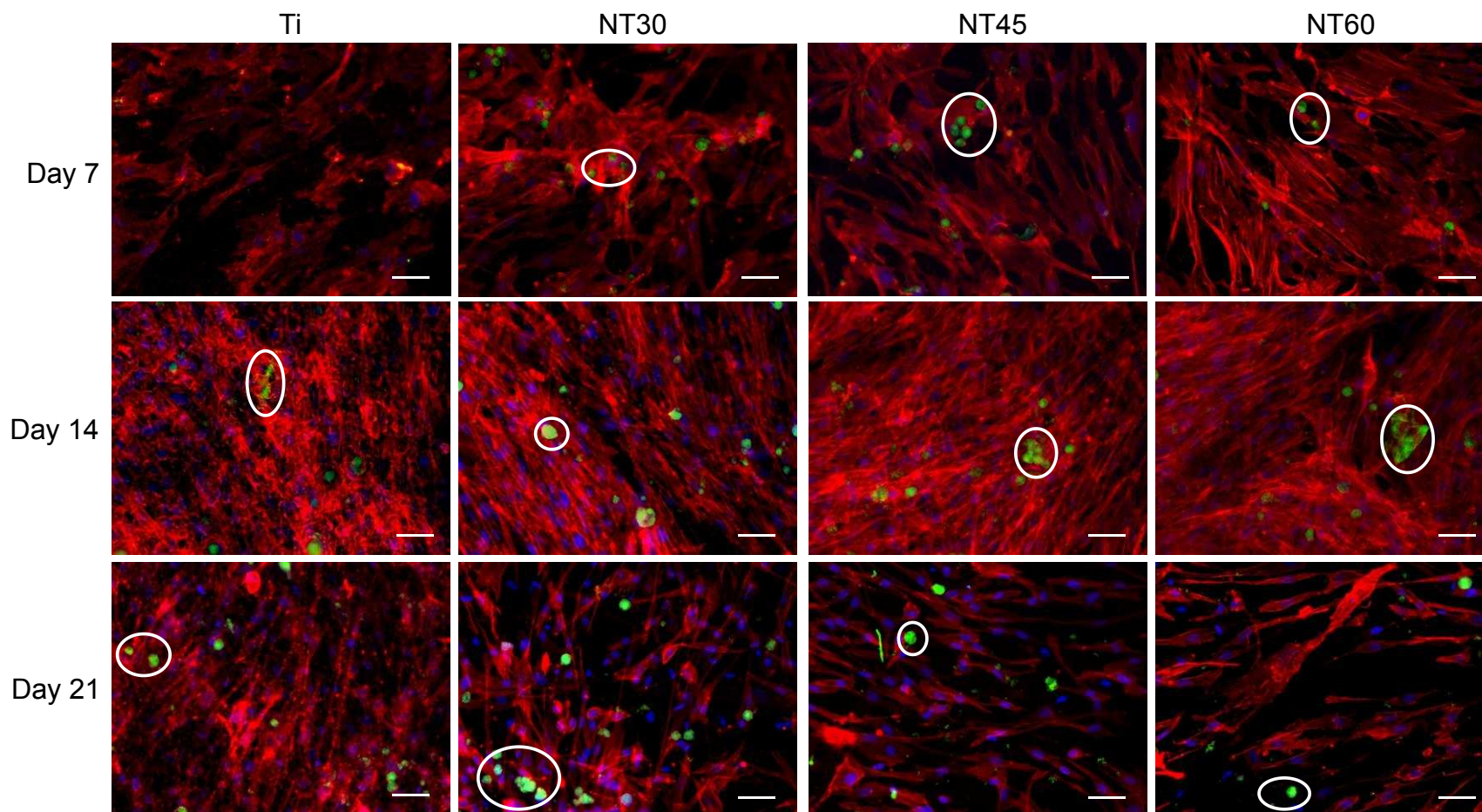


Figure 4.2 Immunofluorescent images of adipose-derived stem cells taken at 20x magnification after 7, 14 and 21 days of induced osteogenesis (Scale bar 50 μ m). Circles enclose osteocalcin proteins.

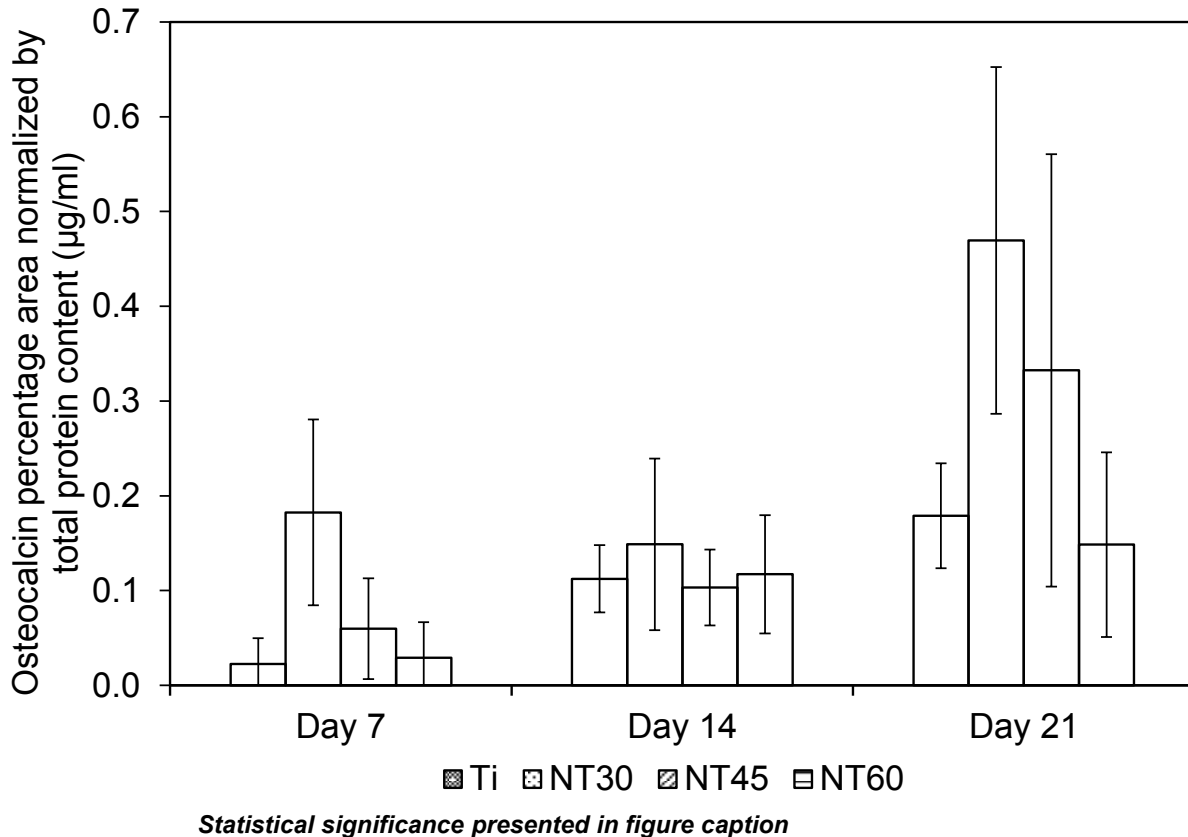
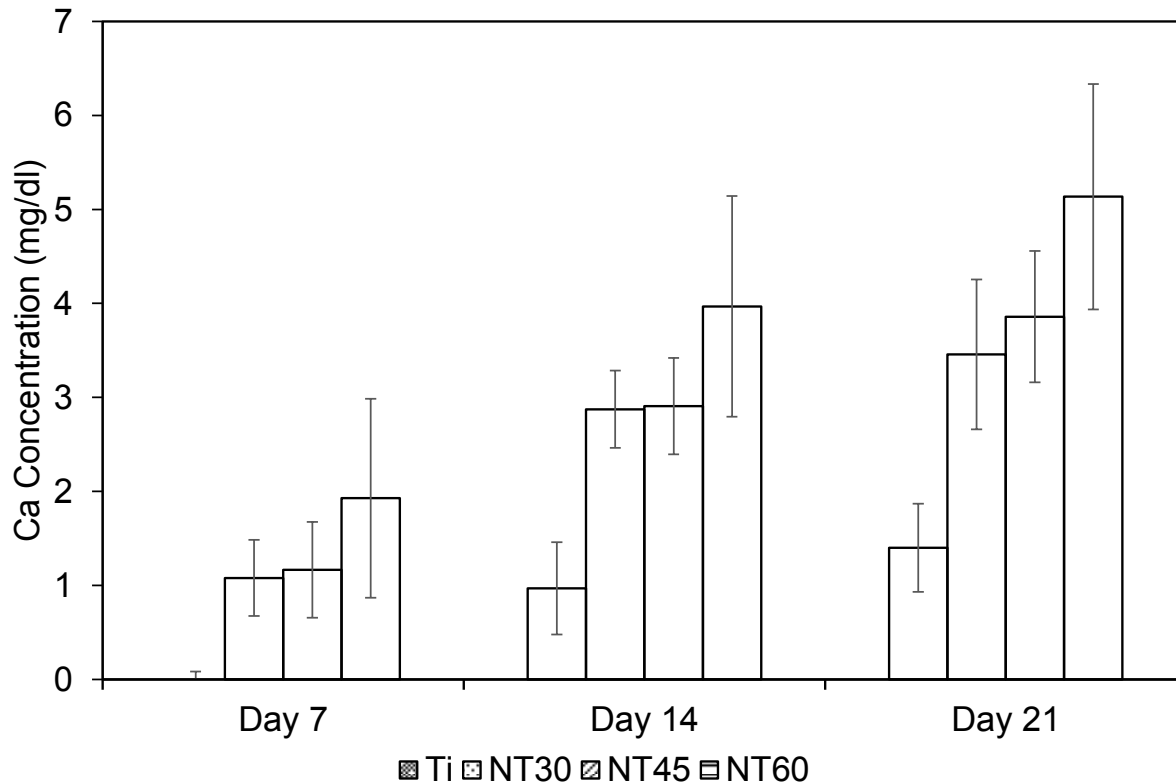


Figure 4.3 Percentage area coverage of osteocalcin normalized by total protein content (Micro BCA assay) after 7, 14 and 21 days induced osteogenesis. When statistically comparing between weeks of the same treatment, Ti: all weeks are significantly different from each other; NT60: Day 7 is significantly different from Day 14 and Day 21; NT30 and NT45: Day 21 is significantly different from Day 7 and Day 14. When comparing between treatments on the same week, Day 7: NT30 is significantly different from Ti, NT45 and NT60; Day 14: no significance between treatments; Day 21: NT30 and NT45 are significantly different from Ti and NT60. (Tukey's HSD $p < 0.05$) Full statistical analysis found in Appendix I.

Results indicated that NT30 and NT45 had the highest average osteocalcin after 21 days. All surfaces displayed higher OCN after 21 days which is to be expected since OCN is a late marker of differentiation. Other studies have also found higher osteocalcin on nanosurfaces than on Ti [26]-[27]. However, in this study the larger NT displayed lower percentages of osteocalcin after 21 days suggesting that osteoblasts perform their function better when adhered to smaller NT sizes. These findings are similar to other studies [17,23,24] but are the opposite of another comparable study using ADSC that

found higher osteocalcin on the largest NT [18]. It should be noted that the standard deviations for some surfaces and days are large. (Full statistical analysis can be found in the caption for **Figure 4.3**).

After increased ALP activity and protein secretion, the next step in the synthesis of bone matrix by osteoblasts is mineralization. Mineralization is when the cells produce hydroxyapatite which is composed of calcium and phosphorus. This occurs when the osteoblasts secrete enzymes that degrade the proteoglycans and phosphate-containing compounds causing the release of calcium and phosphate ions. The phosphate and calcium ions then merge to form hydroxyapatite crystals. Calcium deposited on NT and Ti surfaces was determined using a calcium reagent test after 7, 14, and 21 days of induced osteogenesis (**Figure 4.4**). After 21 days all NT surfaces have significantly larger concentrations of calcium than the Ti surfaces. Other reports show similar findings with calcium mineralization being higher on nanosurfaces than on titanium [15,16,18,21,25]. A couple of studies also comparing size of NT found that calcium deposition decreased as NT diameter increased [24,26]. In contrast, in this study the results reveal that ALP activity and OCN were lower on larger NT, however, higher calcium concentration was found on the larger NT. This may be due to cells on the larger NT having more surface area and thus more nucleation sites available to deposit calcium. Additionally, low ALP activity indicates lower phosphorous production and so there may not be enough phosphorous ions available to merge with the calcium ions and form hydroxyapatite, leaving an excess of calcium ions on the surface of the larger NT.



Statistical significance presented in figure caption

Figure 4.4 Calcium concentration on samples 7, 14 and 21 days after induced osteogenesis determined using a calcium reagent test. When statistically comparing between weeks of the same treatment, for all treatments (Ti, NT30, NT45, and NT60) Day 7 is significantly different from Day 14 and Day 21. When comparing between treatments on the same week, Day 7: Ti is significantly different from NT45 and NT60; Day 14: Ti is significantly different from NT30, NT45, and NT60; Day 21: Ti is significantly different from NT30, NT45, and NT60, NT60 is significantly different from NT30. (Tukey's HSD $p < 0.05$) Full statistical analysis found in Appendix I.

The morphology and mineral deposition of ADSC on NT and Ti surfaces was investigated using SEM images of the surfaces after 21 days of induced osteogenesis (**Figure 4.5**). After 21 days, the surfaces were almost completely covered by differentiated ADSC and mineralized matrix components were prevalent on both NT and Ti surfaces (Arrows indicate minerals in **Figure 4.5**). Dispersive X-Ray Spectrometry (EDS, Oxford instruments X-Max) was also utilized after 21 days of induced osteogenesis and confirmed that calcium and phosphorous minerals were widespread on NT and Ti

surfaces. These depositions may be hydroxyapatite which is a mineral produced by osteoblasts and composed of calcium and phosphorus. SEM images also showed that the NT were still intact and not affected by three weeks of cell culture.

4.3 Conclusions

The goal of this study was to determine the effect of nanotube (NT) diameter on the differentiation of human adipose-derived stem cells (ADSC). Three different NT surfaces were fabricated using anodization and week-long proliferation of ADSC on NT and Ti surfaces was performed before osteogenesis was induced using osteogenic media. Results showed that ADSC differentiated and performed better on NT surfaces than Ti surfaces. Additionally, the size of titania NT also affected the osteogenic differentiation of ADSC. Alkaline phosphatase activity and percent of osteocalcin declined as NT diameter increased, however, calcium concentration increased as NT diameter increased. SEM revealed widespread mineral deposition on all Ti and NT surfaces. This study confirms that NT surfaces promote osteogenic differentiation of human ADSC and may enhance integration of the implant and thus improve long term implant stability.

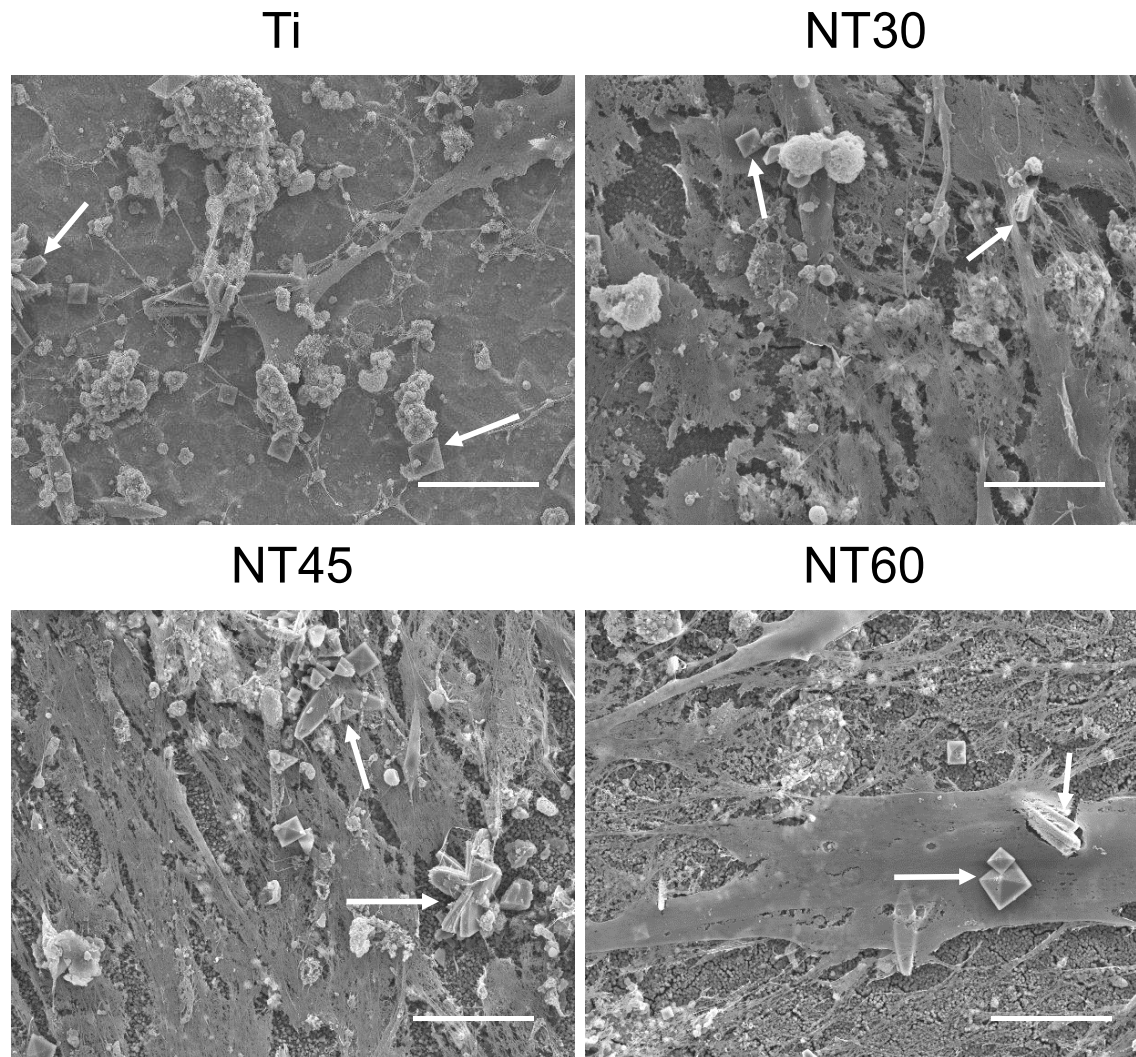


Figure 4.5 SEM images of differentiated adipose-derived stem cells and mineral deposition after 21 days of induced osteogenesis at 1000x magnification (scale bar is 50 μ m). Arrows indicate mineral deposits.

REFERENCES

- [1] K.P. Krafts, The hidden drama Tissue repair, *Organogenesis*. 6 (2010) 225–233. doi:10.4161/org6.4.12555.
- [2] W. Tsuji, Adipose-derived stem cells: Implications in tissue regeneration, *World J. Stem Cells*. 6 (2014) 312. doi:10.4252/wjsc.v6.i3.312.
- [3] J.M. Banovetz, R. Sharp, R. a Probe, J.O. Anglen, Titanium plate fixation: a review of implant failures., *J. Orthop. Trauma*. 10 (1996) 389–94. <http://www.ncbi.nlm.nih.gov/pubmed/8854316>.
- [4] J.P. Berthet, A. Gomez Caro, L. Solovei, M. Gilbert, S. Bommart, P. Gaudard, L. Canaud, P. Alric, C.H. Marty-Ane, Titanium Implant Failure After Chest Wall Osteosynthesis, *Ann Thorac Surg*. 99 (2015) 1945–1952. doi:10.1016/j.athoracsur.2015.02.040.
- [5] M. Geetha, A.K. Singh, R. Asokamani, A.K. Gogia, Ti based biomaterials, the ultimate choice for orthopaedic implants - A review, *Prog. Mater. Sci*. 54 (2009) 397–425. doi:10.1016/j.pmatsci.2008.06.004.
- [6] M. Yaszemski, D.J. Trantolo, *Corrosion and Biocompatibility of Orthopedic Implants*, 2004.
- [7] C.J. Frandsen, K.S. Brammer, S. Jin, Variations to the nanotube surface for bone regeneration, *Int. J. Biomater*. 2013 (2013). doi:10.1155/2013/513680.
- [8] D.L.C. Barbara D Boyan, ChristophH Lohmann, David D Dean, VictorL Sylvia, and Z. Schwartz, Mechanisms Involved in Osteoblast Response to Implant Surface Morphology, *Annu. Rev. Mater. Res*. 31 (2001) 357–371.
- [9] M. Kulkarni, a Mazare, E. Gongadze, Š. Perutkova, V. Kralj-Iglič, I. Milošev, P. Schmuki, A Iglič, M. Mozetič, Titanium nanostructures for biomedical applications, *Nanotechnology*. 26 (2015) 62002. doi:10.1088/0957-4484/26/6/062002.
- [10] M.M. Stevens, Biomaterials for bone tissue engineering, *Mater. Today*. 11 (2008) 18–25. doi:10.1016/S1369-7021(08)70086-5.
- [11] H.-I. Chang, Y. Wang, *Cell Responses to Surface and Architecture of Tissue Engineering Scaffolds*, 2011. doi:10.5772/21983.
- [12] B.A. Bunnell, M. Flaata, C. Gagliardi, B. Patel, C. Ripoll, Adipose-derived stem cells: Isolation, expansion and differentiation, *Methods*. 45 (2008) 115–120. doi:10.1016/j.ymeth.2008.03.006.

- [13] W.A. and A.T.B. Laura de Girolamo, Matteo F. Sartori, Osteogenic differentiation of human adipose-derived stem cells: comparison of two different inductive media, *J. Tissue Eng. Regen. Med.* 1 (2007) 154–157. doi:10.1002/term.12.
- [14] E.E. Golub, K. Boesze-Battaglia, The role of alkaline phosphatase in mineralization, *Curr. Opin. Orthop.* 18 (2007) 444–448. doi:10.1097/BCO.0b013e3282630851.
- [15] A.P. Ross, T.J. Webster, Anodizing color coded anodized Ti6Al4V medical devices for increasing bone cell functions, *Int. J. Nanomedicine.* 8 (2013) 109–117. doi:10.2147/IJN.S36203.
- [16] K.C. Popat, L. Leoni, C. a. Grimes, T. a. Desai, Influence of engineered titania nanotubular surfaces on bone cells, *Biomaterials.* 28 (2007) 3188–3197. doi:10.1016/j.biomaterials.2007.03.020.
- [17] M. Lai, K. Cai, L. Zhao, X. Chen, Y. Hou, Z. Yang, Surface Functionalization of TiO₂ Nanotubes with Bone Morphogenetic Protein 2 and Its Synergistic Effect on the Differentiation of Mesenchymal Stem Cells, (2011) 1097–1105.
- [18] K. Malec, J. Goralska, M. Hubalewska-Mazgaj, P. Glowacz, M. Jarosz, P. Brzewski, G. Sulka, M. Jaskula, I. Wybranska, Effects of nanoporous anodic titanium oxide on human adipose derived stem cells, *Int. J. Nanomedicine.* Volume 11 (2016) 5349–5360. doi:10.2147/IJN.S116263.
- [19] R. Zhang, H. Wu, J. Ni, C. Zhao, Y. Chen, C. Zheng, X. Zhang, Guided proliferation and bone-forming functionality on highly ordered large diameter TiO₂ nanotube arrays, *Mater. Sci. Eng. C.* 53 (2015). doi:10.1016/j.msec.2015.04.046.
- [20] R. Florencio-Silva, G.R.D.S. Sasso, E. Sasso-Cerri, M.J. Simões, P.S. Cerri, Biology of Bone Tissue: Structure, Function, and Factors That Influence Bone Cells, *Biomed Res. Int.* 2015 (2015). doi:10.1155/2015/421746.
- [21] E.F. Andrea Deiwick, Functional Titanium Lotus-Topography Promotes the Osteoinduction of Human Adipose-Derived Stem Cells In Vitro, *J. Nanomed. Nanotechnol.* 5 (2014). doi:10.4172/2157-7439.1000239.
- [22] A. Mazare, M. Dilea, D. Ionita, I. Titorencu, V. Trusca, E. Vasile, Changing bioperformance of TiO₂ amorphous nanotubes as an effect of inducing crystallinity, *Bioelectrochemistry.* 87 (2012) 124–131. doi:10.1016/j.bioelechem.2012.01.002.
- [23] J. Park, S. Bauer, K.A. Schlegel, F.W. Neukam, K. Der Von Mark, P. Schmuki, TiO₂ nanotube surfaces: 15 nm - an optimal length scale of surface topography for cell adhesion and differentiation, *Small.* 5 (2009) 666–671. doi:10.1002/sml.200801476.
- [24] J. Park, S. Bauer, K. Von Der Mark, P. Schmuki, Nanosize and vitality: TiO₂ nanotube diameter directs cell fate, *Nano Lett.* 7 (2007) 1686–1691. doi:10.1021/nl070678d.

- [25] N. Trujillo, K. Popat, Increased Adipogenic and Decreased Chondrogenic Differentiation of Adipose Derived Stem Cells on Nanowire Surfaces, *Materials (Basel)*. 7 (2014) 2605–2630. doi:10.3390/ma7042605.
- [26] W. Yu, X. Jiang, F. Zhang, L. Xu, The effect of anatase TiO₂ nanotube layers on MC3T3-E1 preosteoblast adhesion, proliferation, and differentiation, *J. Biomed. Mater. Res. Part A*. 94 (2010) n/a-n/a. doi:10.1002/jbm.a.32687.

CHAPTER 5

CONCLUSIONS AND FUTURE WORK

5.1 Conclusions

The need for joint replacement will continue to grow and increase significantly in the coming decades due to the aging population. Unfortunately, many joint implants experience failure after 10-15 years requiring revision surgery. Since joint implant materials come into direct contact with bone it is imperative that they mimic the structure of bone to improve osseointegration, or the direct structural and functional connection between living bone and the implant surface. Improving the osseointegration of the implant can increase the stability of the implant, thus, reducing micro motions that cause loosening and lead to implant failure. Current joint implants have microscale coatings and texturing, however, bone is composed of both micro and nano components. In order to mimic the nanostructure of bone many nanotopographies are being studied. These nanostructures have been shown to improve cellular response in terms of adhesion, proliferation and osteogenic differentiation. However, the optimal size of nanosurfaces to promote cell adhesion, proliferation, and differentiation is still disputed. Titania nanotubes (NT) are easily fabricated on titanium surfaces using electrochemical anodization and have been shown to improve cellular response *in vitro* and improve integration *in vivo*.

This thesis examined the surface characteristics of titania NT and the effect of nanotube size on adhesion, proliferation, and differentiation of adipose-derived stem cells (ADSC) *in vitro*. Titania NT with three different diameters were fabricated via anodization in an organic electrolyte solution by altering the voltage and duration of each anodization

process. The manner in which cells interact with a surface is largely determined by the proteins adhered on the surface. The surface characteristics that may affect how proteins interact with the surface are tube diameter and length, surface wettability, crystalline structure, and surface chemistry. These characteristics were evaluated and discussed for all three NT surfaces and titanium (Ti) control. Tube inner diameter and length of NT were characterized via scanning electron microscopy (SEM). Contact angle was used to determine wettability and revealed that all NT surfaces exhibited higher wettability than Ti control. Glancing angle X-ray diffraction (GAXRD) revealed all NT surfaces in this study exhibited high anatase content and x-ray photoelectron spectroscopy (XPS) indicated small percentages of fluoride present on all three NT surfaces. In conclusion, all of these surface characterization tests suggest that these NT surfaces should be ideal for *in vitro* cell studies and have the potential to promote cell adhesion, proliferation and differentiation.

Week long proliferation studies with ADSC on NT and Ti surfaces were performed *in vitro*. Adhesion and proliferation were investigated using a viability assay, fluorescent staining, and scanning electron microscope to visualize cell morphology. The studies revealed elongated cells on NT surfaces and ADSC count was greater on all nanotube surfaces than Ti after seven days proliferation. The smaller diameter nanotubes, NT30 and NT45, were better for ADSC proliferation as they elicited the highest cell counts after day seven.

After week-long proliferation of ADSC on NT and Ti surfaces, osteogenesis was induced using osteogenic media. To confirm osteogenic differentiation and to determine the level of activity of the differentiated ADSC, three assays were performed: alkaline

phosphatase (ALP) activity, total protein content (micro BCA assay), and calcium concentration. Immunofluorescence staining to examine production of osteocalcin and scanning electron microscopy to visualize the cells was also performed. Results showed that ADSC differentiated and performed better on NT surfaces than Ti surfaces. Additionally, the size of titania NT altered the osteogenic differentiation of ADSC. Alkaline phosphatase activity and percent of osteocalcin declined as NT diameter increased, however, calcium concentration increased as NT diameter increased. Scanning electron microscopy revealed widespread mineral deposition on all Ti and NT surfaces.

This thesis confirmed that NT surfaces promote adhesion, proliferation, and osteogenic differentiation of human ADSC and revealed that smaller NT performed this function better than larger NT. Further studies are needed to confirm that implants with NT surfaces enhance osseointegration and to further define their potential to improve implant stability.

5.2 Future Work

Future studies should be directed into four main areas.

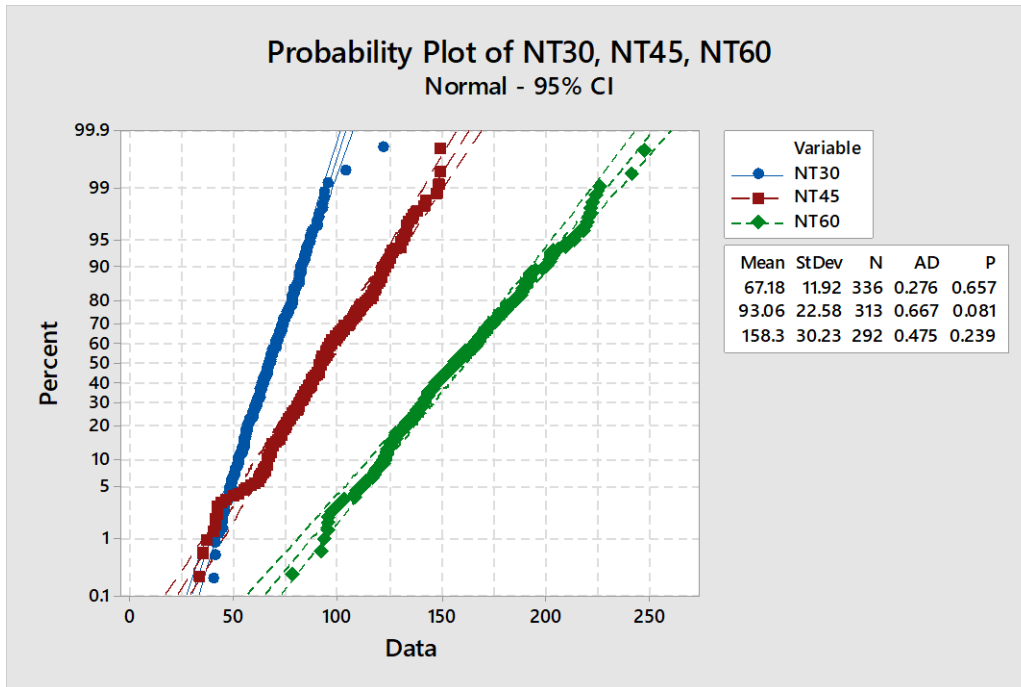
1. Research into understanding the nanoscale mechanisms that affect cell function. Specifically looking at why cell proliferation and differentiation is altered on nanosurfaces and what, if any, biochemical changes occur within the cells due to their interaction with a nanostructured surface.
2. Fabrication of nanotubes on titanium alloys that are commonly used in joint implants today followed by fabrication of nanotubes on hip and knee implant components.

3. Mechanical testing of hip and knee implant (ASTM F1875 - 98(2014)) components that have a nanotube surface topography in a loading environment. Since joint implants experience a large range of motion and multiple forces it is important to determine the stability of the nanotube topography when placed in a simulated loading environment.
4. *In vivo* animal studies using rats, dogs, goat, and/or sheep models. Initial studies to determine whether the osseointegration is improved by adding nanotubes can be done on smaller animal models such as rats. For weight bearing mechanical analysis a larger animal model such as dog, goat or sheep should be utilized.

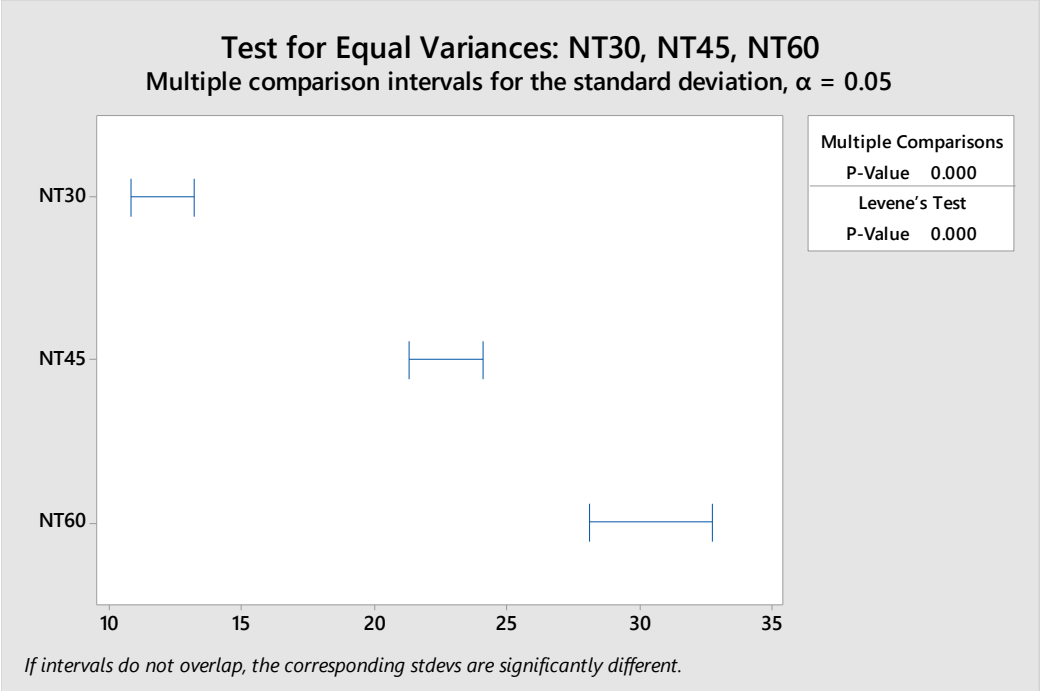
APPENDIX I
Statistical Analysis

Statistical Plots and Analysis for Figure 2.3

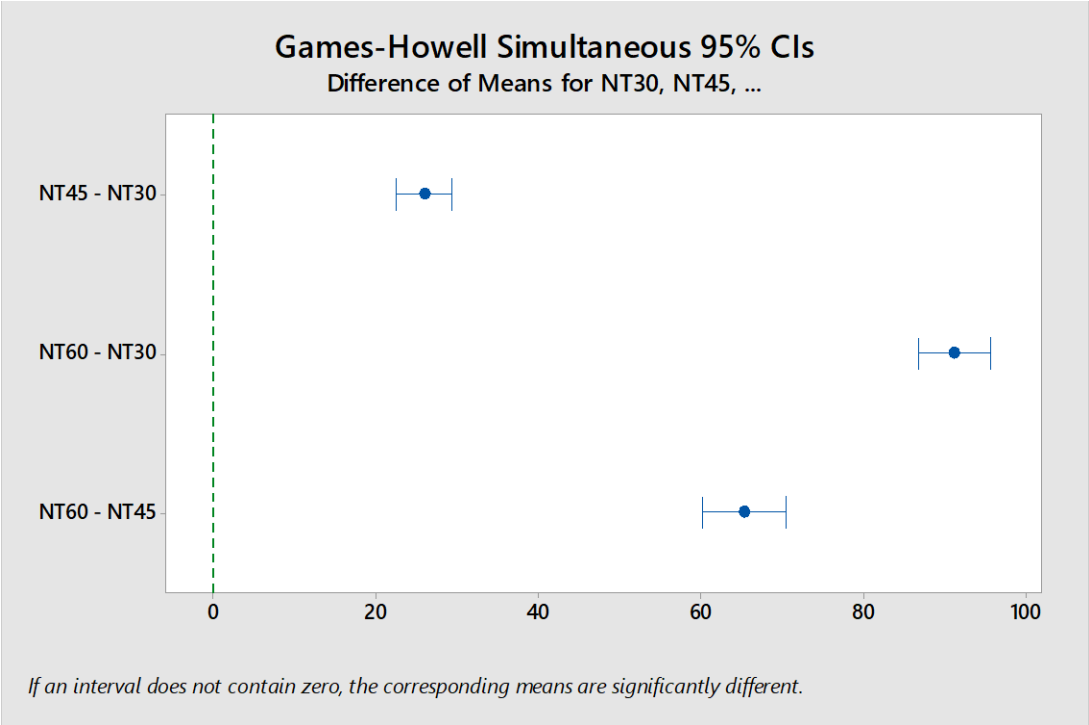
First, analyzing NT inner diameter for NT30, NT45, and NT60.

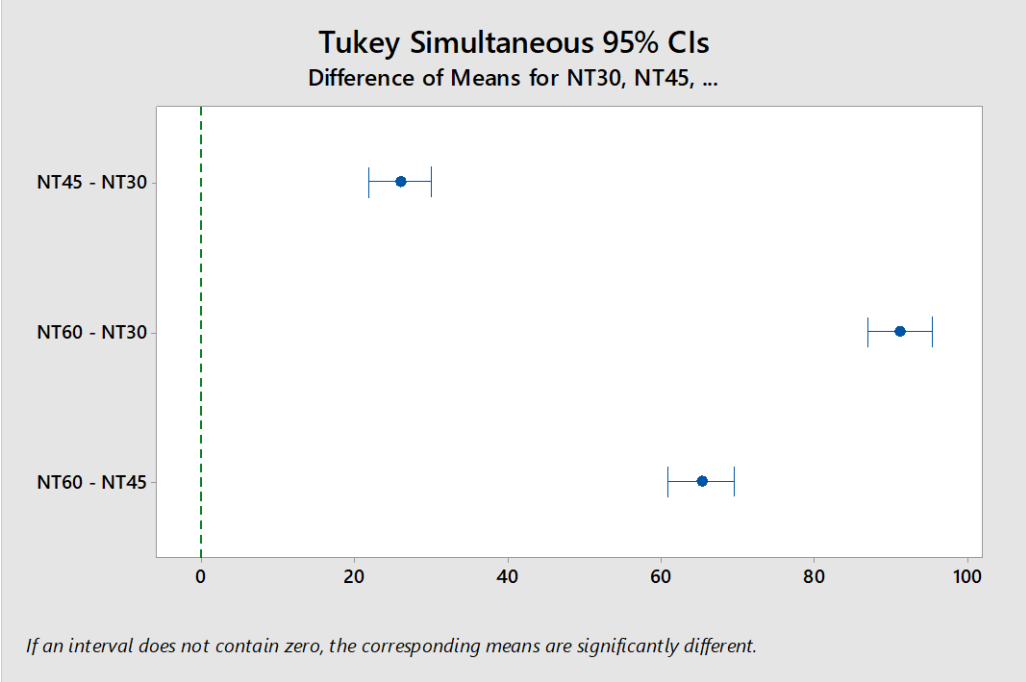


P-values are all greater than 0.05, so we can assume normal distribution for all three NT surfaces.



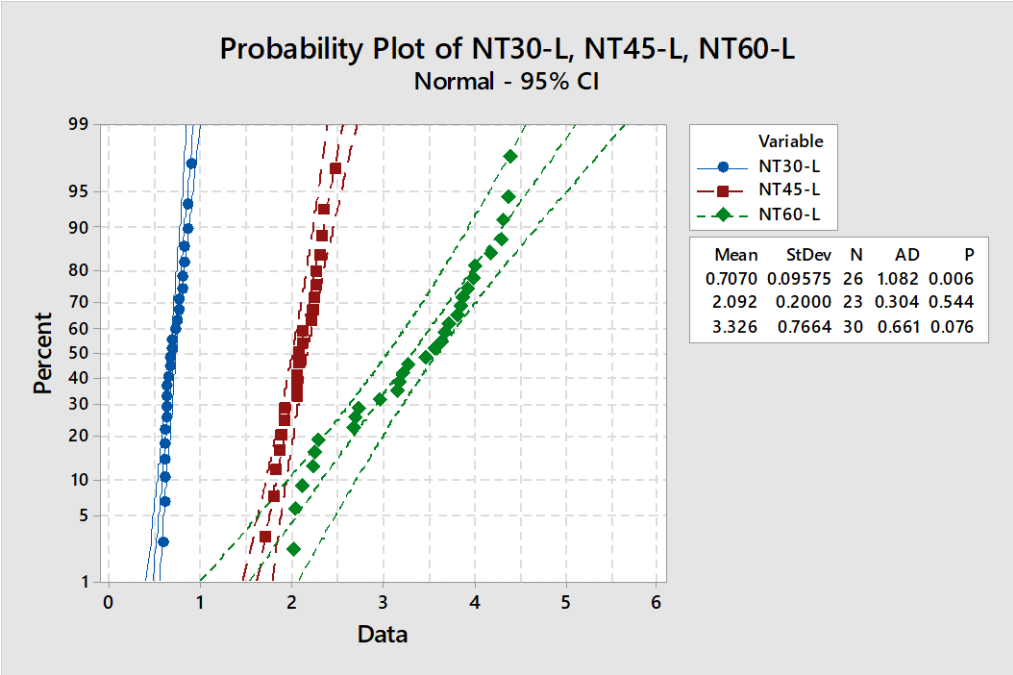
Test for equal variances is not very good so will run ANOVA with a Tukey post hoc analysis and Games-Howell (for non-equal variances) post hoc analysis to double check.



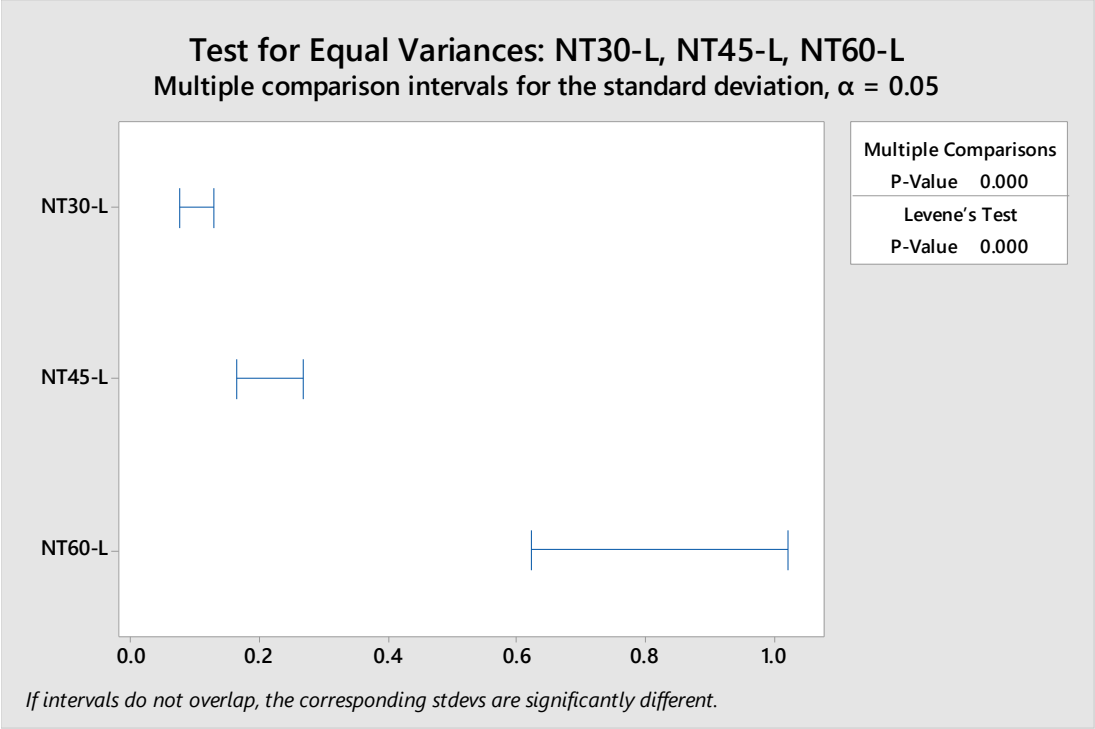


Both Tukey post hoc and Games-Howell find that all three NT surface's inner diameter are significantly different from each other.

Second, analyzing NT length for NT30, NT45, and NT60.

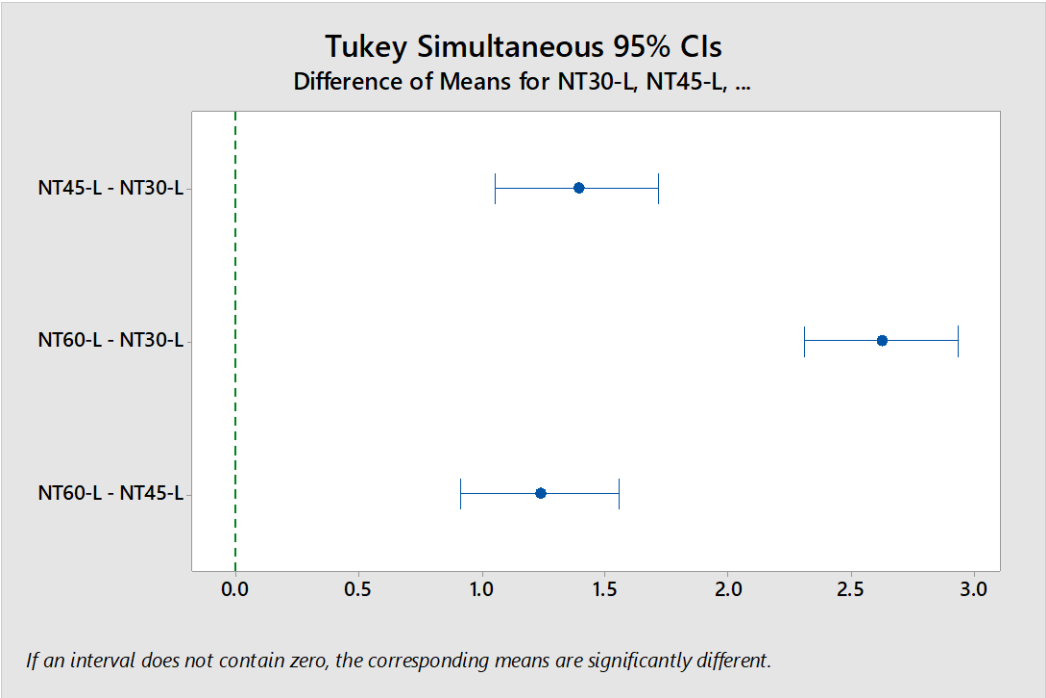


NT45 and NT60 have normal distributions, however, NT30 is not a normal distribution.



NT30 and NT45 have close enough variances, however, NT60 is not very close, but is within 5x of NT45 so should be ok to use an ANOVA.

Ran a one-way ANOVA with a post hoc Tukey even though NT30 is not normal.



Tukey shows that all three NT surfaces are significantly different from each other. Since NT30 is not normal, but dependent variable is continuous, will run a Mann-Whitney (for non-normal sets of data) to confirm that the means of data sets are significantly different with the NT30.

Mann-Whitney Test and CI: NT30-L, NT45-L

N Median

NT30-L 26 0.6780

NT45-L 23 2.0680

Point estimate for $\eta_1 - \eta_2$ is -1.4069

95.2 Percent CI for $\eta_1 - \eta_2$ is (-1.4840,-1.2791)

W = 351.0

Test of $\eta_1 = \eta_2$ vs $\eta_1 \neq \eta_2$ is significant at 0.0000

The test is significant at 0.0000 (adjusted for ties)

Since value is $0.000 < 0.05$, confirms that NT30 and NT45 are significantly different from each other.

Mann-Whitney Test and CI: NT30-L, NT60-L

N Median

NT30-L 26 0.6780

NT60-L 30 3.5165

Point estimate for $\eta_1 - \eta_2$ is -2.7978

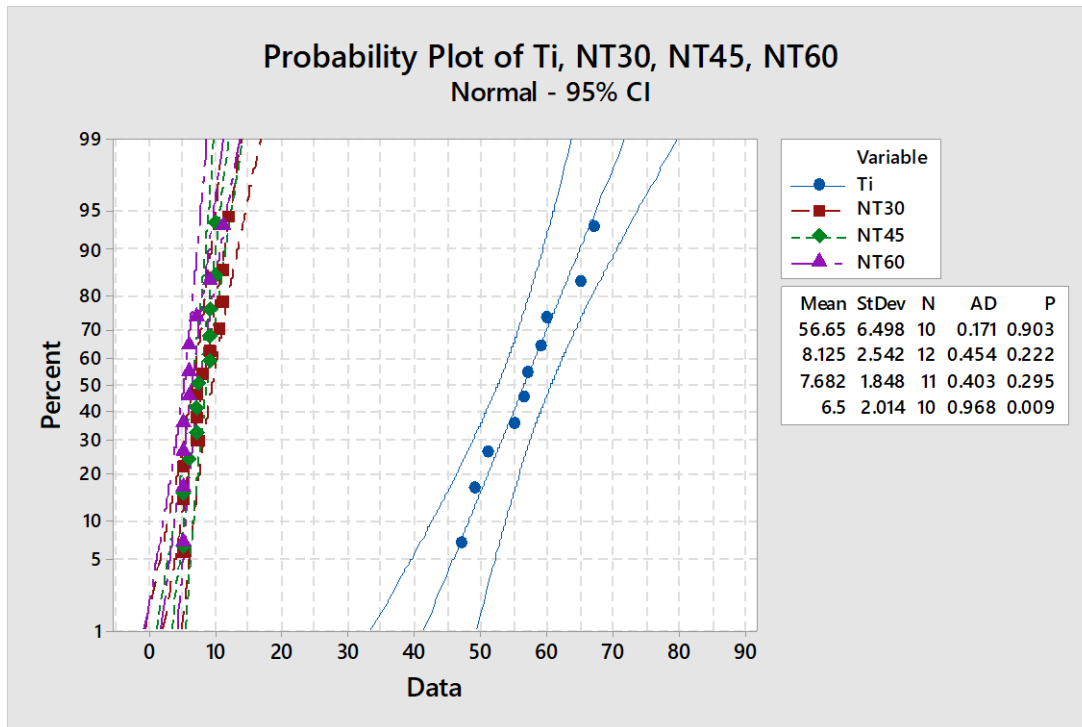
95.0 Percent CI for $\eta_1 - \eta_2$ is (-3.0690,-2.3519)

W = 351.0

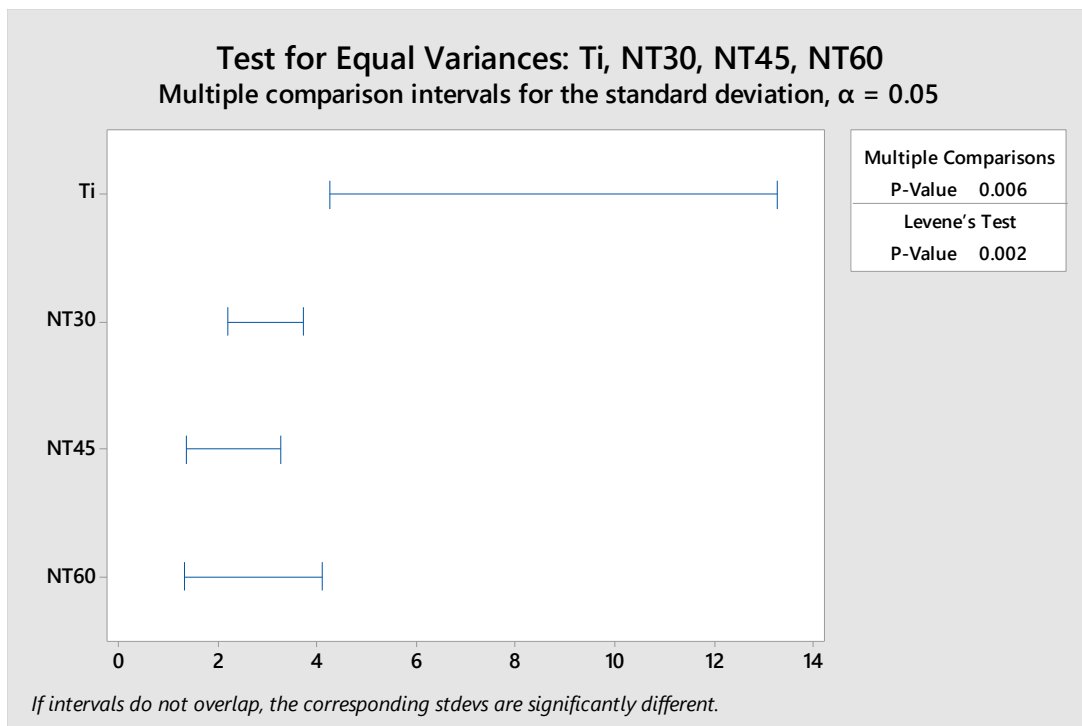
Test of $\eta_1 = \eta_2$ vs $\eta_1 \neq \eta_2$ is significant at 0.0000

Confirms that NT30 and NT60 are significantly different from each other.

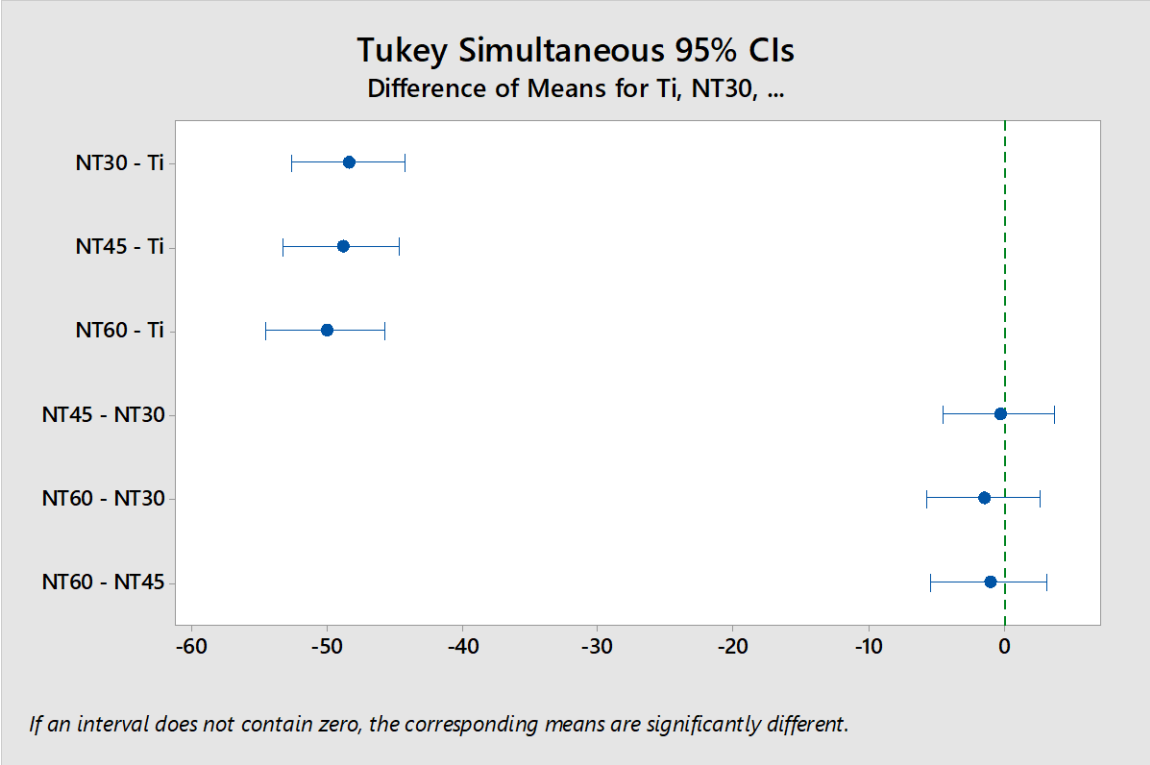
Statistical Plots and Analysis for Figure 2.4



All normally distributed except NT60, but should be ok to run an ANOVA.

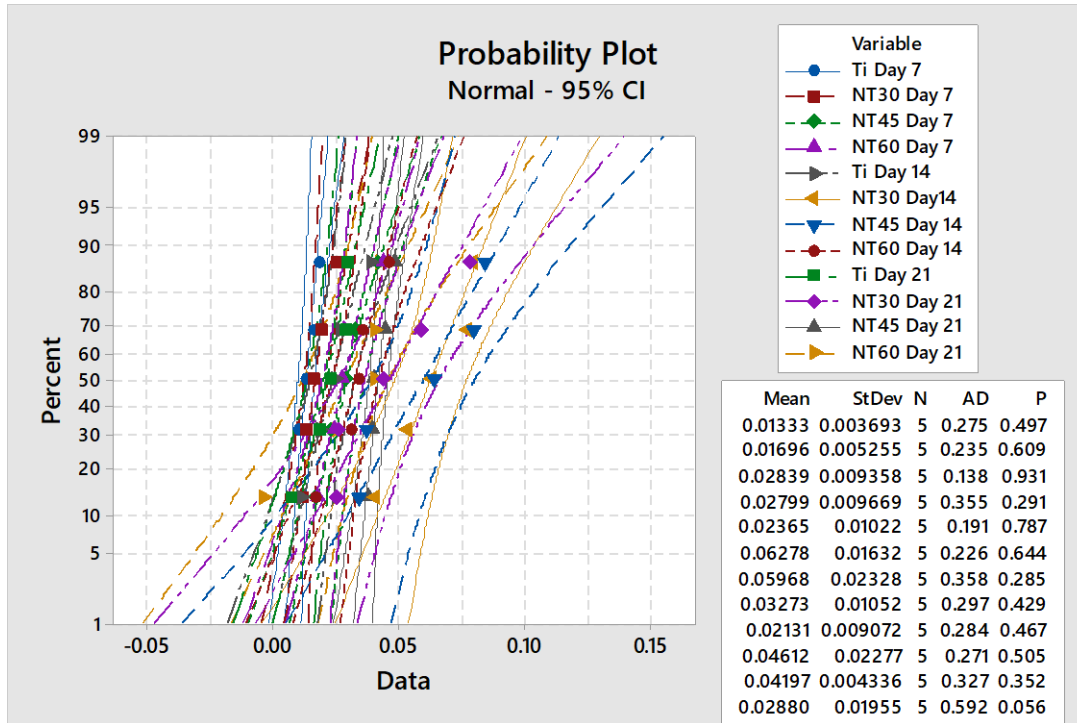


Test for equal variance looks good.

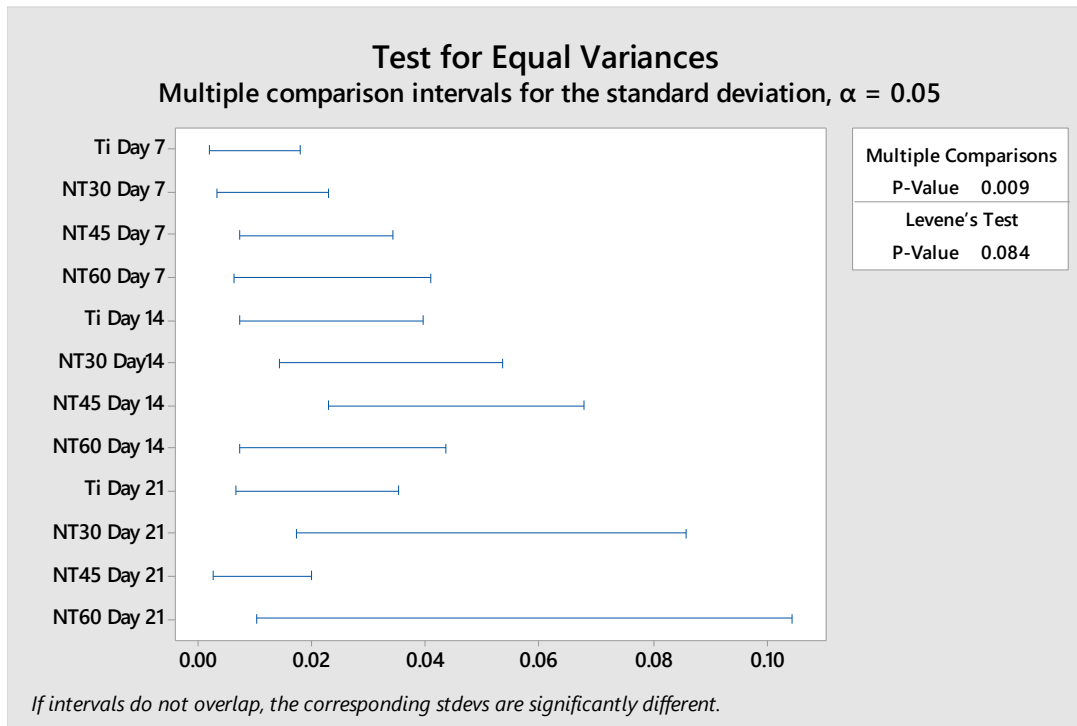


One-way ANOVA with a post hoc Tukey shows that the NT surface contact angles are significantly different from the Ti contact angle.

Statistical Plots and Analysis for Figure 4.1



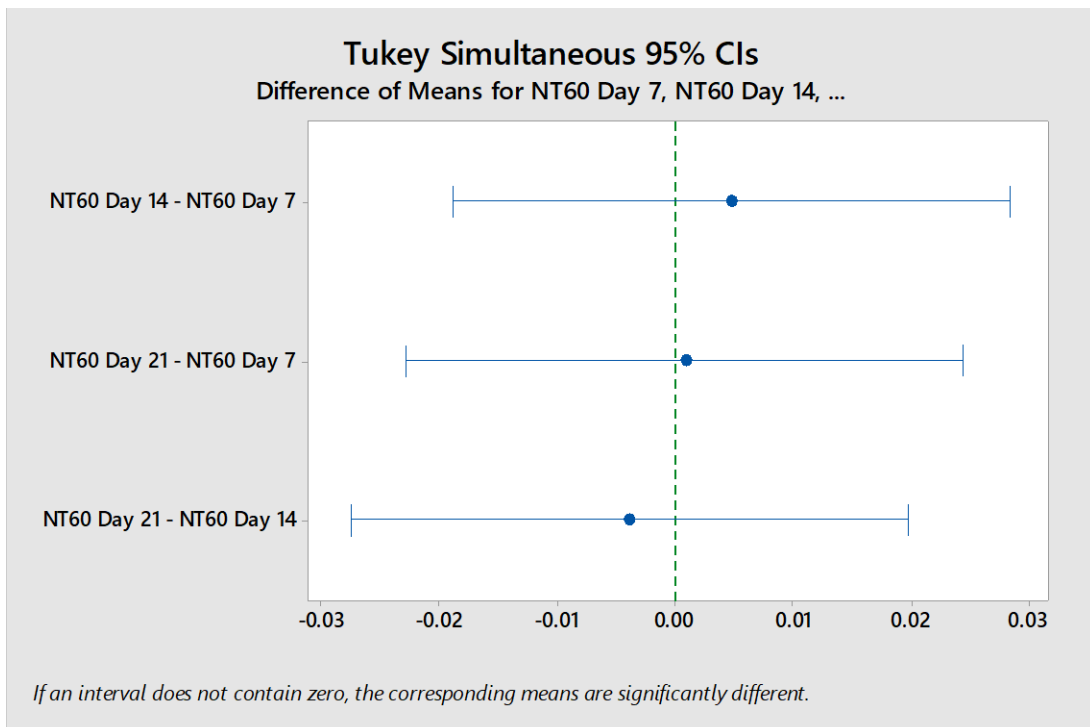
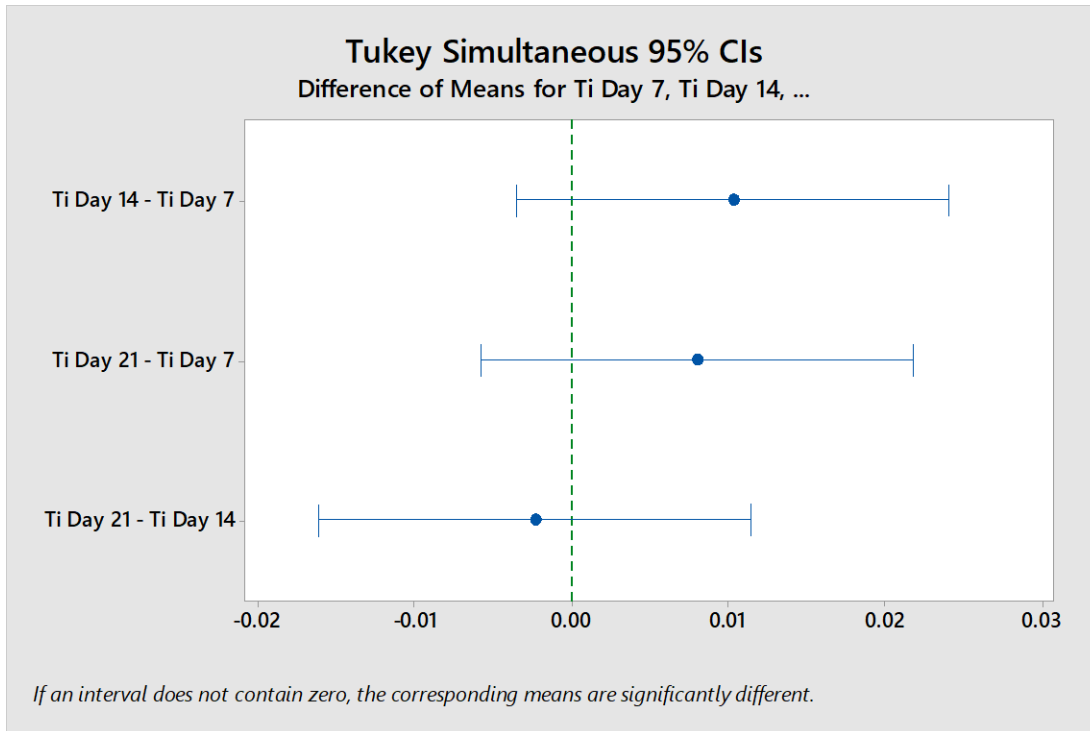
All data sets have normal distribution.



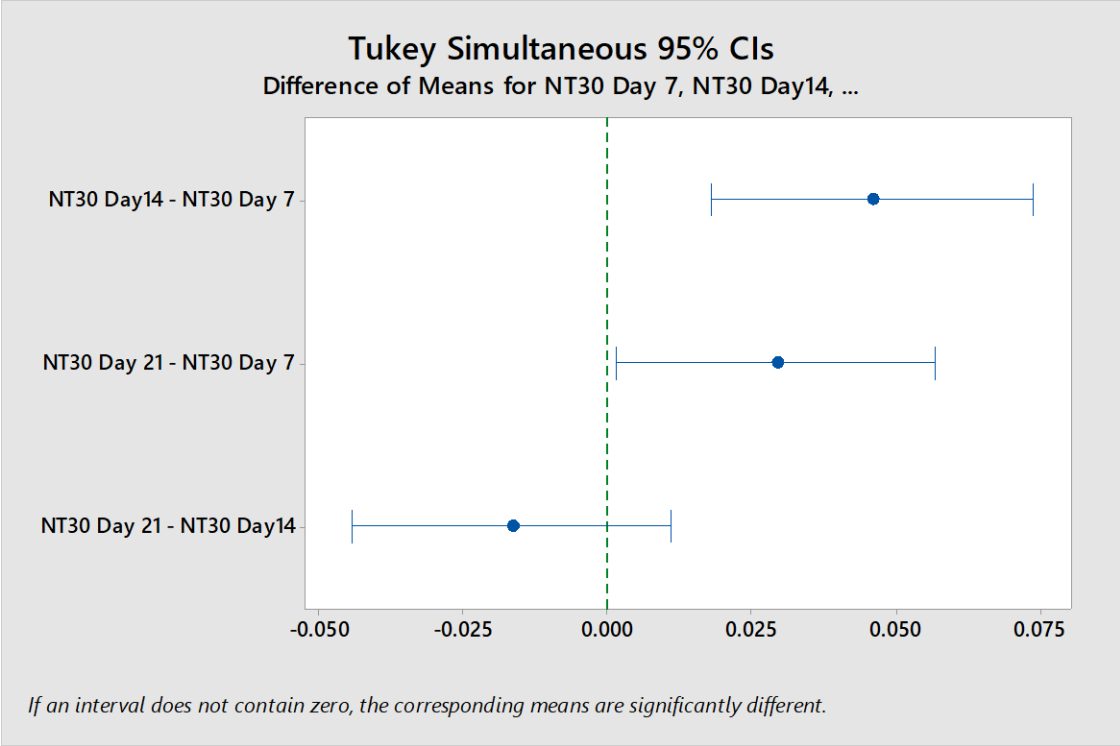
Equal variance looks good as they are all overlapping.

Run a one-way ANOVA with post hoc Tukey to determine significance.

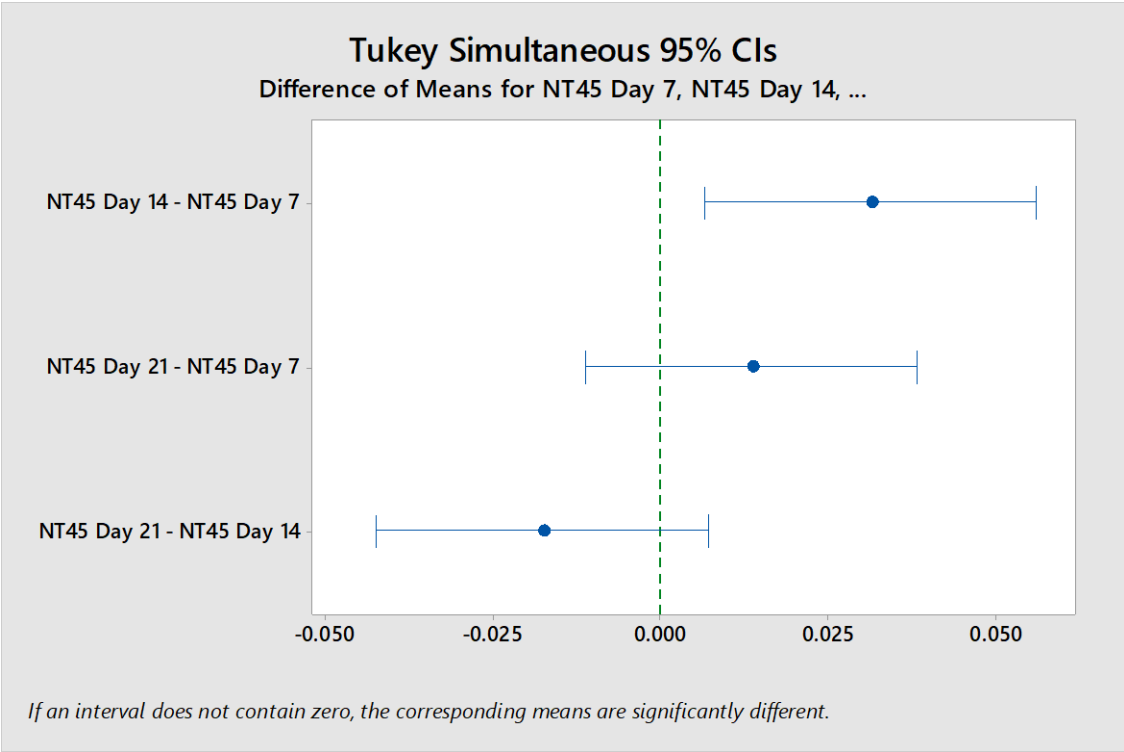
When statistically comparing between weeks of the same treatment:



Ti and NT60 display no significance between weeks.

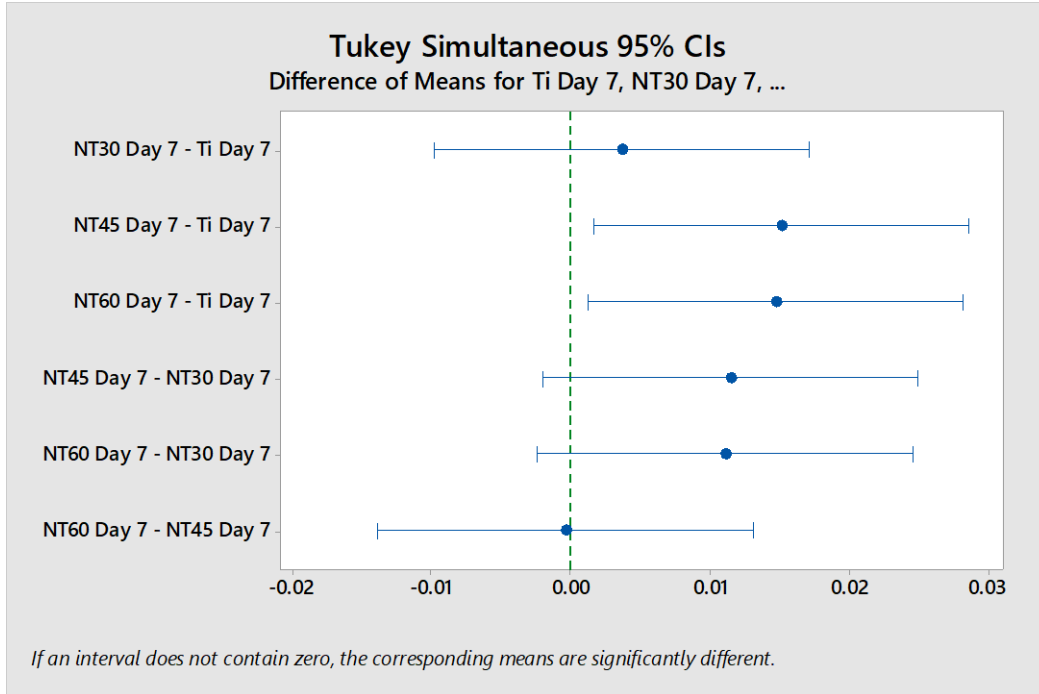


For NT30, Day 7 is significantly different from Day 14 and Day 21.

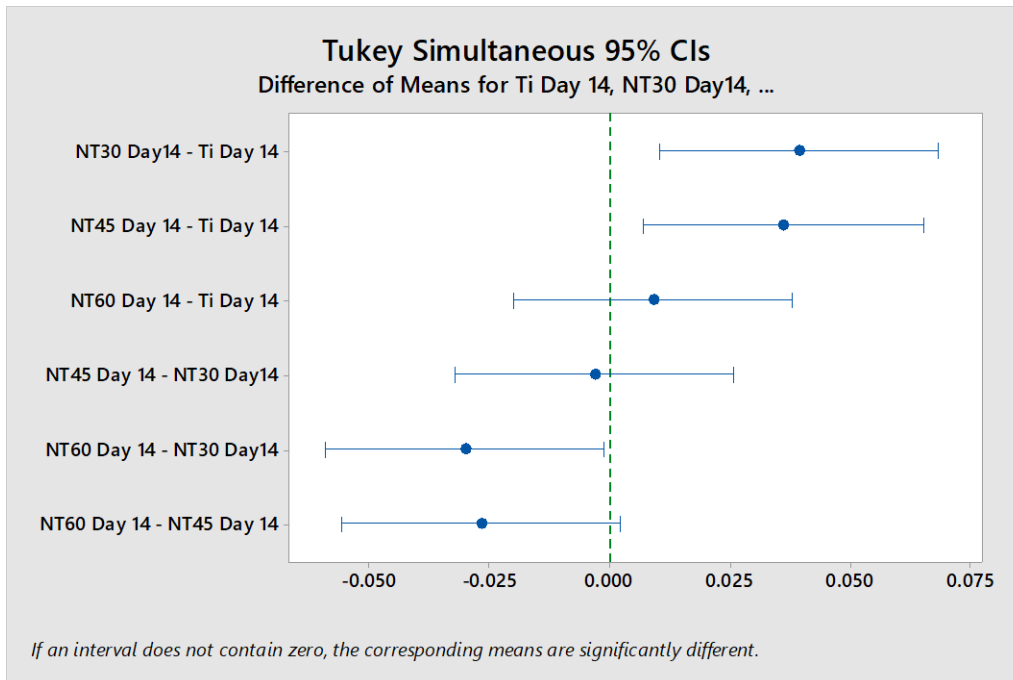


For NT45, Day 7 is significantly different from Day 14.

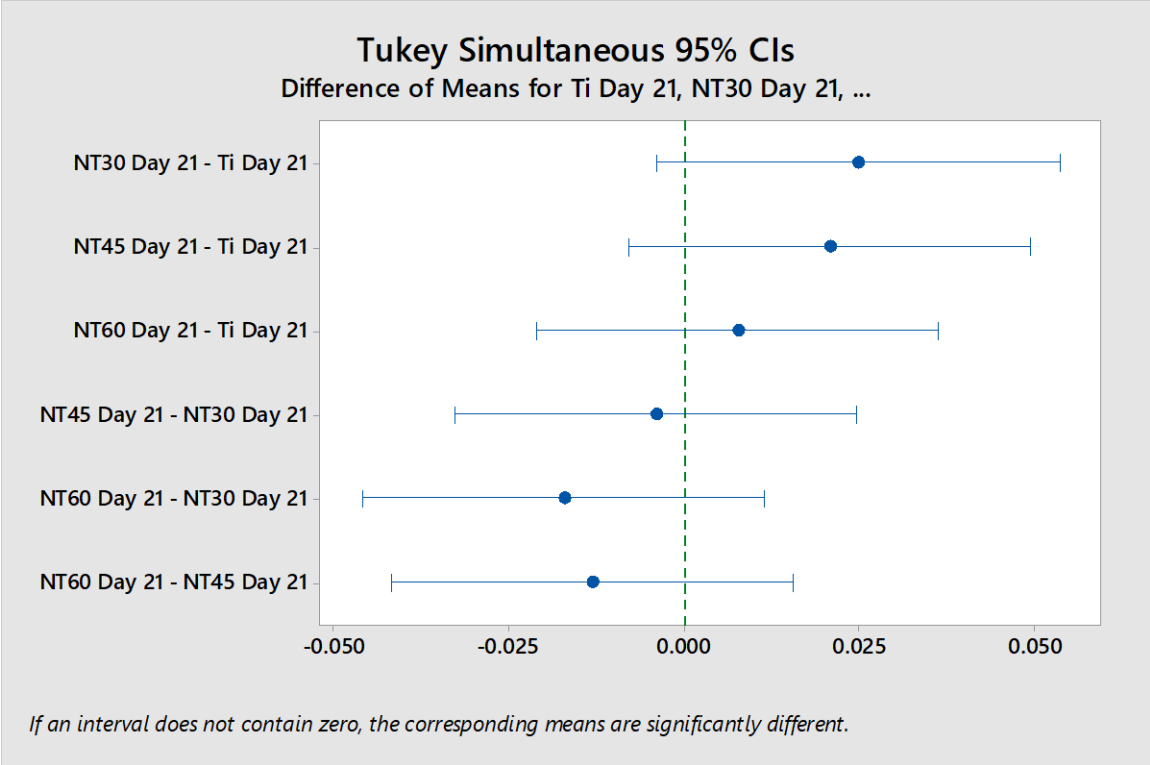
When statistically comparing between treatments on the same week:



For Day 7, Ti is significantly different from NT45 and NT60.



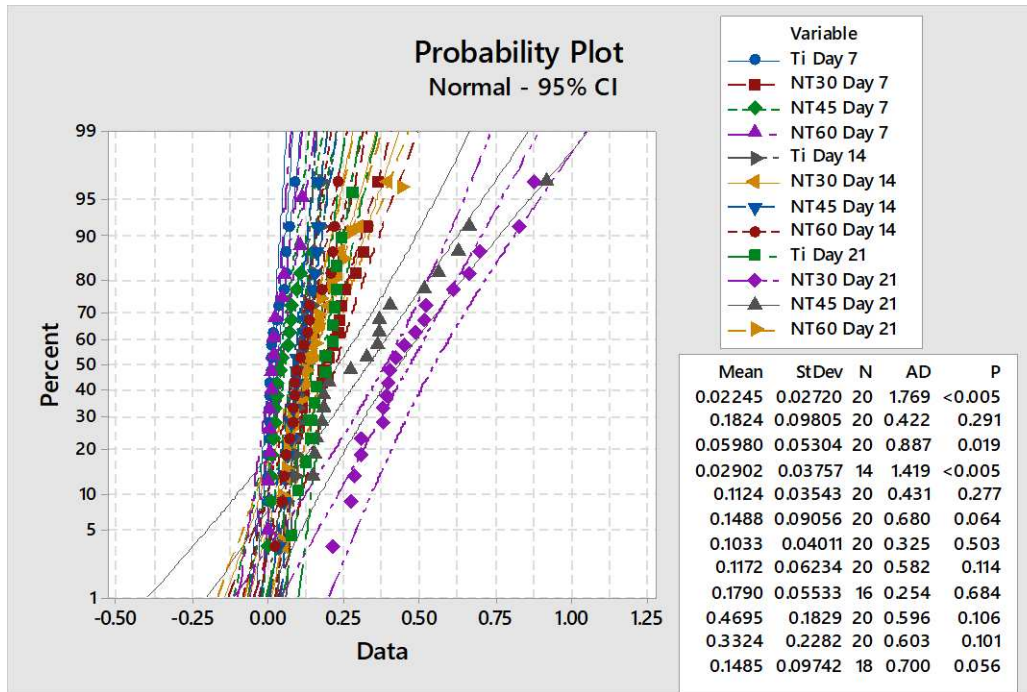
For Day 14, Ti is significantly different from NT30 and NT45, also NT60 is significantly different from NT30.



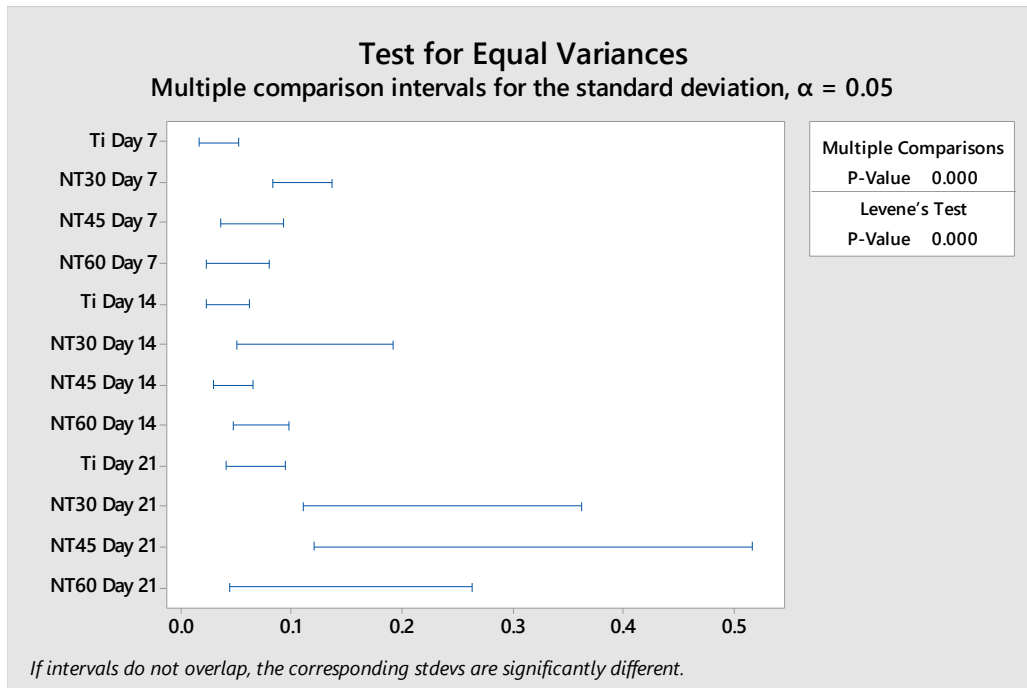
For Day 21, there is no significance between treatments.

Statistical Plots and Analysis for Figure 4.3

Two outliers in NT 60 Day 21 were removed prior to statistical analysis presented.



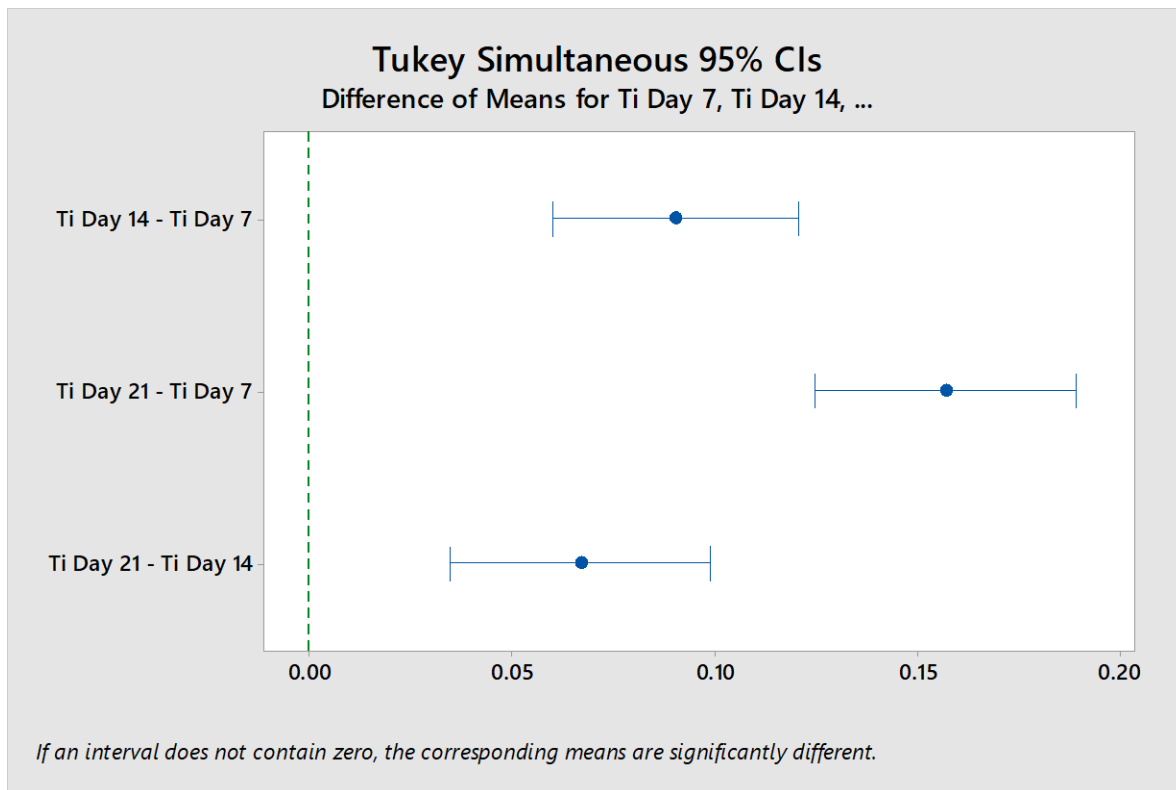
Several data sets on Day 7 are not normal: Ti Day 7, NT45 Day 7, NT60 Day 7.



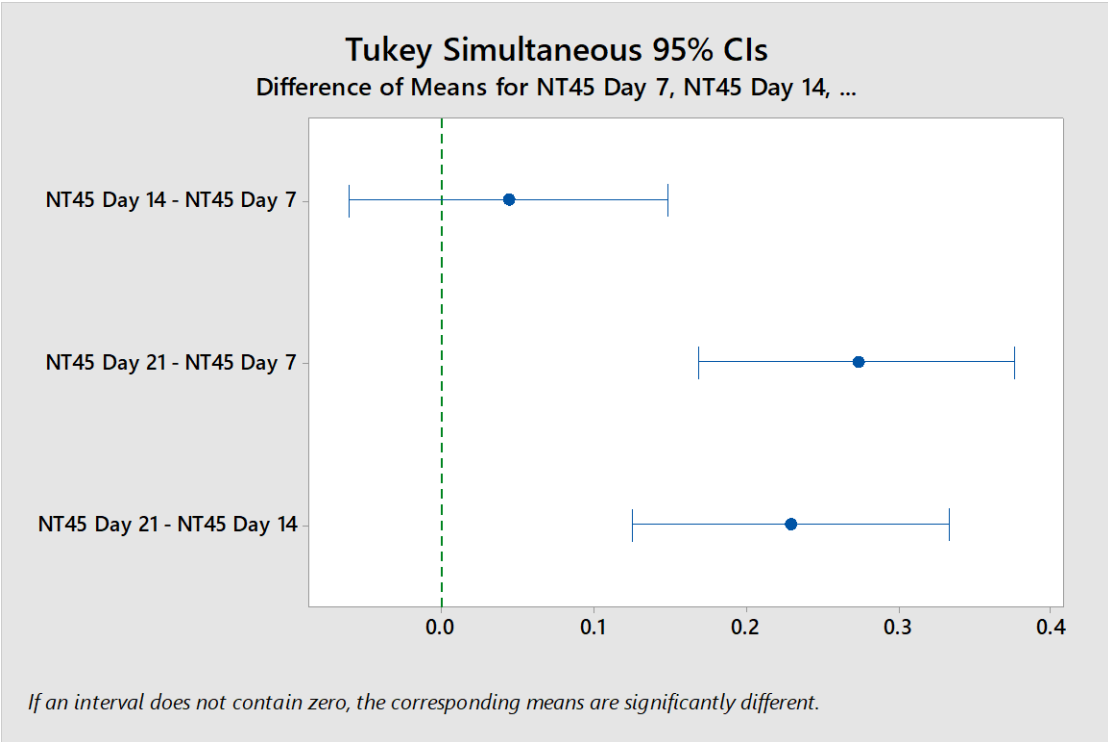
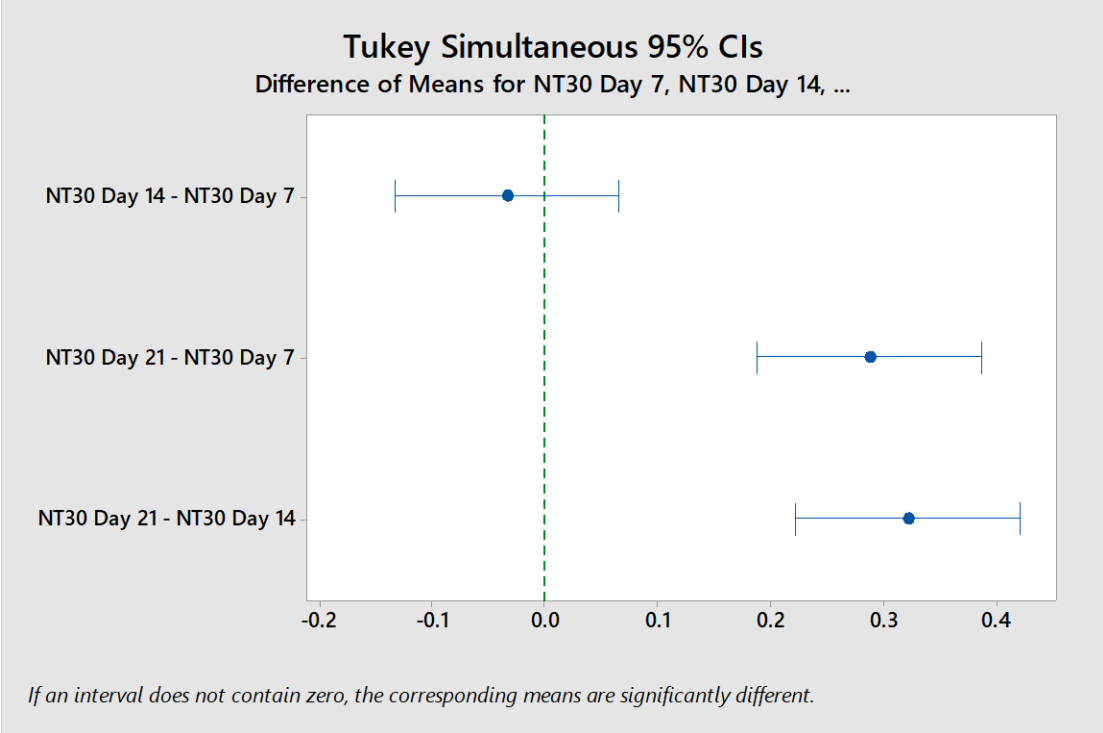
Equal variance is ok, but not great, as not all ranges are overlapping.

Still choosing to run a one-way ANOVA with post hoc Tukey to determine significance as most data sets were normal (just not Day 7) and equal variance is adequate enough for ANOVA.

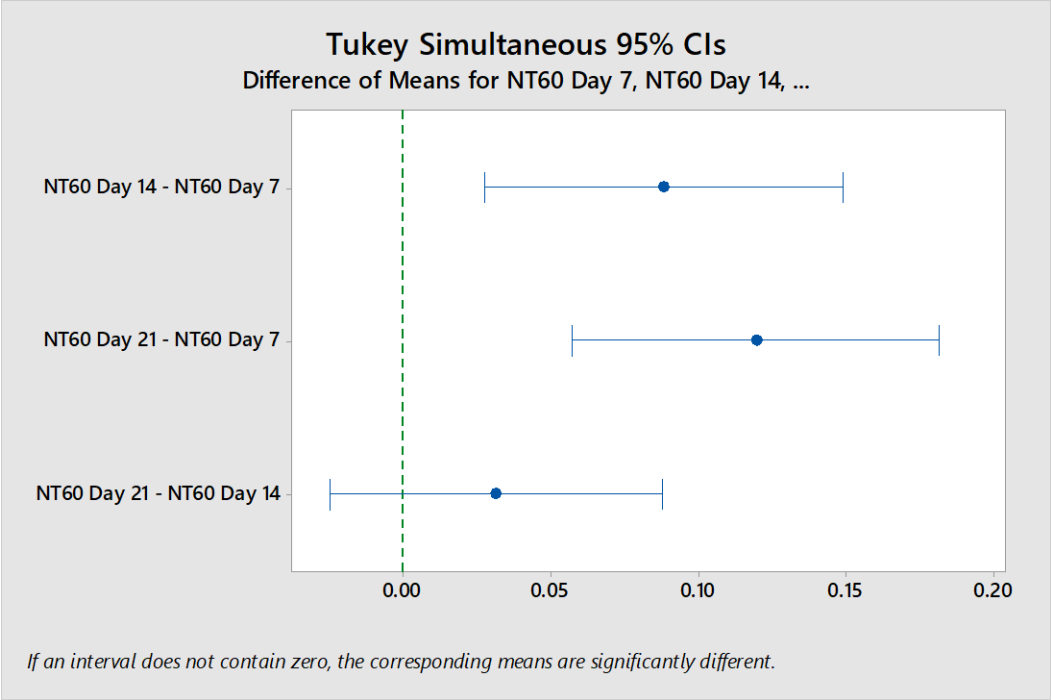
When statistically comparing between weeks of the same treatment:



For Ti, all weeks are significantly different.

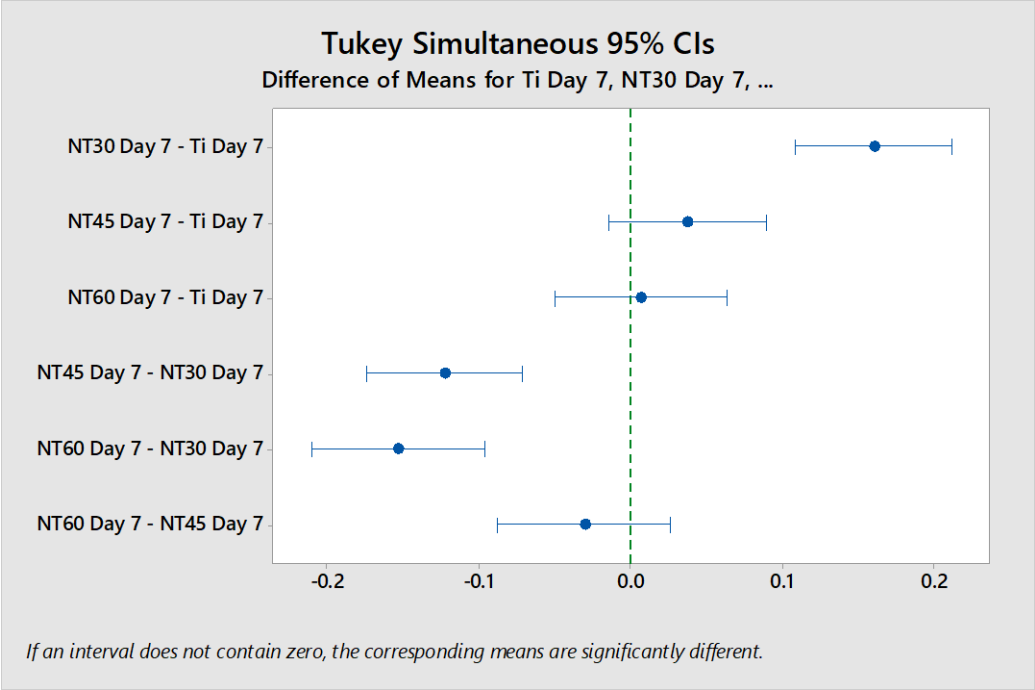


For NT30 and NT45, Day 21 is significantly different from Day 7 and 14.



For NT60, Day 7 is significantly different from Day 14 and Day 21.

When comparing between treatments on the same week:



For Day 7, NT30 is significantly different from Ti, NT45 and NT60.

Since Ti Day 7, NT45 Day 7, and NT60 Day 7 did not have normal distributions, did a Mann-Whitney (used for non-normal data sets) to confirm that NT30 was significantly different from all the other surfaces.

Mann-Whitney Test and CI: NT30 Day 7, Ti Day 7

	N	Median
NT30 Day 7	20	0.19133
Ti Day 7	20	0.00850

Point estimate for $\eta_1 - \eta_2$ is 0.17350

95.0 Percent CI for $\eta_1 - \eta_2$ is (0.08923,0.22194)

W = 596.0

Test of $\eta_1 = \eta_2$ vs $\eta_1 \neq \eta_2$ is significant at 0.0000

The test is significant at 0.0000 (adjusted for ties)

Since value is $0.000 < 0.05$, confirms NT30 and Ti are significantly different.

Mann-Whitney Test and CI: NT30 Day 7, NT45 Day 7

	N	Median
NT30 Day 7	20	0.19133
NT45 Day 7	20	0.04267

Point estimate for $\eta_1 - \eta_2$ is 0.11997

95.0 Percent CI for $\eta_1 - \eta_2$ is (0.05715,0.18267)

W = 560.0

Test of $\eta_1 = \eta_2$ vs $\eta_1 \neq \eta_2$ is significant at 0.0001

Confirms NT30 and NT45 are significantly different.

Mann-Whitney Test and CI: NT30 Day 7, NT60 Day 7

	N	Median
--	---	--------

NT30 Day 7 20 0.19133

NT60 Day 7 14 0.01369

Point estimate for $\eta_1 - \eta_2$ is 0.16293

95.2 Percent CI for $\eta_1 - \eta_2$ is (0.07979,0.22098)

W = 475.0

Test of $\eta_1 = \eta_2$ vs $\eta_1 \neq \eta_2$ is significant at 0.0000

The test is significant at 0.0000 (adjusted for ties)

Confirms NT30 and NT60 are significantly different.

The Mann-Whitney also says that NT45 and Ti are significantly different and NT45 and NT60 are significantly different which did not show up using ANOVA.

Mann-Whitney Test and CI: NT45 Day 7, NT60 Day 7

N Median

NT45 Day 7 20 0.04267

NT60 Day 7 14 0.01369

Point estimate for $\eta_1 - \eta_2$ is 0.02171

95.2 Percent CI for $\eta_1 - \eta_2$ is (0.00117,0.05822)

W = 414.0

Test of $\eta_1 = \eta_2$ vs $\eta_1 \neq \eta_2$ is significant at 0.0263

Mann-Whitney Test and CI: NT45 Day 7, Ti Day 7

N Median

NT45 Day 7 20 0.04267

Ti Day 7 20 0.00850

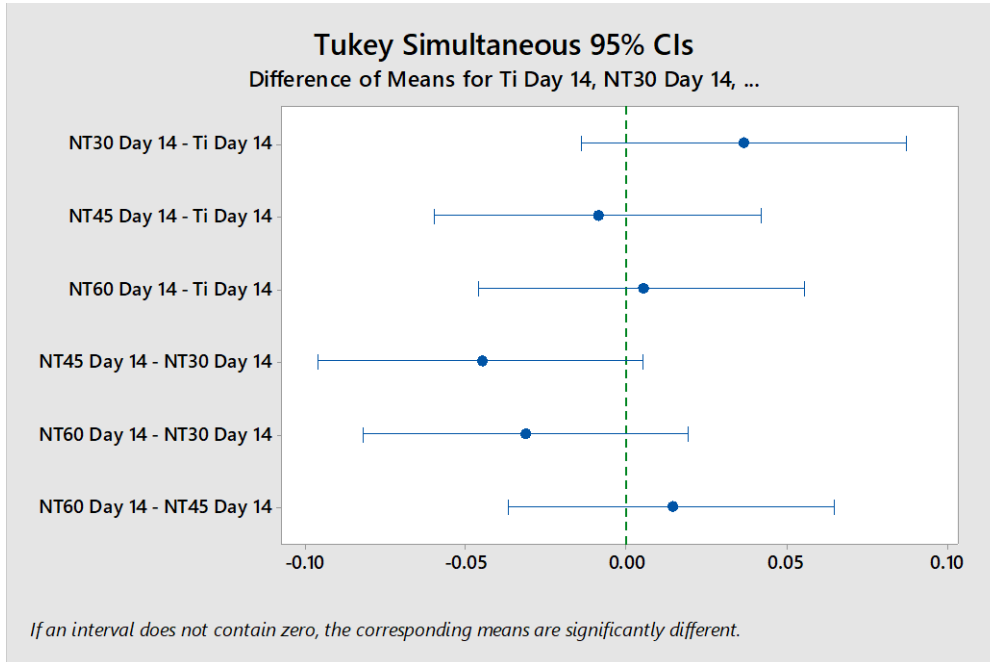
Point estimate for $\eta_1 - \eta_2$ is 0.02256

95.0 Percent CI for $\eta_1 - \eta_2$ is (0.00769,0.06084)

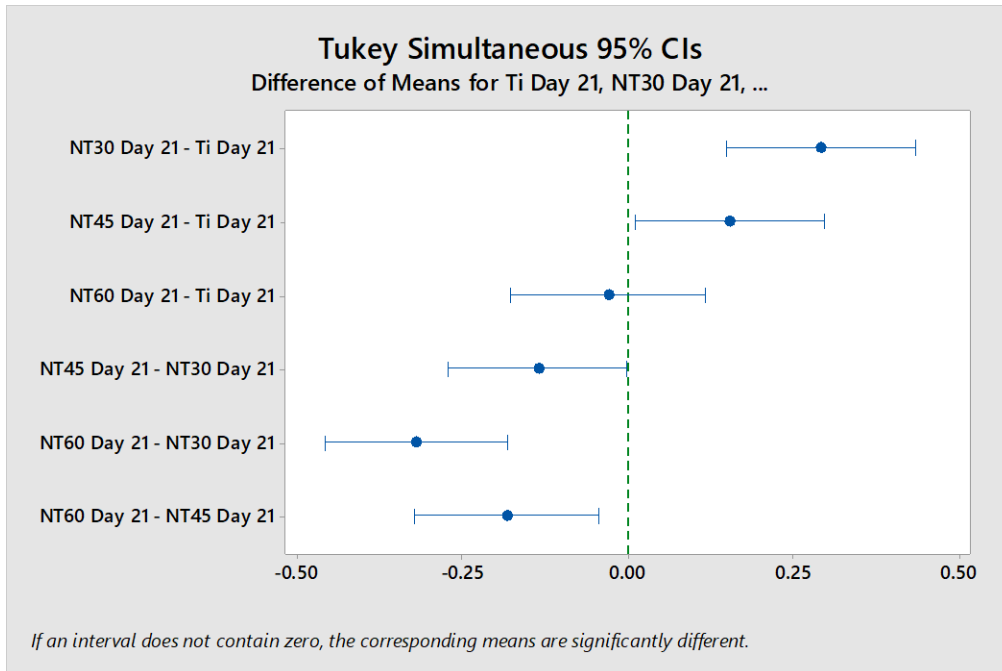
W = 516.0

Test of $\eta_1 = \eta_2$ vs $\eta_1 \neq \eta_2$ is significant at 0.0043

The test is significant at 0.0043 (adjusted for ties)

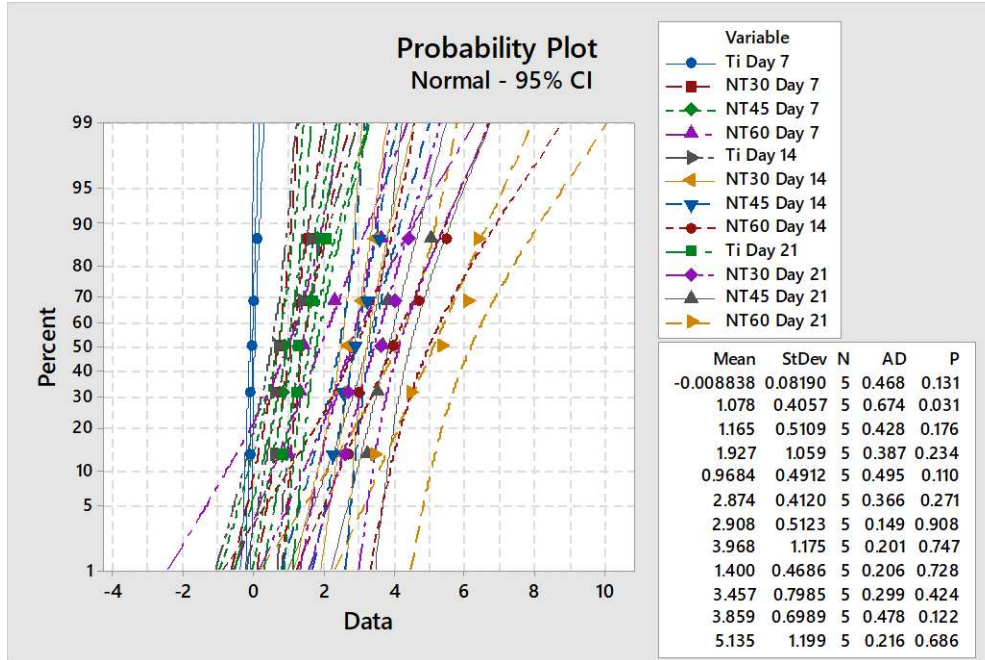


For Day 14, no significance between surfaces.

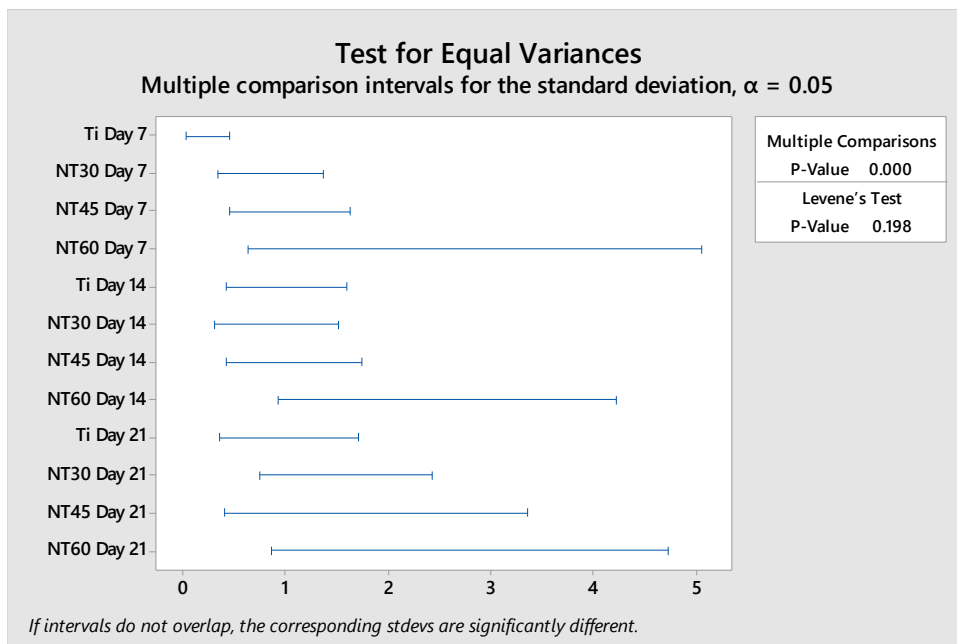


Day 21: NT30 and NT45 are significantly different from Ti and NT60.

Statistical Plots and Analysis for Figure 4.4

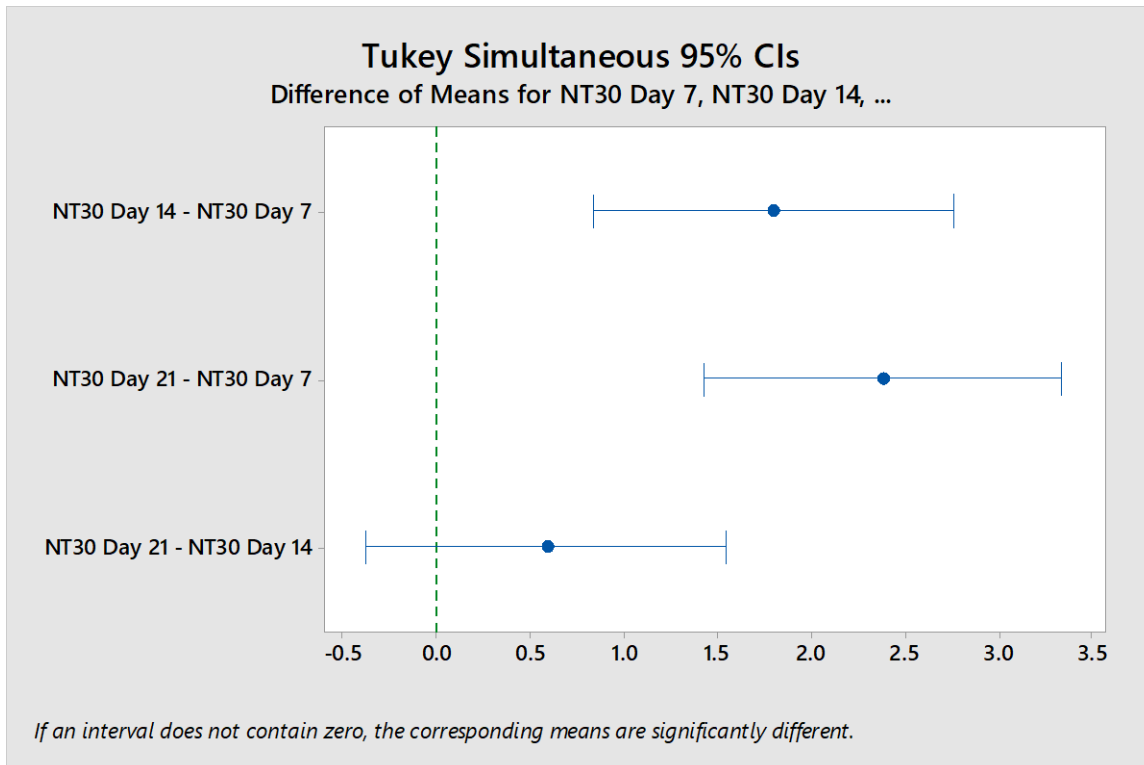
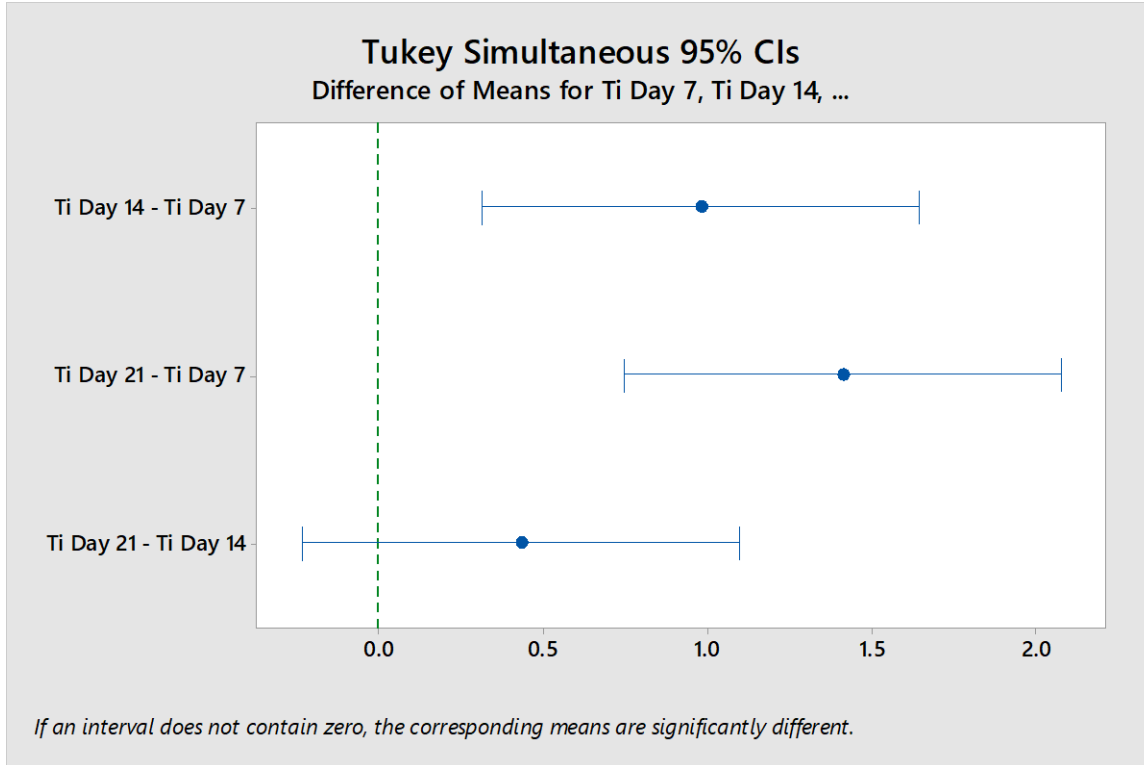


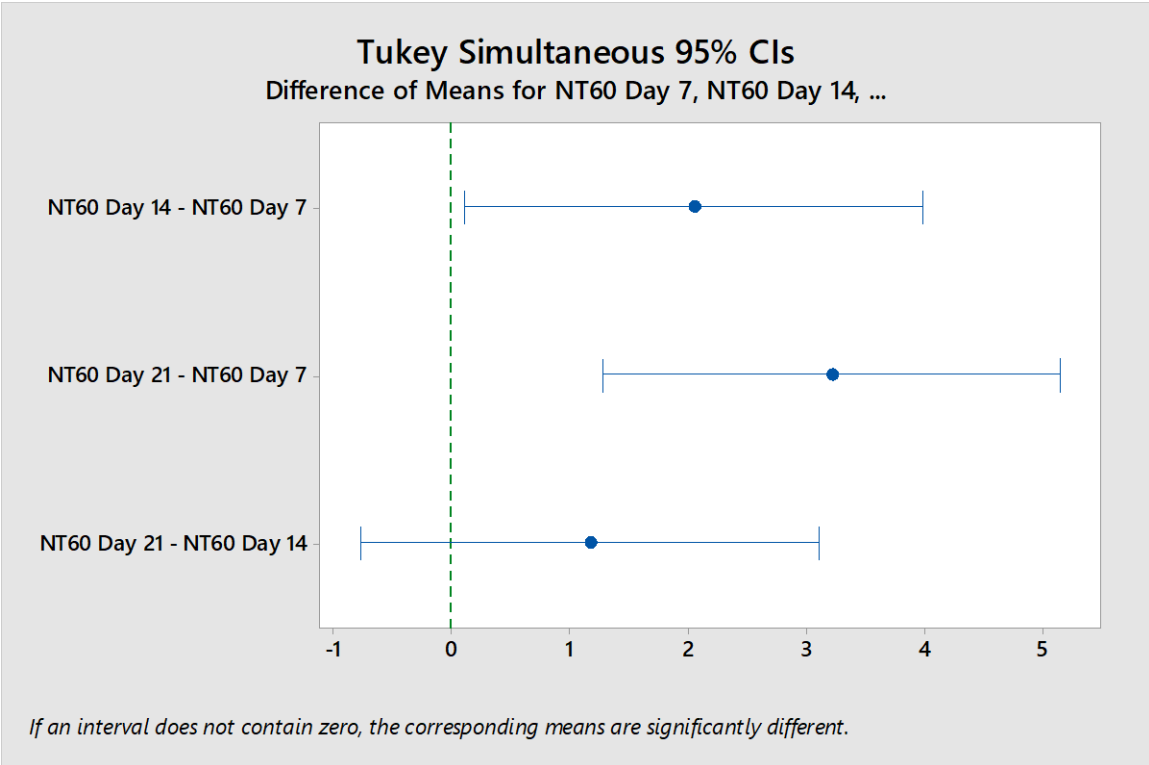
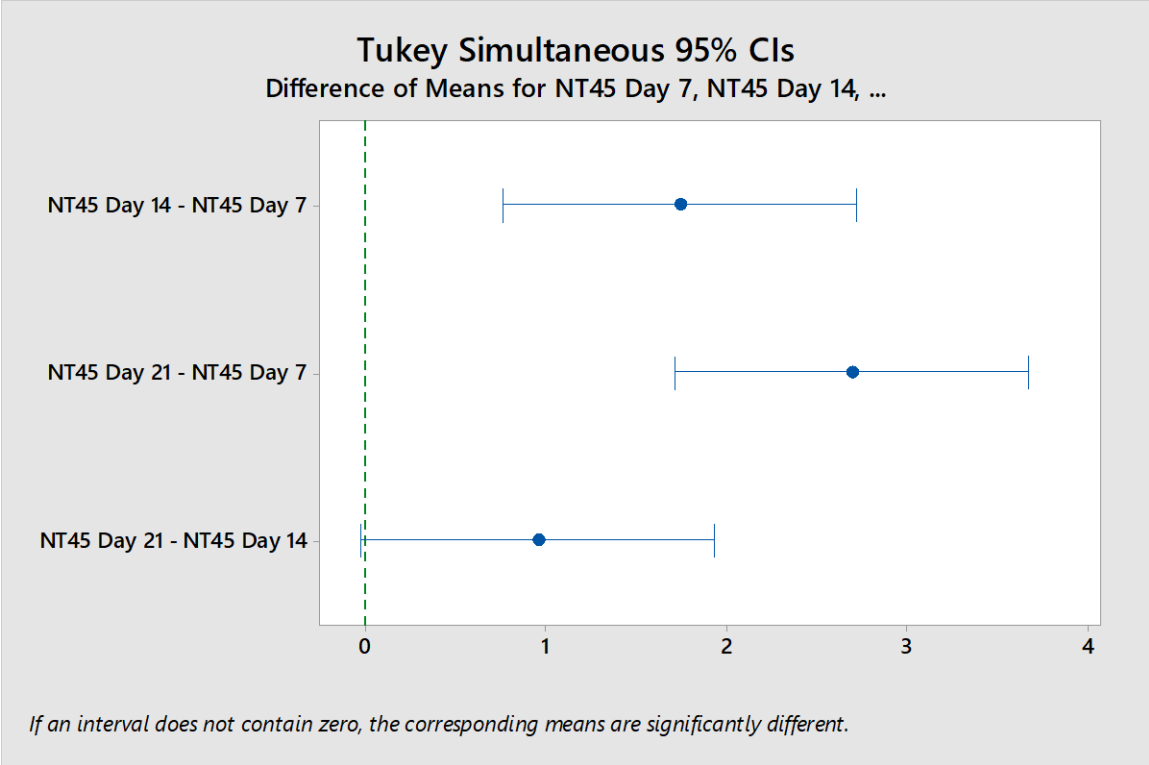
All data sets exhibit normal distribution except NT30 Day 7, but is not very low p-value so it might be fine to treat it as normal distribution.



Test for equal variance looks good. So will run one-way ANOVA with post hoc Tukey, but will look closely at NT30 Day 7 in case need to run Mann-Whitney.

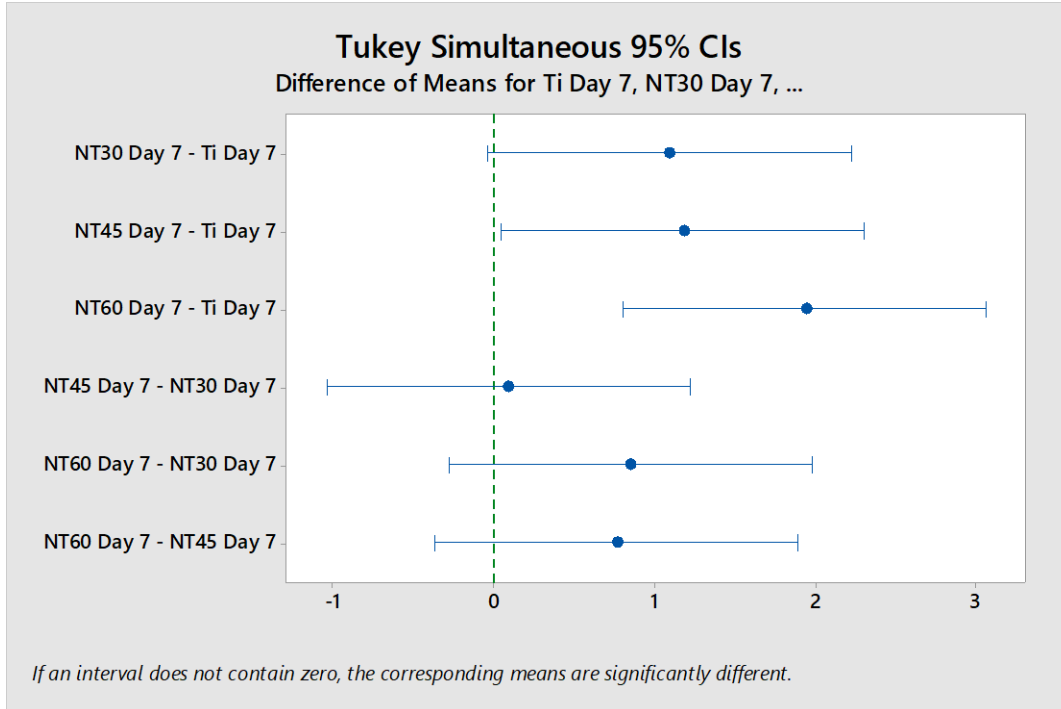
When statistically comparing between weeks of the same treatment:



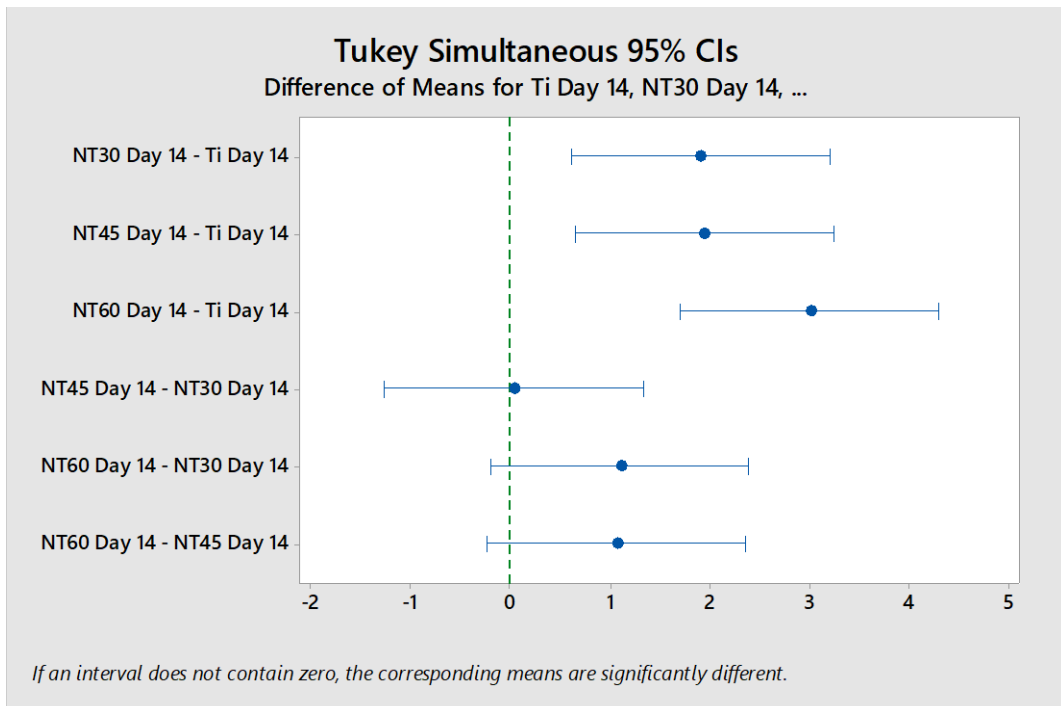


For all treatments (Ti, NT30, NT45, and NT60) Day 7 is significantly different from Day 14 and Day 21.

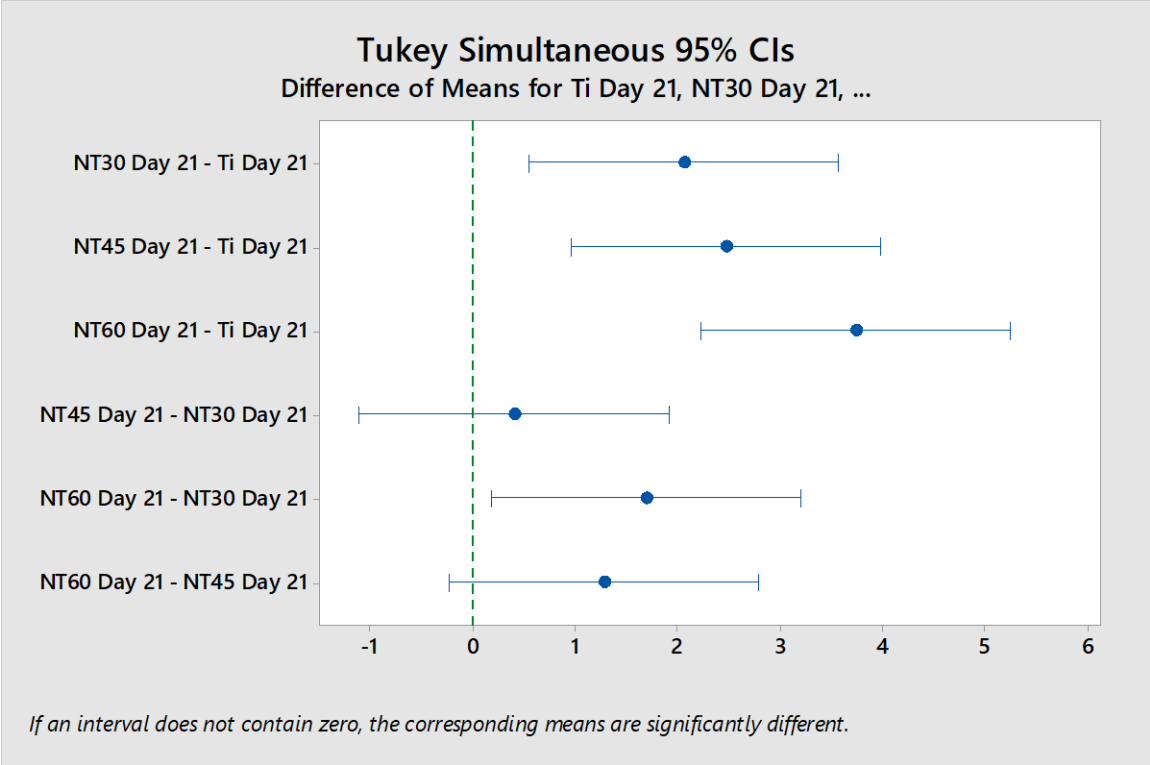
When comparing between treatments on the same week:



For Day 7, Ti is significantly different from NT45 and NT60.



For Day 14, Ti is significantly different from NT30, NT45, and NT60.



For Day 21: Ti is significantly different from NT30, NT45, and NT60. Additionally NT60 is significantly different from NT30.